

Summer 2021

## Developing and Understanding Catalysts for Organic Synthesis

Shelby Dickerson

Follow this and additional works at: <https://scholarcommons.sc.edu/etd>

 Part of the [Chemistry Commons](#)

---

### Recommended Citation

Dickerson, S.(2021). *Developing and Understanding Catalysts for Organic Synthesis*. (Doctoral dissertation). Retrieved from <https://scholarcommons.sc.edu/etd/6415>

This Open Access Dissertation is brought to you by Scholar Commons. It has been accepted for inclusion in Theses and Dissertations by an authorized administrator of Scholar Commons. For more information, please contact [digres@mailbox.sc.edu](mailto:digres@mailbox.sc.edu).

DEVELOPING AND UNDERSTANDING CATALYSTS FOR ORGANIC SYNTHESIS

by

Shelby Dickerson

Bachelor of Science  
University of Southern Mississippi, 2016

---

Submitted in Partial Fulfillment of the Requirements

For the Degree of Doctor of Philosophy in

Chemistry

College of Arts and Sciences

University of South Carolina

2021

Accepted by:

Sheryl L. Wiskur, Major Professor

John Lavigne, Committee Member

Vitaly Rassolov, Committee Member

Christopher Williams, Committee Member

Tracy L. Weldon, Interim Vice Provost and Dean of the Graduate School

© Copyright by Shelby Dickerson, 2021  
All Rights Reserved.

## DEDICATION

This dissertation is dedicated to my family and friends. These were very challenging years with a lot of personal and professional growth. I am humbled to be surrounded by such incredible people.

## ACKNOWLEDGEMENTS

The first person I would like to acknowledge my appreciation for is my advisor Dr. Sheryl Wiskur. You have put up with a lot. Research advisor, teaching advisor, life advisor, you have had every hat a mentor can in all ways of life. I value our conversations in your office and will truly miss having those chats. One of the most valuable skills you have taught me is to be thorough in my work...and then be more thorough. I have become a better scientist and educator under your guidance. As an advisor, you have shown me nothing but kindness, understanding, and an enormous amount of patience. I will always consider myself lucky to have you as a mentor.

As for the Wiskur group, I am so proud to be part of such a supportive scientific community that truly wants the best for each other. Dr. Brandon Redden and Dr. Tian Zhang, you both were my senior grad students who I really viewed as big brothers. We very much were a family, and I loved our group outings. Tian, I'm sorry I never expanded my horizons for Chinese cuisine. Brandon, I can still hear you critiquing my "sad" lunches. Although my project was very different from both of yours, you both never stopped trying to help me or cheer me up when research sucked. Gong, you have really come out of your shell since first year, and I know you are going to be a great "Senior Grad Student." Christian and Nate, watching you both grow during your first year of graduate school, I have no doubt you both will be successful and continue the legacy of the Wiskur group. Keep the laughs going in the lab. Christian, don't start fires and always keep an eye on the balloon supply. Jane and Bronwyn, I could not have asked for better undergraduate

mentees. You both are strong women in science, and I cannot wait to see what you accomplish in your careers.

Grace, I could not have survived each day without you there. My work-wife. My coconspirator. My person. You are one of the most loyal friends I have ever had. You are as much part of my PhD as this dissertation. To you and Abby, thank you for always checking in, always being a text/phone call away, and for all the Five Guys and Monterrey's adventures. I trust we will continue meeting for PokemonGo community days when we can, followed by queso at a beloved Mexican restaurant. Mat, thanks for being down to hang with a pizza and a movie and being a gym buddy.

Tyler, you have brought so much happiness this past year. Thank you for letting me take over your kitchen, for my new Lego addiction, and spoiling Lily with eggs and cheese for breakfast. Kristina, I will never understand how you can talk to me every day and still want to be one of the greatest, and oldest, friends I have. Your endless faith in me is a treasure, and I cherish every part of our friendship. I will never forget meeting you at Starbucks for a lab group coffee break in undergrad. Katherine, I appreciate that when life gets too busy for us to keep in touch, we can always meet up like no time has passed. I can always count on you to fill my Snapchat with puppy videos and keep my "to read" list full. Thanks buddy.

Lastly, I want to thank my parents, Alma and Ken Dickerson. I am lucky to have such a supportive family. I always looked forward to every trip y'all made for football games, holidays, or "just cause." You brought a piece of home every time.

I also acknowledge the National Science Foundation (NSF) for funding this research.

## ABSTRACT

Organic synthesis relies on improving catalyst designs and understanding reaction mechanisms for the advancement of the field. This dissertation will describe projects in both of these areas. First it will cover new photocatalysts in the aim of maintaining reactivity while increasing solubility in less polar solvents, and second understanding the importance of intermolecular interactions between new nucleophilic catalysts and substrates.

Photocatalysis has become a major focus as a sustainable pathway for chemical reactions with visible light photocatalysts performing a large range of reactions such as redox reactions, cyclization reactions, and energy transfer reactions. Chapter 1 will discuss classes of organic photocatalysts commonly used in the field and the goals for developing future catalysts. Silicon phthalocyanines have been largely ignored as photocatalysts in photocatalytic reactions, despite their low energy excitation, long triplet lifetimes, and their ability to form singlet oxygen. In chapter 2, we will discuss three silicon phthalocyanine catalysts we developed for photocatalysis. Using cyclic voltammetry and Stern Volmer quenching studies, we have shown silicon phthalocyanines can act as electron donors or acceptors with appropriate substrates. We have successfully used silicon phthalocyanines in a reductive quenching reaction and in energy transfer reactions utilizing singlet oxygen as a reactant. These reactions, as well as the photophysical and electrochemical experiments will be discussed.

In asymmetric catalysis, intra- and intermolecular interactions can be important for influencing catalyst/substrate arrangements to obtain selective reactions. Cation- $\pi$  interactions are one such interaction, that is frequently suggested to aid in reaction control. Isothiourea catalysts are nucleophilic catalysts that tend to form a cationic intermediate during the reaction and are hypothesized to participate in cation- $\pi$  interactions. Chapter 3 will directly focus on the cation- $\pi$  interaction we believe is occurring during an alcohol silylation reaction by analyzing electron rich and electron poor nonchiral isothiourea catalysts to understand how changes in the catalyst affect interactions with substrates. Competition studies with electron-rich and electron-poor substrates are used as a tool to probe this interaction and the results obtained will be discussed.



## TABLE OF CONTENTS

Dedication.....	iii
Acknowledgements .....	iv
Abstract.....	vi
List of Tables .....	x
List of Figures .....	xi
List of Schemes.....	xv
Chapter 1: Background on Photocatalysis.....	1
1.1 Photocatalysis in organic synthesis.....	1
1.2 Organic photocatalysts .....	5
1.3 Silicon phthalocyanines.....	11
1.4 Conclusions .....	15
Chapter 2 Silicon Phthalocyanines as Photocatalysts .....	17
2.1 Introduction .....	17
2.2 Synthesis of silicon phthalocyanines .....	20
2.3 Photophysical and photochemical properties of silicon phthalocyanines.....	21
2.4 Silicon phthalocyanines in an energy transfer reaction.....	36
2.5 Silicon phthalocyanines in an electron transfer reaction.....	38
2.6 Conclusions and outlook .....	42
2.7 Experimental.....	46

## Chapter 3 Investigating the Electronic Effect on Isothiourea-Based

Catalysts in Competition Studies with Trans-2-Phenylcyclohexanols .....	50
3.1 Introduction .....	50
3.2 Experimental Design.....	63
3.3 Synthesis of isothiourea catalysts and alcohol derivatives.....	65
3.4 Competition studies of isothiourea catalysts .....	68
3.5 Conclusions and outlook .....	82
3.6 Experimental.....	83
References.....	91

## LIST OF TABLES

<b>Table 2.1</b> Ground state and excited state redox potentials of photocatalysts. ....	29
<b>Table 2.2</b> The [4+2]-cycloaddition of pyridone <b>2.6</b> to endo-peroxide <b>2.7</b> . ....	31
<b>Table 2.3</b> Dehalogenation Reaction.....	33
<b>Table 2.4</b> Large Scale of Dehalogenation Reaction and Catalyst Stability Study. ....	35
<b>Table 3.1</b> Alcohol study by Birman for catalysts with different pi systems.....	46
<b>Table 3.2</b> Conversions and selectivities of substituted aryl alcohols in acylation kinetic resolution by Smith .....	48
<b>Table 3.3</b> Conversion and selectivities of substituted alkenyl group in acylation kinetic resolution by Smith.....	49
<b>Table 3.4</b> Conversions and selectivities seen with ester derivatives in kinetic resolution of chiral secondary alcohols .....	52
<b>Table 3.5</b> Competition study results using the methoxy alcohol with <b>3.8a</b> to determine the amount of methoxy alcohol remaining and methoxy product generated in the reaction .....	62
<b>Table 3.6</b> Control kinetic resolution runs with benzotetramisole catalyst.....	66
<b>Table 3.7</b> Results of competition study for catalyst and alcohol derivatives.....	67

## LIST OF FIGURES

<b>Figure 1.1</b> Simplified Jablonski diagram of photocatalytic process. ....	1
<b>Figure 1.2</b> Structure of $\text{Ru}(\text{bpy})_3^{2+}$ .....	2
<b>Figure 1.3</b> Examples of different organocatalysts.....	3
<b>Figure 1.4</b> Organic dyes investigated by Zeitler group .....	4
<b>Figure 1.5</b> Silicon phthalocyanine structure .....	9
<b>Figure 1.6</b> Structure of derivatized silicon phthalocyanine dendrimer .....	11
<b>Figure 1.7</b> Proposed silicon phthalocyanine structures .....	14
<b>Figure 2.1</b> Silicon phthalocyanine derivatives.....	17
<b>Figure 2.2</b> Synthetic routes for silicon phthalocyanine catalysts <b>1.1-1.3</b> .....	18
<b>Figure 2.3</b> A. UV-vis absorption spectrum of <b>2.1</b> in $\text{CHCl}_3$ at 0.005 mM. B. UV-vis absorption spectrum of <b>2.2</b> in $\text{CHCl}_3$ at 0.002 mM. C. Emission spectrum of <b>2.1</b> at 0.8 $\mu\text{M}$ with excitation at 670 nm in $\text{CHCl}_3$ . D. Emission spectrum of <b>2.2</b> at 0.3 $\mu\text{M}$ with excitation at 670. 22.....	19
<b>Figure 2.4</b> Oxidation and reduction cyclic voltammetries of <b>2.1</b> at 1.7 mM and <b>2.2</b> at 2 mM at 0.1 Vs-1 in $\text{CHCl}_3/\text{TBAPF}_6$ .....	21
<b>Figure 2.5</b> The oxidative (left) and reductive (right) scans of <b>2.2</b> at multiple scan rates (100, 80, 60, 40, and 20 V/s in chloroform.....	22
<b>Figure 2.6</b> Linear dependence of peak current for <b>2.1</b> in chloroform. A) Oxidative Peak B) First Reductive Peak C) Second Reductive Peak. ....	22
<b>Figure 2.7</b> The oxidative (left) and reductive (right) scans of <b>2.1</b> at multiple scan rates (100, 80, 60, 40, and 20 V/s in chloroform.....	23

<b>Figure 2.8</b> Linear dependence of peak current for <b>2.2</b> in chloroform. A) Oxidative Peak. B) Reductive Peak.....	23
<b>Figure 2.9</b> Oxidation and reduction cyclic voltammetries of <b>2.1</b> at 1.7 mM, <b>2.2</b> at 2 mM, and <b>2.3</b> at 1 mM at 0.1 Vs-1 in CH <sub>2</sub> Cl <sub>2</sub> / TBAPF <sub>6</sub> . ....	24
<b>Figure 2.10</b> The oxidative (left) and reductive (right) scans of <b>2.1</b> at multiple scan rates (100, 80, 60, 40, and 20 V/s in dichloromethane .....	25
<b>Figure 2.11</b> Linear dependence of peak current for <b>2.1</b> . A) Oxidative Peak. B) First Reductive Peak. C) Second Reductive Peak .....	25
<b>Figure 2.12</b> Oxidation (left) and reduction (right) overlaps of multiple scan rates for <b>2.2</b> in dichloromethane .....	26
<b>Figure 2.13</b> Linear dependence of peak current for <b>2.2</b> in dichloromethane. A) Oxidative Peak. B) First Reductive Peak. C) Second Reductive Peak.....	26
<b>Figure 2.14</b> Oxidation (left) and reduction (right) scans of multiple rates (100, 80, 60, and 40 V/s) overlap for <b>2.3</b> in dichloromethane .....	27
<b>Figure 2.15</b> Linear dependence of peak current for <b>2.3</b> in dichloromethane. A) Oxidative Peak. B) First Reductive Peak. C) Second Reductive Peak.....	27
<b>Figure 2.16</b> A. Normalized absorbance and emission overlap of <b>2.1</b> . B. Normalized absorbance and emission overlaps of <b>2.2</b> . Emission excitation was at 675 nm.....	28
<b>Figure 2.17</b> A. Stern-Volmer quenching study of <b>2.1</b> at 0.8 $\mu$ M and iPr <sub>2</sub> EtN at 0-0.33 M in CHCl <sub>3</sub> . The emission spectra from 630-800 nm, excitation at 675 nm. B. Stern-Volmer quenching study of <b>2.2</b> at 0.3 $\mu$ M and iPr <sub>2</sub> EtN at 0-0.31 M in CHCl <sub>3</sub> . The emission spectra from 630-800 nm, excitation at 675 nm. C. Stern-Volmer quenching study of <b>2.3</b> at 1.0 mM and iPr <sub>2</sub> EtN at 0-0.5 M in CHCl <sub>3</sub> . The emission spectra from 630-800 nm, excitation at 675 nm.....	29
<b>Figure 2.18</b> A (Left). Stern Volmer quenching studies of <b>2.1</b> (8 x 10 <sup>-7</sup> M) and <b>2.2</b> (3 x10 <sup>-7</sup> M). B (Right). Stern Volmer quenching with <b>2.1</b> , <b>2.2</b> , and <b>2.3</b> (1.0 mM) with Hünig's base in chloroform. Catalysts <b>2.1</b> , <b>2.2</b> , and <b>2.3</b> were excited at	

675 nm and emission was collected from 630 – 800 nm. I <sub>0</sub> is in reference to 676.5 nm.....	30
<b>Figure 2.19</b> Tetraphenylporphyrin (TPP) .....	31
<b>Figure 3.1</b> Structures for tetramisole ( <b>3.1</b> ) and benzotetramisole ( <b>3.2</b> ).....	44
<b>Figure 3.2</b> Transition state of the cation- $\pi$ and $\pi$ - $\pi$ interaction suggested by the Birman group in the resolution of chiral alcohols for amidine-based catalysts .....	45
<b>Figure 3.3</b> Birman catalyst development for better pi overlap .....	45
<b>Figure 3.4</b> Predicted cation- $\pi$ interaction in transition state in the Wiskur group's silylation reactions .....	51
<b>Figure 3.5</b> Predicted cation-pi intermediate of nonchiral isothiurea catalysts and secondary alcohols .....	54
<b>Figure 3.6</b> Derivatized isothiurea-based catalysts.....	55
<b>Figure 3.7</b> HPLC trace of competition study .....	59
<b>Figure 3.8</b> Select compounds investigated for HPLC internal standard.....	60
<b>Figure 3.9</b> GC trace of competition study.....	61
<b>Figure 3.10</b> Competition study crude <sup>1</sup> H NMR of reaction mixture in CDCl <sub>3</sub> .....	63
<b>Figure 3.11</b> <sup>1</sup> H NMR comparison of crude reaction mixture before (bottom) and after (top) acylating unreacted alcohols in CDCl <sub>3</sub> .....	65
<b>Figure 3.12</b> Linear free energy relationship diagrams for <b>3.5a-c</b> using sigma plus constants .....	68
<b>Figure 3.13</b> Proposed interactions between methoxy catalyst and chloro alcohol in competition study .....	70
<b>Figure 3.14</b> Suggested chiral isothiurea catalysts for future kinetic resolutions.....	73
<b>Figure 3.15</b> Suggested isothiurea catalyst derivatives with ring containing nitrogens expanded from five- to six-membered... ..	73
<b>Figure 3.16</b> Dual pi system of secondary alcohol for future competition studies.....	74

## LIST OF SCHEMES

<b>Scheme 1.1</b> Model reactions to test eosin Y as organophotocatalyst <b>A.</b> Photoredox dehalogenation reaction. <b>B.</b> Asymmetric $\alpha$ -alkylation reaction.....	5
<b>Scheme 1.2</b> Tautomerization equilibrium of eosin Y.....	6
<b>Scheme 1.3</b> Synthesis of iodo-Bodipy derivative.....	8
<b>Scheme 2.1</b> Synthetic routes for silicon phthalocyanine catalysts <b>2.1-2.3</b> .....	18
<b>Scheme 3.1</b> Birman's kinetic resolution of secondary alcohols.....	44
<b>Scheme 3.2</b> Smith's kinetic resolution of secondary alcohols with HyperBTM .....	47
<b>Scheme 3.3</b> Proposed transition states by Smith and coworkers for multiple possible cation- $\pi$ interactions.....	47
<b>Scheme 3.4</b> Previous silylation-based kinetic resolutions performed by the Wiskur group .....	50
<b>Scheme 3.5</b> Reaction for competition studies .....	55
<b>Scheme 3.6</b> Synthesis of catalysts <b>3.5a-c</b> .....	57
<b>Scheme 3.7</b> Synthesis of alcohol derivatives .....	57
<b>Scheme 3.8</b> Scheme of acylating alcohol derivatives to generate fluoro esters for $^{19}\text{F}$ NMR .....	64
<b>Scheme 3.9</b> Controlled kinetic resolution with benzotetramisole catalyst <b>3.2</b> to generate acylated fluorinated esters .....	65

# CHAPTER 1

## BACKGROUND ON PHOTOCATALYSIS

### 1.1. Photocatalysis in organic synthesis

In the past fifteen years, synthetic chemists have increasingly employed photocatalysis, specifically using visible-light, for unique organic transformations, including photo-cycloadditions and C-H bond activations, just to name two.<sup>1</sup> Photocatalysts provide mild, sustainable pathways for reactions to occur by producing excited species (commonly singlet or triplet state species) that achieve intricate molecular transformations not always possible by established protocols or traditional reagents. The two processes most accepted for photocatalysis are electron and energy transfer.<sup>2,10</sup> In these processes, a photocatalyst absorbs energy from light, to reach an excited singlet state. This excited species can then undergo intersystem crossing to its excited triplet state. The triplet state is where photochemistry occurs and is the species that can either undergo an energy

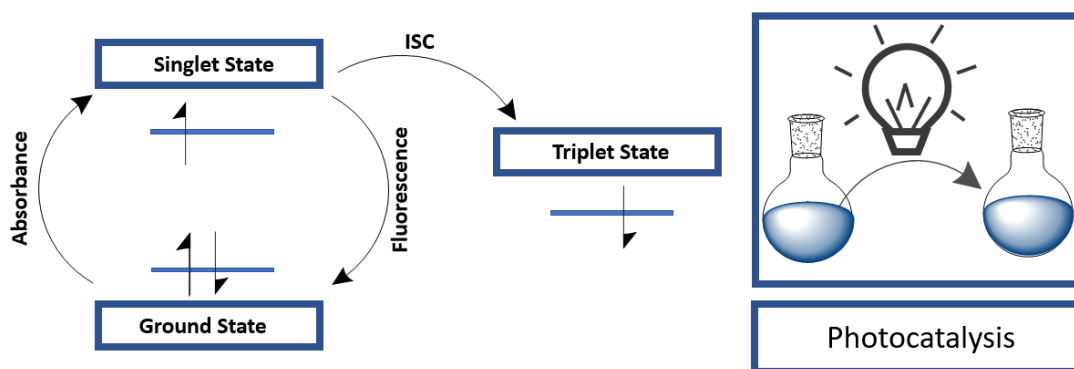


**Figure 1.1** Simplified Jablonski diagram of photocatalytic process.



or electron transfer to produce other reactive species in the reaction (Figure 1.1).<sup>7,8,10</sup> The MacMillan, Yoon, and Stephenson research groups were fundamental in initiating the boom photoredox catalysis has had in organic synthesis.<sup>2,3,4,5,6,7,8</sup> Their research employed

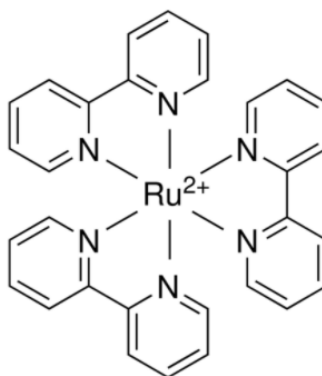


**Figure 1.2** Structure of  $\text{Ru}(\text{bpy})_3^{2+}$

$\text{Ru}(\text{bpy})_3^{2+}$  (bpy is 2,2'-bipyridine as shown in Figure 1.2) or derivatives of  $\text{Ru}(\text{bpy})_3^{2+}$ , to achieve what were synthetically challenging transformations, such as the *enantio*-selective intermolecular  $\alpha$ -alkylation of aldehydes,<sup>2</sup> [2+2] cycloaddition of enones,<sup>3</sup> and reductive dehalogenation,<sup>4</sup> all using visible light photocatalysis. These groups were able to perform very different reactions with essentially the same catalyst, expanding its application to a wide set of reactions. What made this catalyst so versatile was its ability to efficiently undergo single electron transfer (SET) and energy transfer (ET) processes, both photocatalytic pathways.<sup>9,10</sup> In these reactions, the excited  $\text{Ru}(\text{bpy})_3^{2+}$  would accept an electron from a sacrificial donor, then donate the electron to a different substrate that would then perform the desired chemistry. Since then, numerous studies have incorporated ruthenium-based photocatalysts to continue expanding the application of these catalysts in various types of reactions.<sup>6,7,8</sup>

While ruthenium-based photocatalysts have shown to be valuable photocatalysts, a push for more sustainable catalysts, specifically organic-based photocatalysts, emerged to reduce the use of these precious metals and limit metal waste.<sup>11,12,13</sup> Porphyrinoids,<sup>14</sup> acridinium salts,<sup>15</sup> (thio)xanthene dyes,<sup>16</sup> pyriliums,<sup>17</sup> benzophenones,<sup>18</sup> phenalenones,<sup>19</sup> thiazines,<sup>20</sup> and BODIPY<sup>21,30</sup> (Boron-dipyrromethene) are just a few of the many classes of organophotocatalysts that have developed in hopes of replacing metal-based photocatalysts (Figure 1.3).<sup>21</sup> These compounds have desirable qualities, including simple

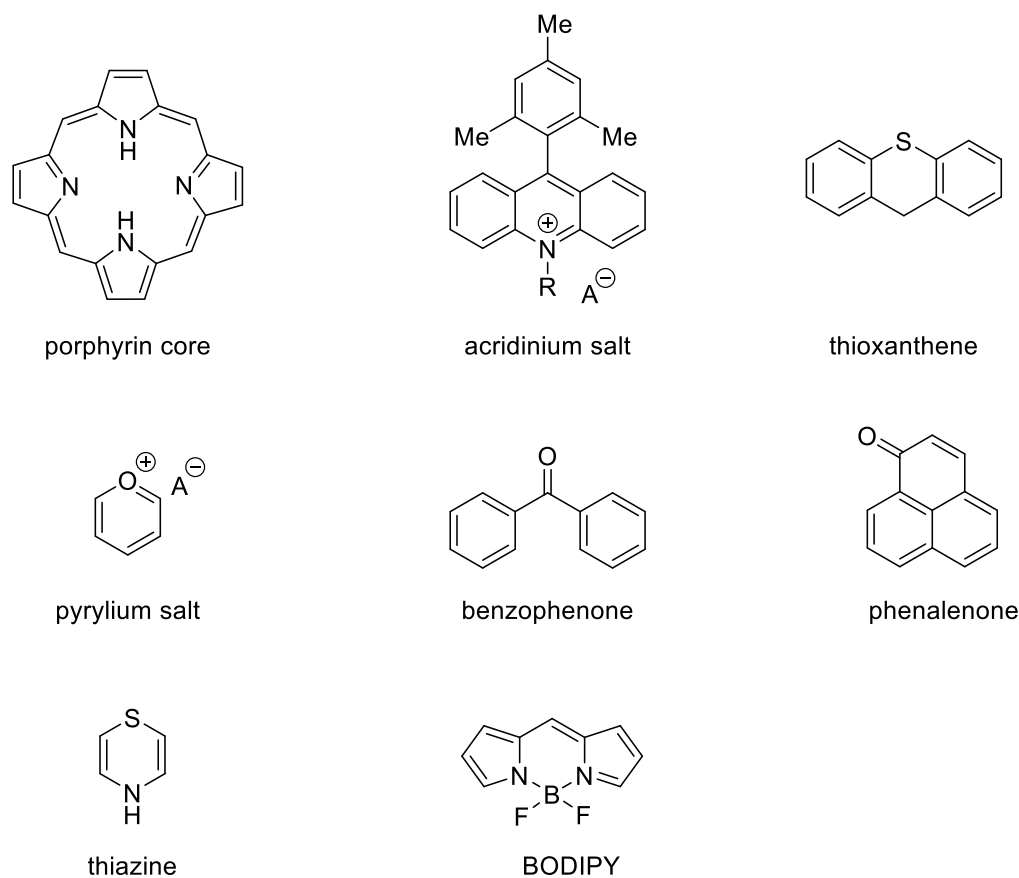


**Figure 1.3** Examples of different organocatalysts

structural modifications for tuning of physical properties, photostability, and redox properties similar to ruthenium-based catalysts. While significant strides have been made in developing organic photocatalysts with these families, there are still several issues to

address, including solubility in diverse solvents, tolerance towards changes in pH, and achieving redox potentials competitive with metal-based photocatalysts. In this dissertation, a select few of these families will be further discussed and analyzed in terms of their contribution to photocatalysis.

## 1.2 Organic Photocatalysts

### 1.2.1 Eosin Y

In 2010, the Zeitler group investigated various organic dyes in hopes of developing an efficient photocatalyst for organic transformations.<sup>22</sup> They began their study with organic dyes (Figure 1.4) that displayed similar properties to ruthenium- and iridium-based catalysts, specifically their absorbance max wavelengths and redox potentials. The Zeitler group modeled Stephenson and coworker's dehalogenation of  $\alpha$ -bromoacetophenone to

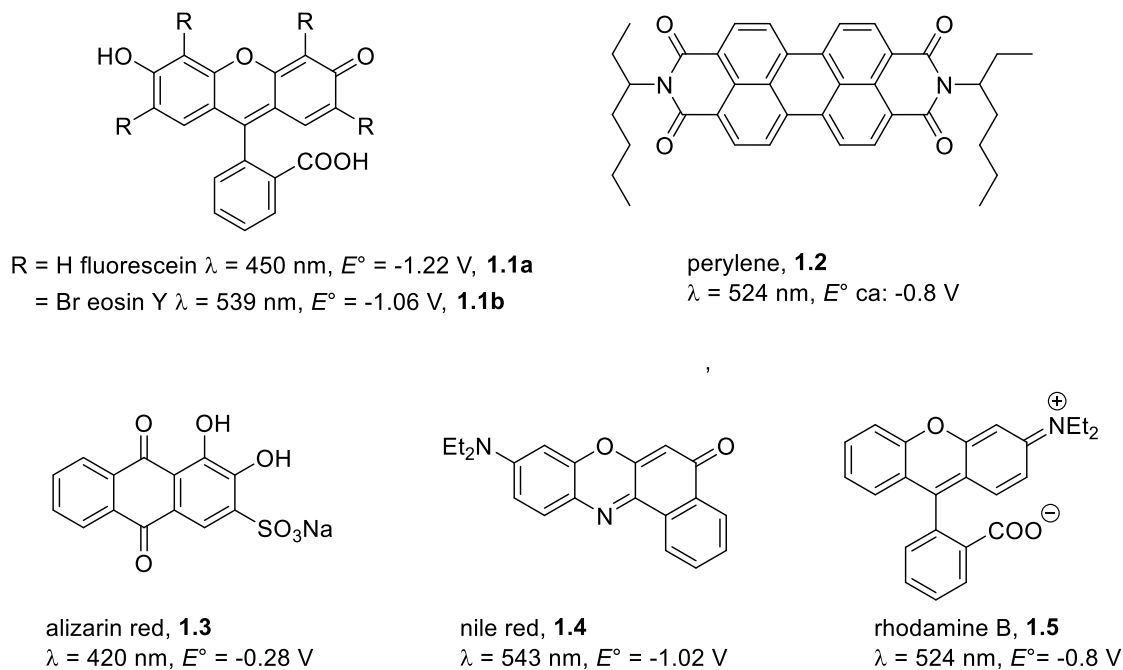
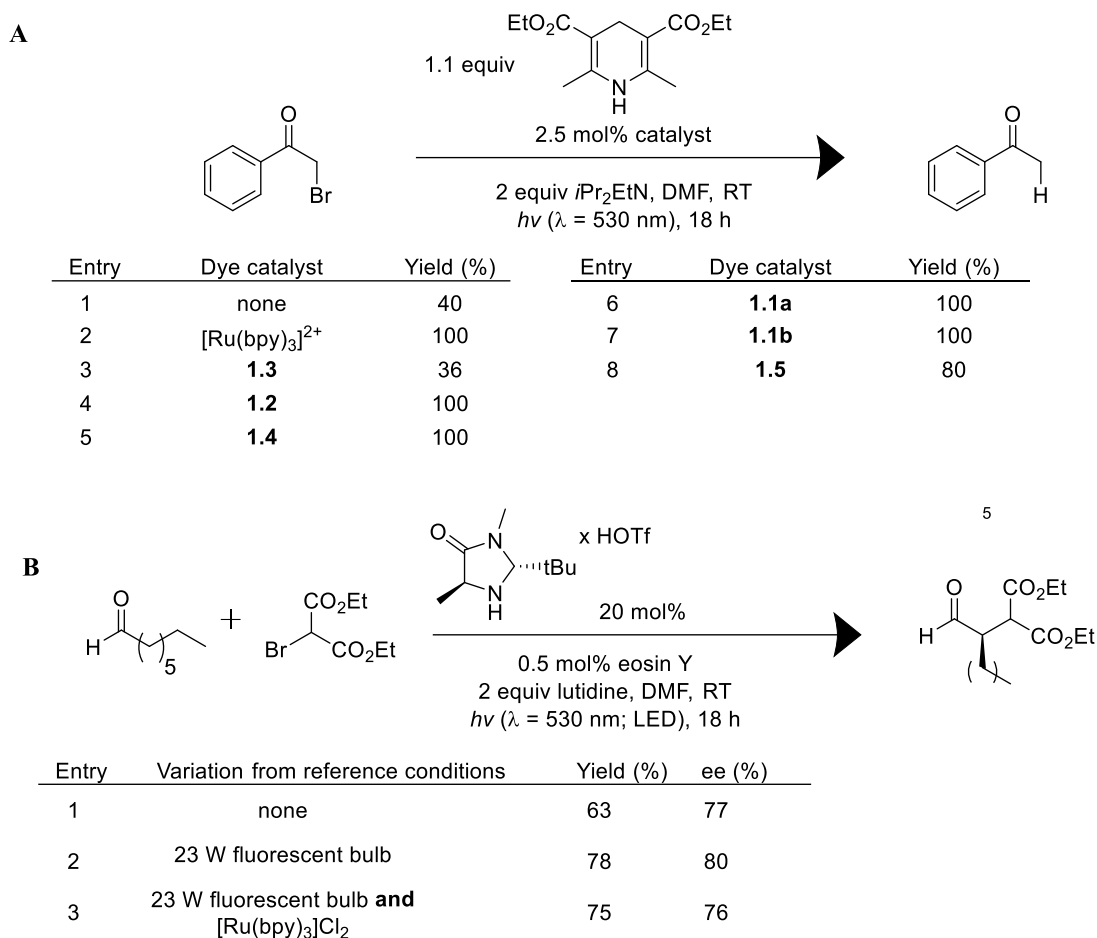


**Figure 1.4** Organic dyes investigated by Zeitler group.

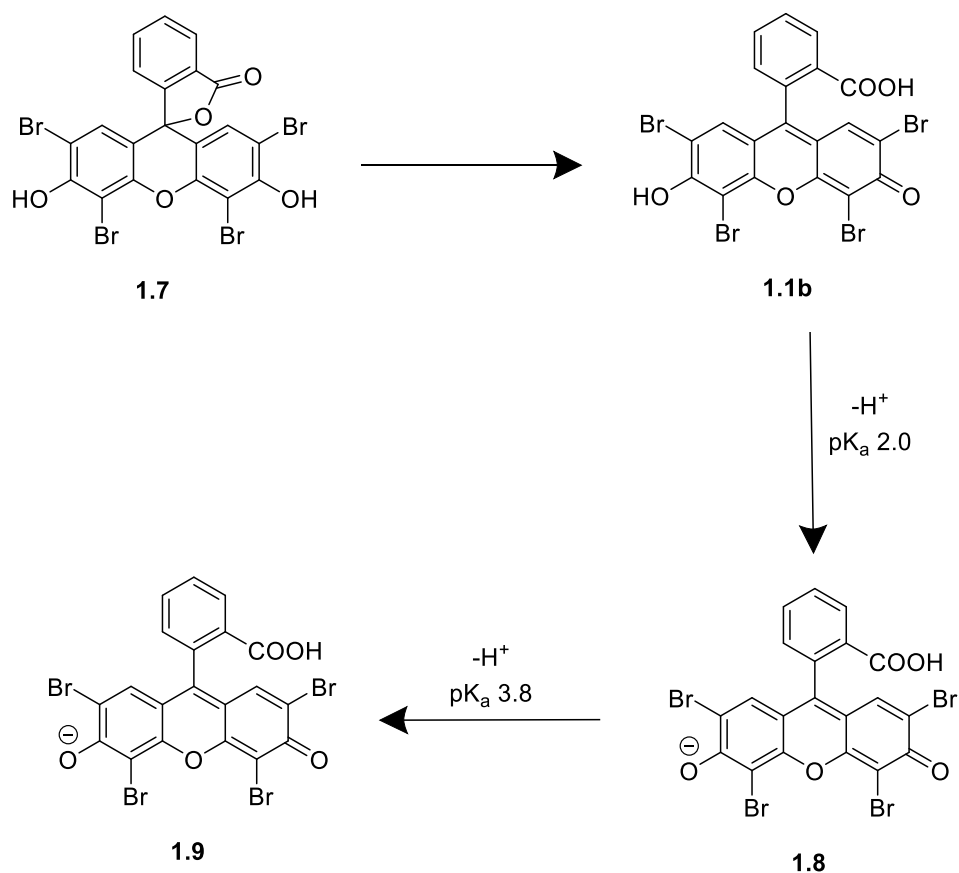


**Scheme 1.1** Model reactions to test eosin Y as organophotocatalyst. **A.** Photoredox dehalogenation reaction. **B.** Asymmetric  $\alpha$ -alkylation reaction.

analyze each dye's potential for photoredox processes (Scheme 1.1A).<sup>4,22</sup> They saw most dyes were successful in achieving full conversion under a variety of light sources, but noticed the brominated derivative of eosin Y provided very clean product and suffered minimum photo-bleaching (when photo-induced damage occurs that prevents fluorescence) when using higher powered LEDs.<sup>22</sup> They also analyzed eosin Y's performance in MacMillan's asymmetric  $\alpha$ -alkylation reaction to test its ability to produce enantioselective products (Scheme 1.1B).<sup>2,22</sup> They saw comparable conversion and selectivities to MacMillan's use of Ru(bpy)<sub>3</sub><sup>2+</sup>, and concluded eosin Y is similar to ruthenium-based catalysts where both serve as electron acceptors. The success of this

catalyst has provided more sustainable methods for organic transformations and lead to an upsurge of eosin Y derivatives to continue enhancing and developing its photochemical and photophysical properties for more diverse applications.<sup>28,29</sup>

Eosin Y derivatives have been employed in various reactions, including reductions,<sup>23</sup> oxidations,<sup>24</sup> brominations,<sup>25</sup> and arylation reactions,<sup>26</sup> just to name a few. While eosin Y and its derivatives seem to be a great solution to replace metal photocatalysts, there are limitations that prevent it from being a truly universal catalyst. One is the dependence on pH and solvent, preferring solutions with pH > 4.<sup>27,28</sup> Scheme 1.2 depicts the acid-base behavior eosin Y can undergo, where the deprotonated forms (**1.8**



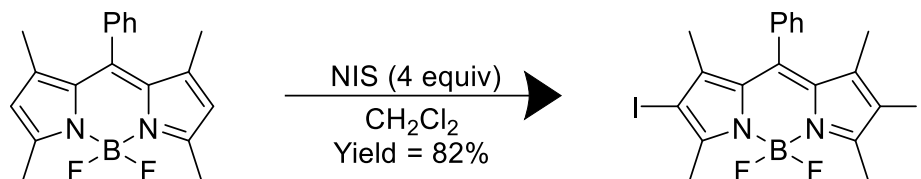
**Scheme 1.2** Tautomerization equilibrium of eosin Y.

and **1.9**) are catalytically active.<sup>27,28</sup> The closed form **1.7** tautomer does not absorb visible light because the closed form (also known as spirocyclic) interrupts the conjugation of the ring system and **1.1b** has weak absorbance of visible light. Because of this sensitivity to pH, the literature agrees that more basic organic solvents, such as DMSO, show better performance with eosin Y compared to other solvents such as acetonitrile unless base is added to the reaction.<sup>28</sup> Also, since eosin Y is a salt in its active form, it does not tolerate nonpolar solvents and has issues with solubility in reactions. Even derivatives of eosin Y, including addition of organic moieties in place of the core bromines to increase its solubility in organic solvents, have limited success.<sup>29</sup> Therefore, photocatalysts that are more tolerant to different environmental conditions are needed to address these limitations of eosin Y.

### **1.2.2 BODIPY-based photocatalysts**

BODIPY (boron-dipyrromethene)-based photocatalysts have also attracted much attention for photocatalysis due to their easily tunable photophysical and photochemical properties through derivatization, strong absorption of visible light, and good photostability.<sup>21,30</sup> Additionally, BODIPY derivatives are more tolerable to pH and temperature changes and modifications to the boron can enhance the chemical stability of these structures, which addresses concerns seen with eosin Y derivatives discussed previously.<sup>31,32,33</sup> The structural modifications that BODIPY can undergo to enhance its photochemical and electrochemical properties has made these structures favorable for

photocatalysis. For example, the addition of two iodine atoms to the BODIPY core (Scheme 1.3), greatly enhances the triplet state lifetime to over 57  $\mu\text{s}$  whereas its unsubstituted core has a feeble triplet state lifetime of 0.02  $\mu\text{s}$ .<sup>34,35,36</sup> This is very impressive considering photocatalyst  $\text{Ru}(\text{bpy})_3\text{Cl}_2$  has a reported triplet state lifetime of only 1.1  $\mu\text{s}$ .<sup>37</sup>



**Scheme 1.3** Synthesis of iodo-BODIPY derivative.

The length of a triplet state lifetime can be very valuable for photocatalysis. As mentioned above, the triplet state is an excited state produced from the excitation of a photocatalyst, through the absorption of light, and is what actively participates in the electron or energy transfer in photocatalytic cycles.<sup>2,10</sup> The extended triplet state lifetime is due to the heavy atom effect (in this case iodine), which is well-known to promote intersystem crossing and extend triplet state lifetimes, allowing more time for the excited species to react.<sup>38</sup> In 2013, Huang and Zhao utilized this iodo-derivatized BODIPY catalyst to undergo photoredox processes and saw the catalyst was able to act as both an electron donor and electron acceptor in three separate photoredox reactions.<sup>39</sup> Traditionally, BODIPY derivatives primarily act as photooxidants (electron acceptors) and have limited applications in acting as electron donors.<sup>21</sup> While the dual capability of this catalyst was significant, the iodo-BODIPY catalyst also outperformed favored  $\text{Ru}(\text{bpy})_3\text{Cl}_2$ ,  $\text{Ir}(\text{ppy})_3$ , and eosin Y catalysts, becoming a formidable organic photocatalyst.<sup>39</sup> However, despite these advantages, the iodo-BODIPY derivative also experience limitations. While the iodine atom increases the triplet state lifetime due to the heavy atom effect, halogenation on the BODIPY core

decreases the reduction values to less negative potentials, limiting its ability to interact with diverse substrates.<sup>40</sup> More recently, several groups have employed metal complexes with BODIPY derivatives to further enhance its triplet state lifetime and retain favorable electrochemistry, generating dual catalysis systems.<sup>21,41,42,43,44</sup> While this can improve catalyst performance, whether that be through increased product yields or further manipulation of the heavy atom effect to enhance triplet lifetimes, this technique also counteracts the goal of reducing the use of metal-based catalysts, specially complexes containing ruthenium and iridium.<sup>42</sup> It would be beneficial to generate photocatalysts where tuning the structure would enhance the catalyst properties instead of adding additional catalysts, further complicating the reaction cycle.

### 1.3 Silicon Phthalocyanines

To address the limitations mentioned above with commonly used photocatalysts, we proposed silicon phthalocyanines (Figure 1.5) as a viable option for organophotocatalysis. Commonly used in dyes and pigments,<sup>45</sup> silicon phthalocyanines have the desired properties, such as structural tunability for solubility,<sup>45</sup> visible light

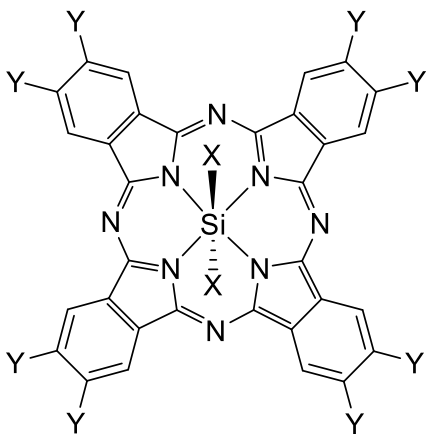


**Figure 1.5** Silicon phthalocyanine structure



absorption ( $\sim 700$  nm),<sup>46</sup> and are organic based. The structural tunability of these compounds, specifically the ability to substitute any ligand in the axial (denoted as X in Figure 1.5) and peripheral (denoted as Y in Figure 1.5) positions allow these structures to have limitless potential in any field. Cancer phototherapy,<sup>47</sup> organic photovoltaic devices,<sup>48</sup> supramolecular organic thin films,<sup>49</sup> solar cells,<sup>50</sup> and polymer chemistry<sup>51</sup> are just a few fields silicon phthalocyanines have been utilized in. The axial ligands influence the solubility in two ways. The axial position to the phthalocyanine ring allows the ligands to disrupt any  $\pi$ - $\pi$  stacking that can occur between the planar phthalocyanine molecules, increasing the solubility of these structures. Since potentially any type of ligand can be put in the axial position, the polarity of the ligands can be modified for these structures to be soluble in different types of solvent systems, whether that be organic or aqueous.<sup>46</sup> Therefore, these structures are valuable for organic photocatalysis because they are not limited to polar or nonpolar solvents, rather the structures can be tuned for any reaction system required.

Substitution in the axial position as well as the peripheral positions can also impact the redox properties of these structures.<sup>52</sup> A majority of the literature on the electronic properties of these structures focuses on the application of photovoltaic devices with limited data utilizing these compounds in photoredox processes in organic systems.<sup>46</sup> These studies have mostly centered around solar energy conversion and homogeneous photocatalysis.<sup>46</sup> The consensus of these studies appear to agree that the sterics of the axial ligands have little influence on the electrochemical potentials but did influence the solubility of the structures which lead to increased device performance.<sup>53</sup> Reports of incorporating electron-withdrawing groups on the axial positions have impacted the

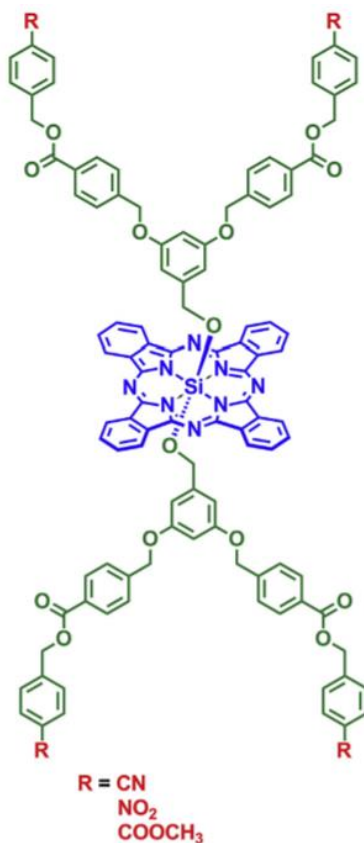


**Figure 1.1.6** Structure of derivatized silicon phthalocyanine dendrimer.

electron donating and accepting properties of these structures with improved device performance reported.<sup>54</sup> However, one study by Yang and Peng investigated electrochemical behaviors of silicon phthalocyanines with aryl benzyl ether dendrimer ligands containing nitro, cyano, or ether terminal groups on the axial positions using cyclic voltammetry (Figure 1.6).<sup>55</sup> While high negative reduction potentials were seen for the derivatives, producing structures that require higher energy to reduce, little difference was seen between the redox values for the different axial ligands.<sup>55</sup> This conflicts with the idea that electron-withdrawing groups improve the electron transfer process as stated in literature with photovoltaic devices. Therefore, further research is needed to better

understand how the axial and peripheral ligands participate in the stabilization of electrochemical processes for silicon phthalocyanines.

In addition to ligand substitution, the use of silicon phthalocyanines as second generation photosensitizers in photodynamic therapy (PDT) also makes these structures attractive for photocatalysis.<sup>56,57</sup> In a PDT process, when light irradiates on a photosensitizer, or photocatalyst in context with this dissertation, a photon is absorbed and excites the molecule from its ground state to its excited singlet state, undergoing intersystem crossing to the triplet state.<sup>56</sup> Once in the triplet state, two accepted processes can occur to initiate PDT: an energy or electron transfer with molecular oxygen to produce highly reactive singlet oxygen or superoxide anions, respectively, which initiate cell death.<sup>56</sup> This process is nearly identical to photocatalytic cycles where an excited photocatalyst in its triplet state transfers energy or an electron to a substrate during the reaction sequence (Figure 1.1). Therefore, since phthalocyanines are already used in the generation of reactive species in PDT, we assume that they can also be used in photocatalytic reactions.

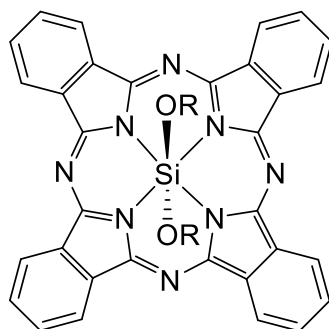
One last application of silicon phthalocyanines is their ability to generate hydrogen from water splitting for an alternate energy carrier.<sup>58,59</sup> Lu and coworkers developed a system that covalently linked a silicon phthalocyanine structure with a phenyl group linking it to graphene with Pt nanoparticles loaded on the graphene sheets as a cocatalyst.<sup>59</sup> In this system, the silicon phthalocyanine is excited with visible light, referred to as light harvesting, and accepts an electron from the sacrificial donor triethanolamine. This electron is then transferred to the graphene. The Pt cocatalyst then “traps” the electron and facilitates proton reduction to afford hydrogen.<sup>60</sup> This system had poor performance due to  $\pi$ - $\pi$

stacking aggregation between hydrophobic graphene and the silicon phthalocyanine phenyl structures. To address the aggregation they added surfactants, which are known to prevent aggregation. The graphene interacts with the surfactant through either ionic or  $\pi$ - $\pi$  interactions which helps distribute the graphene in different solvents and disrupts the intermolecular interactions that cause aggregation.<sup>61,62</sup> Once the surfactants were added to the system, more than double the amount of hydrogen was produced versus without the surfactant. Additionally, the amount of hydrogen produced was four times higher than normal graphene. It was concluded that the strong absorbance of silicon phthalocyanines was responsible for the increase in performance and efficient charge transfer to the graphene. The Pt further enhanced the hydrogen production because it lowers the electrochemical proton reduction overpotential for water splitting and is able to collect the photoexcited electrons from the graphene to generate hydrogen.<sup>59</sup> Several other systems have utilized silicon phthalocyanine/graphene combinations for hydrogen generation because of the optimal absorption properties and efficient electron transfer. Therefore, we believe these structures could also be extended to organic photocatalysts for photoredox processes.

## 1.4 Conclusions

Silicon phthalocyanines show great promise as photocatalysts for both electron and energy transfer reactions. Their absorption of visible light, structural tunability and ability to participate in PDT processes are desired traits for visible light photocatalysis in organic reactions. While the literature reports redox potentials for these structures, limited research is available on using them as photocatalysts in organic synthesis.<sup>46</sup> In chapter 2, three silicon phthalocyanines (**1.1**, **1.2**, and **1.3** in Figure 1.7) with pentoxy, trihexylsilyloxy, and

triphenylsilyloxy groups for axial ligands will be investigated. The electrochemical profile for each compound was measured to determine its redox potentials and how stable these



**1.1** R = —O(CH<sub>2</sub>)<sub>4</sub>CH<sub>3</sub>

**1.2** R = —OSi((CH<sub>2</sub>)<sub>5</sub>CH<sub>3</sub>)<sub>3</sub>

**1.3** R = —OSiPh<sub>3</sub>

**Figure 1.1.7** Proposed silicon phthalocyanine structures.

compounds are for electron transfer processes, ideally for photoredox reactions. Fluorescence quenching studies analyzed how efficiently each catalyst transfers electrons with increasing concentration of a known fluorescence quencher. Finally, the performance of each catalyst in a photoredox reaction, specifically a reductive quenching reaction where the catalyst donates an electron, and energy transfer reaction is discussed.

## CHAPTER 2

### SILICON PHTHALOCYANINES AS PHOTOCATALYSTS

#### 2.1 Introduction

With relevance to cancer therapy,<sup>63</sup> biomedical applications,<sup>64,65</sup> and waste water treatment,<sup>66</sup> photocatalysis has proven to be a powerful, versatile tool. Within the last fifteen years, synthetic chemists have increasingly employed photocatalysis, specifically using visible-light, for unique organic transformations, including photo-cycloadditions and C-H bond activations, just to name two.<sup>67,68,69,70,71</sup> Photocatalysts provide mild, sustainable pathways for reactions to occur by producing excited species that achieve intricate molecular transformations not always possible by established protocols or traditional reagents. For example, selective activation of vinyl halides to generate alkyl radicals has been a key goal in modern organic synthesis but has been difficult to achieve due to high reduction potentials.<sup>72</sup> However, common photocatalysts afford reduction potentials complementary to vinyl halides and allow new C-C bond forming routes under mild reaction conditions.<sup>73</sup>

Many photocatalytic reactions are promoted by ruthenium- and iridium-based catalysts<sup>70,74</sup> because of their long-lived triplet state lifetimes and large redox properties; however, a push towards reducing the use of these precious metals has led to a growing interest in organic photocatalysts<sup>75,76,77</sup>, such as Eosin Y<sup>78,79,80,81</sup> and derivatives,<sup>82</sup> BODIPY derivatives<sup>83</sup>, acridinium salts<sup>84,85</sup>, Rose Bengal,<sup>86</sup> and some newer amine

heterocycles<sup>87,88,89,90</sup> just to name a few. Despite the rapid growth of organic photocatalysts there are still limitations that need to be overcome. For example, many of the organic photocatalysts are salts, therefore they have limited solubility in non-polar organic solvents. Additionally, there is a need to develop highly reducing catalysts that are competitive with ruthenium and iridium photocatalysts.<sup>75</sup> The focus of this study is to develop two axially-substituted silicon phthalocyanine organocatalysts that are soluble in a wide range of organic solvents and are competitive with ruthenium- and iridium-based photocatalysts. Silicon phthalocyanines are neutral compounds, where the substituents in the axial positions can alter their solubility, stability, and photophysical and photochemical properties. We found our silicon phthalocyanines are soluble in a range of solvents and possess redox potentials competitive with existing organic photocatalysis. These catalysts were successfully employed in an energy transfer reaction and redox reaction where the silicon phthalocyanines were competitive or out-performed the original organic photocatalysts under similar conditions.

Silicon phthalocyanines are porphyrin-based structures with phenyl rings fused on the porphyrin core and this class of compounds has great potential as visible-light mediated photocatalysts due to their ability to absorb long wavelengths and their high structural tunability.<sup>91</sup> The extended conjugation of these molecules allows for long wavelength absorption, usually varying in the red region (600-800 nm range).<sup>92,93</sup> The energy absorbed promotes the compound into an excited state, which allows for one of two processes: energy transfer or electron transfer, the two most common pathways for photocatalysis to occur. Most commonly, silicon phthalocyanines are known to participate in an energy transfer process when activated by light as shown by their use in photodynamic therapy.<sup>94</sup>

When the excited molecule interacts with molecular oxygen, energy is transferred to produce highly reactive singlet oxygen, which reacts with cancer cells and initiates cell death.<sup>95,96</sup> While redox values for silicon phthalocyanines have been reported and are conducive for photoredox reactions,<sup>97,98,99</sup> there are limited examples of their use in these reactions,<sup>100,101</sup> i.e. the direct electron transfer from the photocatalyst to the substrate or a secondary catalyst to perform the desired catalytic reaction.<sup>102</sup> It is known that the photophysical and photochemical properties of silicon phthalocyanines can be modulated by substituting the compounds in various positions,<sup>103</sup> but there is a lack of data showing how these changes affect electron transfer efficiency and stability/reversibility of electron transfer in organic reactions. Our research focused on variations in substitution in the axial position (R on **1.1**, **1.2**, and **1.3**) and employing these catalysts in electron and energy transfer processes. The work herein analyzes how axially-substituting silicon phthalocyanines with pentyl (**1.1**), trihexylsilyl (**1.2**), and triphenylsilyl (**1.3**) groups on the silicon center influence the redox stability and the photophysical and photochemical properties of the silicon phthalocyanines (Figure 2.1). The ability of the catalysts to

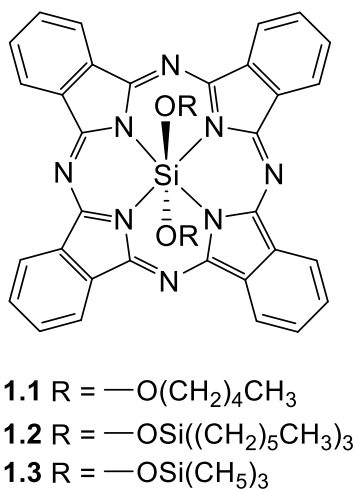


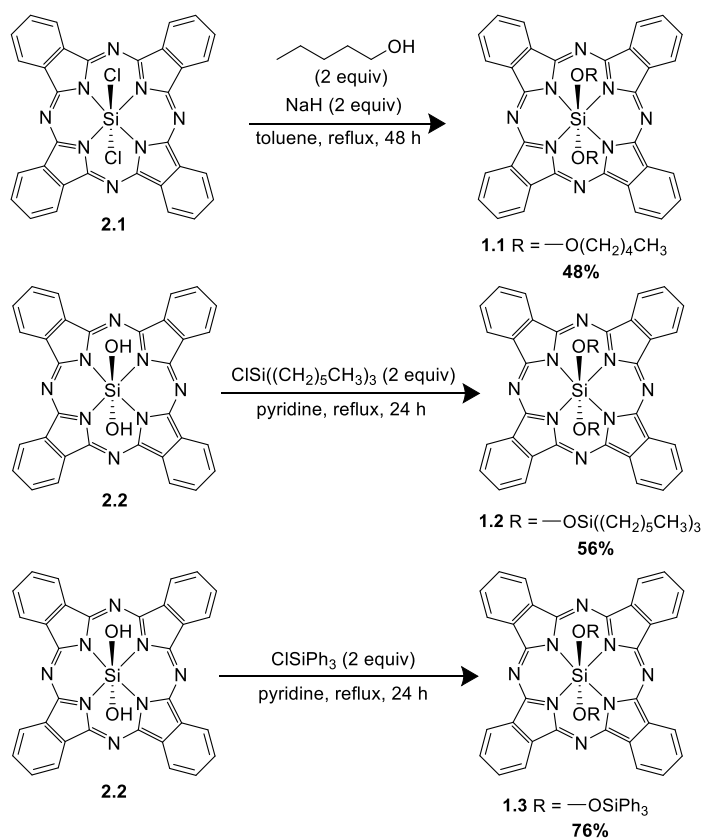
**Figure 2.1** Silicon phthalocyanine derivatives.



promote two reactions were investigated: (1) an energy transfer cycloaddition reaction involving singlet oxygen and (2) an energy transfer dehalogenation reaction. Additionally, full characterization of the compounds was undertaken, including their electrochemical properties and their stabilities under these conditions.

## 2.2 Synthesis of silicon phthalocyanines

The synthesis and characterization of the silicon phthalocyanine catalysts were undertaken following literature procedures. The synthesis of pentoxy substituted catalyst **1.1** followed the procedure outlined by Chen and coworkers, where deprotonated pentanol displaced two chlorides on the silicon center of silicon phthalocyanine dichloride **2.1** with moderate yields (Scheme 2.1).<sup>104</sup> The synthesis of the silyl protected catalyst **1.2** and **1.3**



**Scheme 2.1** Synthetic routes for silicon phthalocyanine catalysts **1.1-1.3**.

were adapted from Lessard et al. starting with the dihydroxyl silicon phthalocyanine **2.2**.<sup>98</sup> The hydroxyl groups were protected by reacting them with trihexylsilyl chloride to obtain **1.2** in moderate yields or triphenylsilyl chloride to obtain **1.3** in higher yields with one step (Scheme 2.1). Regarding **1.3**, issues with purification resulted in limited characterization of the compound and no reactivity was collected for this catalyst.

## 2.3 Photophysical and photochemical properties of silicon phthalocyanines

The absorption and emission profiles for **1.1** and **1.2** were collected and are shown in Figure 2.2. The absorbance spectra for silicon phthalocyanines commonly report distinctive Q band and Soret bands around 670-680 nm and 350 nm, respectively.<sup>109,105</sup>

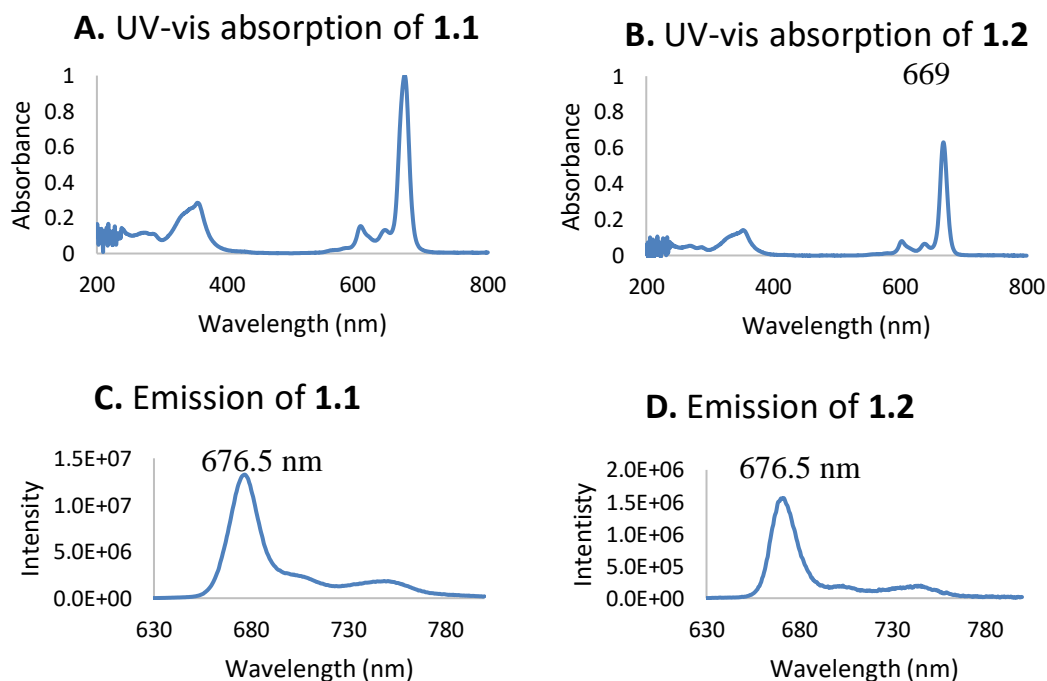


**Figure 2.2** **A.** UV-vis absorption spectrum of **1.1** in  $\text{CHCl}_3$  at 0.005 mM. **B.** UV-vis absorption spectrum of **1.2** in  $\text{CHCl}_3$  at 0.002 mM. **C.** Emission spectrum of **1.1** at 0.8  $\mu\text{M}$  with excitation at 670 nm in  $\text{CHCl}_3$ . **D.** Emission spectrum of **1.2** at 0.3  $\mu\text{M}$  with excitation at 670.

These bands refer to the transitions from the ground to the first excited state (Q band) and from ground state to the second excited state (Soret band).<sup>106</sup> The absorption profiles for both **1.1** and **1.2** in chloroform include a maximum absorption ( $\lambda_{\text{max}}$ ) at 672.5 nm and 669 nm with extinction coefficients ( $\epsilon$ ) of  $1.01 \times 10^5 \text{ M}^{-1}\text{cm}^{-1}$  and  $3.16 \times 10^5 \text{ M}^{-1}\text{cm}^{-1}$ , respectively, and broad peaks around 355 nm and 358 nm, respectively. This fits where the Q bands and Soret bands are reported for silicon phthalocyanines.<sup>104,107</sup> The maximum emission peaks for **1.1** and **1.2** (676.5 nm for both) produce Stokes shifts (difference between maximum absorbance wavelength and maximum fluorescence wavelength) of 4 nm and 7.5 nm, respectively in chloroform. For the emission spectra, the excitation wavelengths used were the absorption maximum wavelengths (672.5 nm for **1.1** and 669 nm for **1.2**) gathered from the absorption profiles. Chloroform was the chosen solvent for all absorption and emission spectra because both catalysts were fully soluble in this system. Despite the alkyl chain of the pentoxo catalyst **1.1**, this catalyst had difficulties dissolving in most nonpolar solvents and some polar solvents, such as acetonitrile to name one. Trihexylsilyl catalyst **1.2** was more soluble in various solvents, including nonpolar solvents, such as hexanes, but also had difficulties with acetonitrile and other polar solvents. We believe catalyst **1.2** was more soluble in nonpolar solvents because of its bulkier, alkyl ligands. It is expected that these nonpolar, branched alkyl groups would easily dissolve in nonpolar solvents, because they aid in disrupting any pi-pi stacking that could occur between phthalocyanine rings. It is possible that the ligand for **1.1** is too small to disrupt these interactions as efficiently as **1.2**. Therefore, since both catalysts readily dissolved in chloroform, all initial characterization utilized chloroform as the solvent.

Voltammetric studies of the pentyl catalyst (**1.1**) and the trihexylsilyl catalyst (**1.2**) were carried out in chloroform with a 0.1 M tetrabutylammonium hexafluorophosphate (TBAPF<sub>6</sub>) electrolyte (Figure 2.3). CV studies have been reported for **1.2** but to the best of our knowledge, **1.1** has not been reported. Based off the literature, we expect **1.1** to display similar responses to **1.2** since most cyclic voltammetry studies on silicon phthalocyanines in the literature show little variation in electrochemical studies.<sup>81,110</sup> Therefore, we expect **1.1** and **1.2** to have one reversible oxidation peak and two reversible reduction peaks.<sup>81,110</sup> Looking at Figure 2.3, **1.1** does have the expected oxidation peak and two reduction peaks. The oxidative peak at  $E_{1/2} = 0.9$  V is quasi-reversible. Quasi-reversible is defined as having

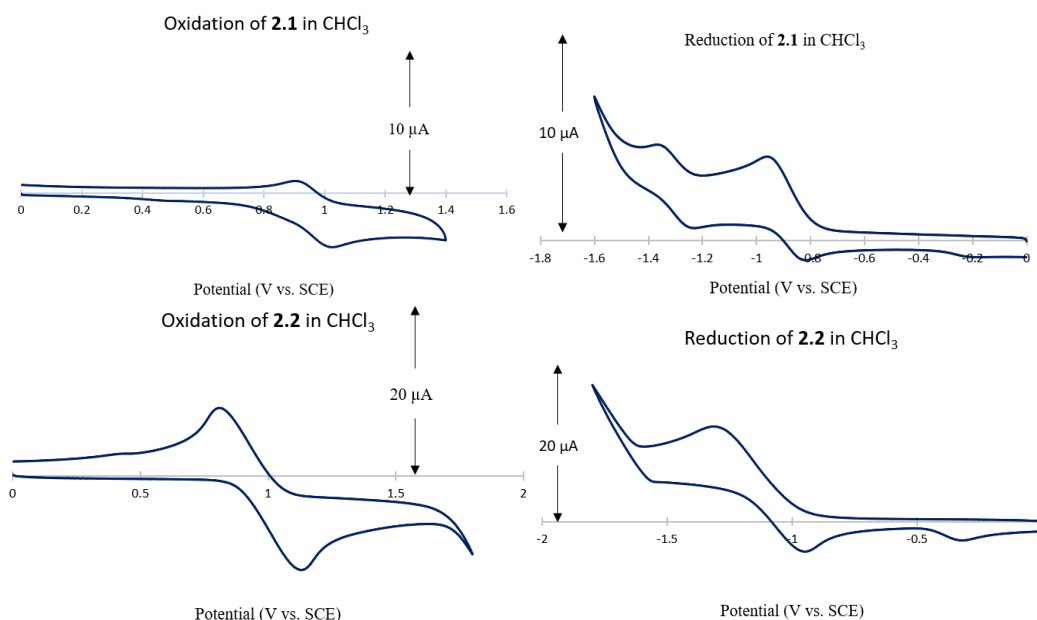


**Figure 2.3** Oxidation and reduction cyclic voltammograms of **1.1** at 1.7 mM and **1.2** at 2 mM at 0.1 V/s in CHCl<sub>3</sub>/ TBAPF<sub>6</sub>.

a cathodic to anodic peak current ( $i_{p,c}/i_{p,a}$ ) at unity, but a peak to peak separation of greater than 100 mV. Multiple scan rates (20, 40, 60, 80, and 100 V/s) were used to analyze the linear dependence of peak current (Figure 2.4). Figure 2.5 shows the linear dependence graphs produced from the scans for **1.1** in chloroform. The oxidative peak of **1.1** did produce a linear correlation (Figure 2.5), indicating the process has reversibility; however,

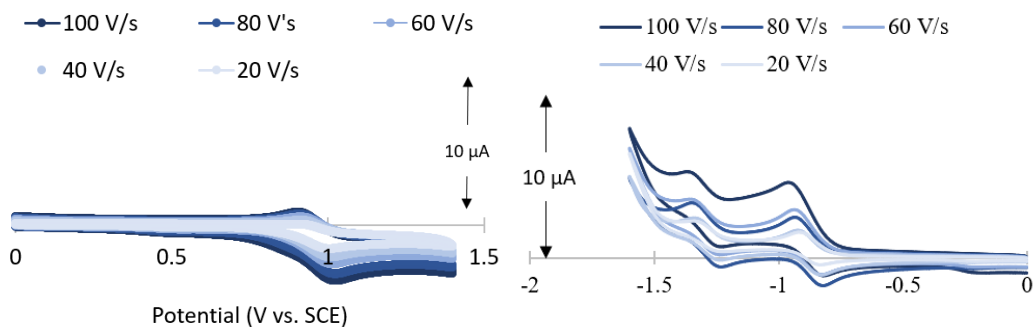


**Figure 2.4** The oxidative (left) and reductive (right) scans of **1.1** at multiple scan rates (100, 80, 60, 40, and 20 V/s in chloroform).

this peak is still quasi-reversible due to how long the time between the structure is oxidized and then reduced back to its neutral state. Catalyst **1.1** showed two reduction peaks  $E = -0.96$  V and  $E = -1.4$  V, both being irreversible due to the lack of linear correlation in their linear dependence graphs (Figure 2.5).

Interestingly, compared to **1.1** and the reported literature, **1.2** in chloroform is missing the second reduction wave the literature reports.<sup>81,110</sup> One explanation for this could be the solvent system. In the literature the CV studies of **1.2** was conducted in dichloromethane and DMSO.<sup>81,110</sup> It is possible that the radical produced in the first reduction is not stable enough in chloroform to allow the second reduction to occur. This is unexpected since we predicted the bulky trihexyl branches of **1.2** to stabilize the

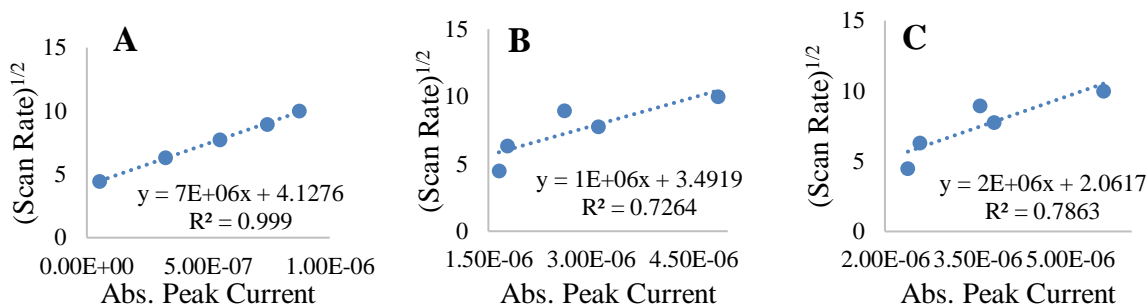


**Figure 2.5** Linear dependence of peak current for **1.1** in chloroform. A) Oxidative Peak. B) First Reductive Peak. C) Second Reductive Peak.

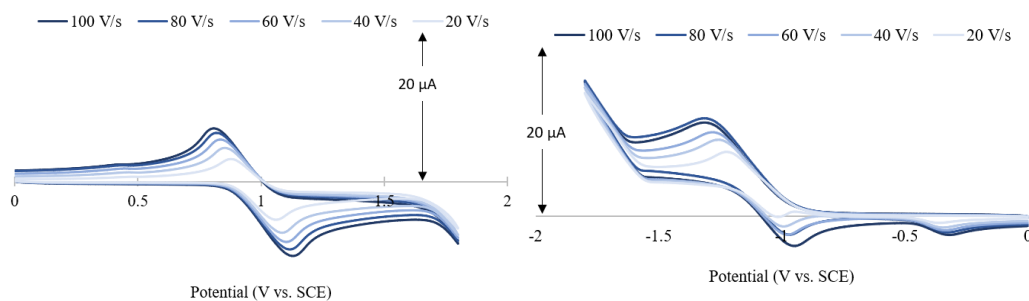


**Figure 2.6** The oxidative (left) and reductive (right) scans of **1.2** at multiple scan rates (100, 80, 60, 40, and 20 V/s in chloroform.

complex. Multiple scan rates (20, 40, 60, 80, and 100 V/s) were used to analyze the linear dependence of peak current (Figure 2.6). Both oxidative (0.81 V) and reductive (-1.3 V) peaks are irreversible due to the lack of linearity from the data points with some data points stacking in one area of the linear dependence graphs (Figure 2.7). Regardless, we repeated

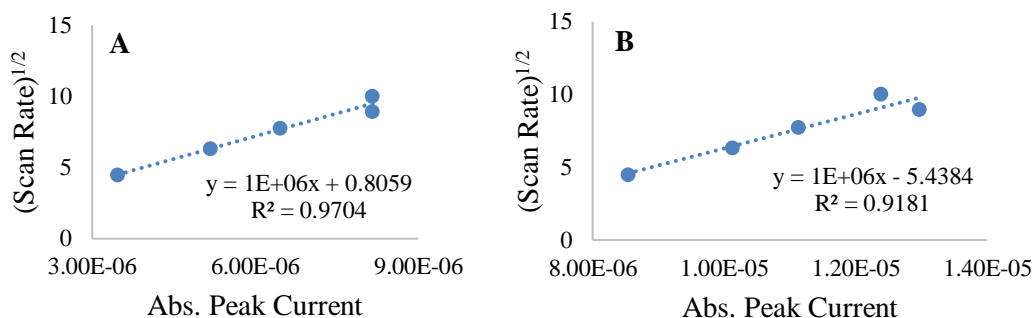


**Figure 2.7** Linear dependence of peak current for **1.2** in chloroform. A) Oxidative Peak. B) Reductive Peak.

the CVs of **1.1** and **1.2** in dichloromethane to reproduce the conditions of the literature.<sup>81,110</sup>

Figure 2.8 shows the new scans for **1.1**, **1.2**, and **1.3** in dichloromethane, and we do see the second reductive wave for **1.2**. Catalyst **1.3** also show redox properties reported in literature when using dichloromethane.<sup>81,110</sup>

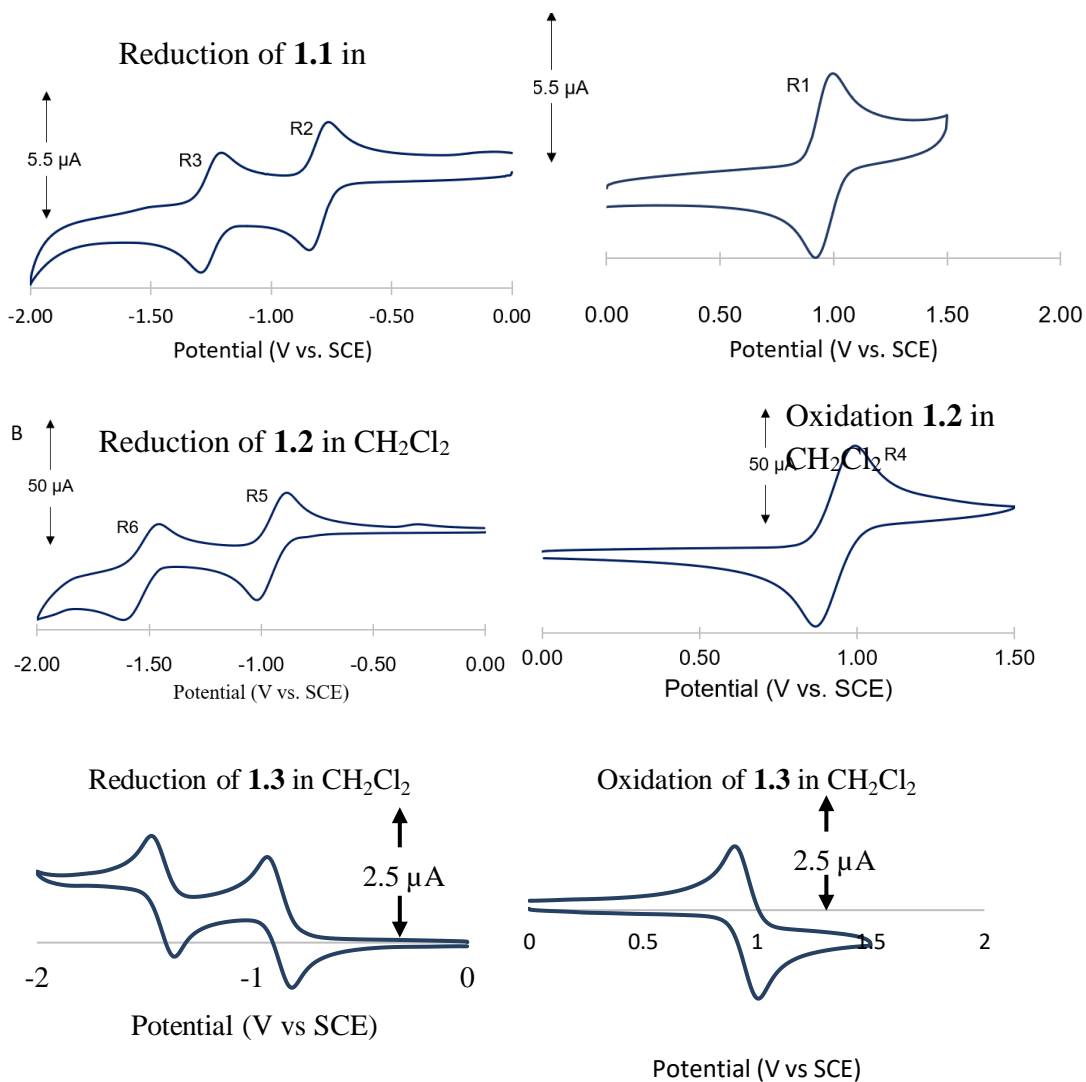


**Figure 2.8** Oxidation and reduction cyclic voltammeteries of **1.1** at 1.7 mM, **1.2** at 2 mM, and **1.3** at 1 mM at 0.1 Vs-1 in  $\text{CH}_2\text{Cl}_2$ /  $\text{TBAPF}_6$ .

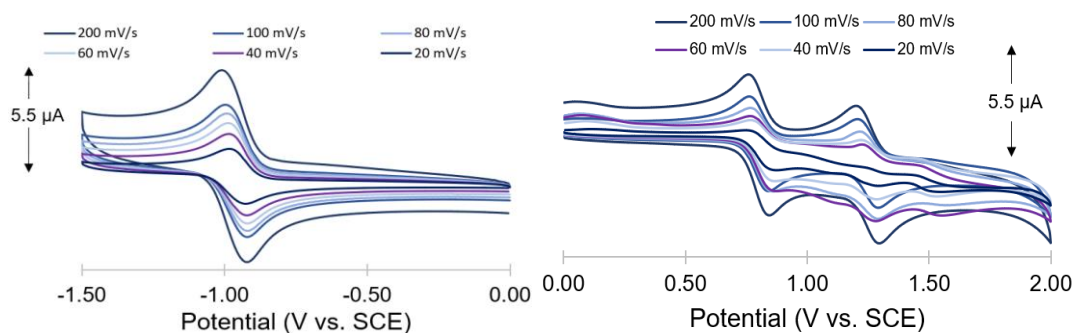


**Figure 2.9** The oxidative (left) and reductive (right) scans of **1.1** at multiple scan rates (100, 80, 60, 40, and 20 V/s in dichloromethane).

Silicon phthalocyanine **1.1** exhibited one quasi-reversible oxidation process at  $E_{1/2} = 0.95$  V, labeled as  $R_1$ . Figure 2.9 shows the multiple scan rates overlapped for the oxidation for **1.1** and Figure 2.10 shows the linear dependence graphs produced from the scans. The oxidative peak of **1.1** did produce a linear correlation (Figure 2.10), indicating the process has reversibility; however, this peak is still quasi-reversible due to how long the time between the structure is oxidized and then reduced back to its neutral state. For the reductive scan, **1.1** exhibited two primarily irreversible reduction processes labeled as

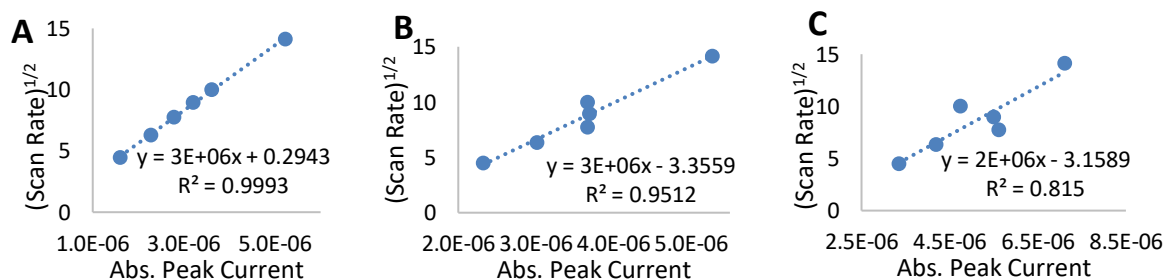


**Figure 2.10** Linear dependence of peak current for **1.1**. A) Oxidative Peak. B) First Reductive Peak. C) Second Reductive Peak.

$R_2$  ( $E = -0.8$  V) and  $R_3$  ( $E = -1.2$  V). As shown below in Figure 2.6, both reduction waves for **1.1** do not follow the predicted linear dependence of peak current ( $i_p$ ) on the square root of scan rate ( $v^{1/2}$ ) that occurs for reversible redox processes due to both having low  $R^2$



values and a lack of linear correlation. This absence of electrochemical reversibility of **1.1** indicates a deficiency of chemical stability upon reduction and is consistent with previous reports that show these class of silicon phthalocyanines complexes require extremely bulky axial groups to exhibit chemical stability.<sup>108,109</sup>

Compound **1.2** does contain two, bulky trihexylsilyl groups into the axial position, which we predicted would better stabilize the structure for redox processes. The CVs of **1.2** show both a quasi-reversible oxidation ( $R_4$ ,  $E_{1/2} = 0.95$  V) and a fully reversible first

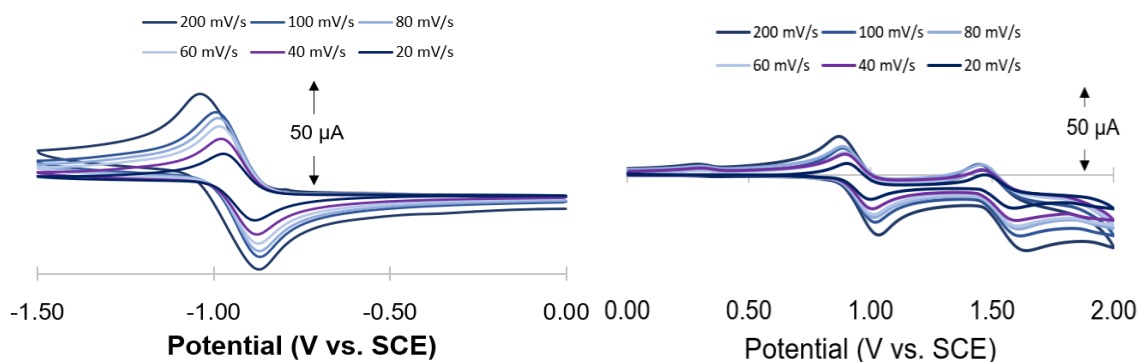


**Figure 2.11** Oxidation (left) and reduction (right) overlaps of multiple scan rates for **1.2** in dichloromethane.

reduction ( $R_5$ ,  $E_{1/2} = -0.93$  V) followed by a quasi-reversible second reduction ( $R_6$ ,  $E_{1/2} = -1.5$  V) (Figure 2.12). The multiple scan rates (100, 80, 60, 40, and 20 V/s) overlap (Figure 2.11) and linear dependence graphs (Figure 2.12) for **1.2** are shown. With significant  $R^2$

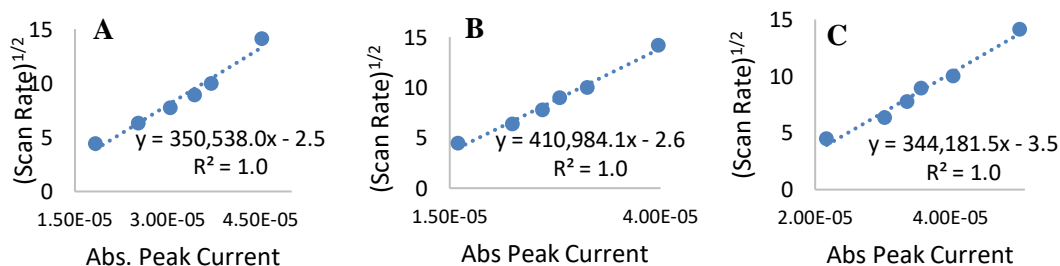


**Figure 2.12** Linear dependence of peak current for **1.2** in dichloromethane. A) Oxidative Peak. B) First Reductive Peak. C) Second Reductive Peak.

values closer to one and cathodic/anodic peak separations less than 100 mV, the CVs thus show that compound **1.2** is more stable towards one oxidative and two reductive processes, and this stability can likely be attributed to the bulkier axial groups when compared to **1.1**.

Compound **1.3** also contains two large, bulky ligands, so we expected to see similar reversibility as we did with **1.2**. The CVs for **1.3** in Figure 2.4 resemble **1.2** in that it has one oxidative peak and two reductive peaks. Figure 2.13 shows the multiple rates overlaps (100, 80, 60, and 40 V/s) and the linear dependence for each peak is in Figure 2.14. The oxidative peak showed linear dependence, indicating it is quasi-reversible in combination with the difference between its cathodic and anodic peaks ( $E_{1/2} = 0.89$  V), one irreversible reduction peak ( $E_{1/2} = -0.94$  V), and one quasi-reversible reduction peak ( $E_{1/2} = -1.47$  V).

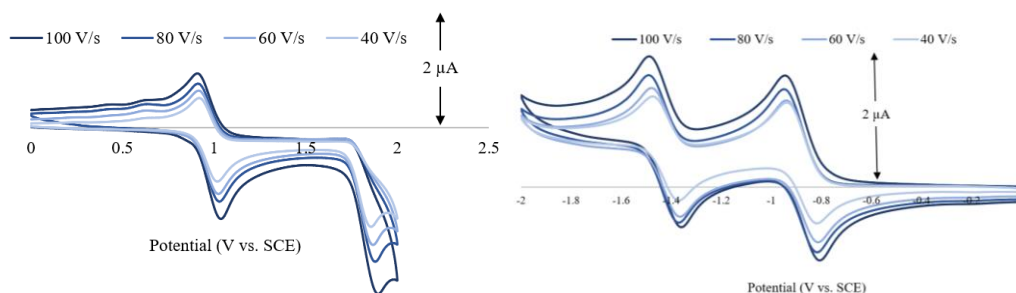


**Figure 2.13** Oxidation (left) and reduction (right) scans of multiple rates (100, 80, 60, and 40 V/s) overlap for **1.3** in dichloromethane.

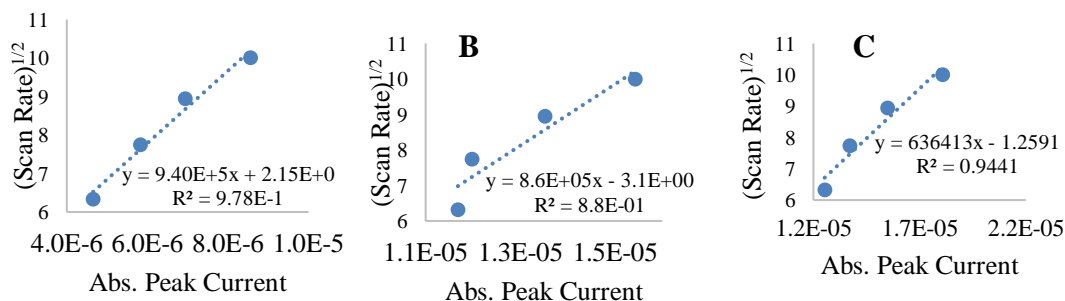


**Figure 2.14** Linear dependence of peak current for **1.3** in dichloromethane. A) Oxidative Peak. B) First Reductive Peak. C) Second Reductive Peak.

Stability of compounds while undergoing one-electron redox processes is an important attribute of photoredox catalysts. It is also worth noting that the electrochemistry reported here for **1.2** and **1.3** in CH<sub>2</sub>Cl<sub>2</sub> is consistent with previously reported data on **1.2** and **1.3**.<sup>110</sup>

Since photochemistry primarily occurs in the triplet state of silicon phthalocyanines, the excited state redox potentials were calculated to accurately depict the

$$E_{red}^* (\text{cat}^*/\text{cat}^{\bullet-}) = E_{red} (\text{cat}/\text{cat}^{\bullet-}) + E_{0,0} \quad \text{Equation 2.1}$$

$$E_{ox}^* (\text{cat}^{\bullet+}/\text{cat}^*) = E_{ox} (\text{cat}^{\bullet+}/\text{cat}) - E_{0,0} \quad \text{Equation 2.2}$$

redox potentials used for catalysis. Therefore equations 2.1 and 2.2<sup>Error! Bookmark not defined.</sup> were used to find the excited state potentials where  $E_{red}^*$  depicts the excited state reduction potential and  $E_{ox}^*$  is the excited state oxidation potential. Absorption and emission profiles

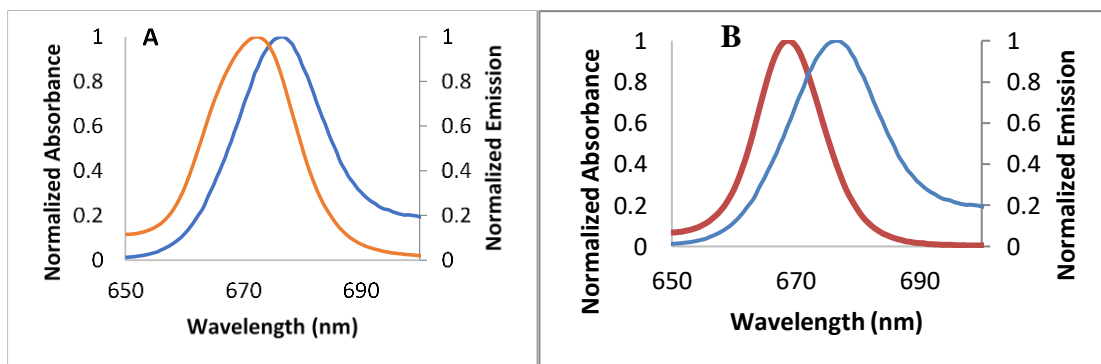


**Figure 2.15** A. Normalized absorbance and emission overlaps of **1.1**. B. Normalized absorbance and emission overlaps of **1.2**. Emission excitation was at 675 nm.

were measured for **1.1** and **1.2** and used to find the excitation energy  $E_{0,0}$  for each by finding the intersecting wavelength of the normalized absorption and fluorescence profiles (Figure 2.15). Table 2.1 includes the excited state potentials of our catalysts and Eosin Y for comparison.<sup>111</sup> Compared to Eosin Y, our silicon phthalocyanines have lower excited

oxidation potentials, limiting the substrates it can oxidize, but a larger range of excited reduction potentials for various substrates when considering all reduction potentials.

The ability of photocatalysts **1.1**, **1.2**, and **1.3** to be reductively quenched by

**Table 2.1** Ground state and excited state redox potentials of photocatalysts.

	$E_{1/2}^{OX}$ (V)	$E_{1/2}^{RED}$ (V)	$E_{ox}^*$ (CAT <sup>•+</sup> /CAT*) (V)	$E_{red}^*$ (CAT*/CAT <sup>•-</sup> ) (V)
<b>1.1</b>	0.95	-0.8, -1.2	-0.89	1.04, 0.64
<b>1.2</b>	0.95	-0.93, -1.5	-0.895	0.915, 0.345
<b>EOSIN Y</b>	0.78	-1.06	-1.11	0.83

increasing amounts (0-0.5 M) of Hünig's base, a commonly used sacrificial electron donor, was then explored with fluorescence quenching in CHCl<sub>3</sub> and a Stern-Volmer analysis to determine if they could efficiently transfer an electron (Figure 2.16a and Figure 2.17b). Figure 2.17a and Figure 2.17b compares the quenching of **1.1**, **1.2**, and **1.3** by Hünig's base where the linear correlation is indicative of effective electron transfer from Hünig's base to the excited-state pentyl **1.1**, trihexylsilyl **1.2**, and triphenylsilyl **1.3** species.<sup>23</sup> The increased slope for **1.1** compared to **1.2** and **1.3**, indicates faster electron transfer kinetics,

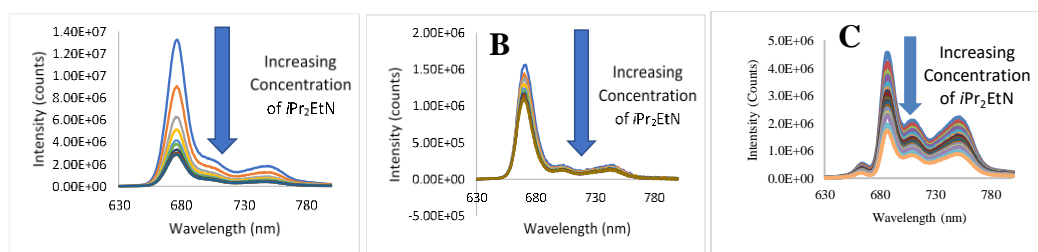


**Figure 2.16** **A.** Stern-Volmer quenching study of **1.1** at 0.8  $\mu$ M and *i*Pr<sub>2</sub>EtN at 0-0.33 M in CHCl<sub>3</sub>. The emission spectra from 630-800 nm, excitation at 675 nm. **B.** Stern-Volmer quenching study of **1.2** at 0.3  $\mu$ M and *i*Pr<sub>2</sub>EtN at 0-0.31 M in CHCl<sub>3</sub>. The emission spectra from 630-800 nm, excitation at 675 nm. **C.** Stern-Volmer quenching study of **1.3** at 1.0 mM and *i*Pr<sub>2</sub>EtN at 0-0.5 M in CHCl<sub>3</sub>. The emission spectra from 630-800 nm, excitation at 675 nm.

as shown in Figure 2.17. Figures 2.16b and 2.17b include the data for **1.3**, but it should be noted the concentration for **1.3** did not have an absorbance below one. Therefore, it cannot be confirmed whether the quenching was due to electron transfer with the introduced quencher or due to self-quenching because the solution was very concentrated. The data

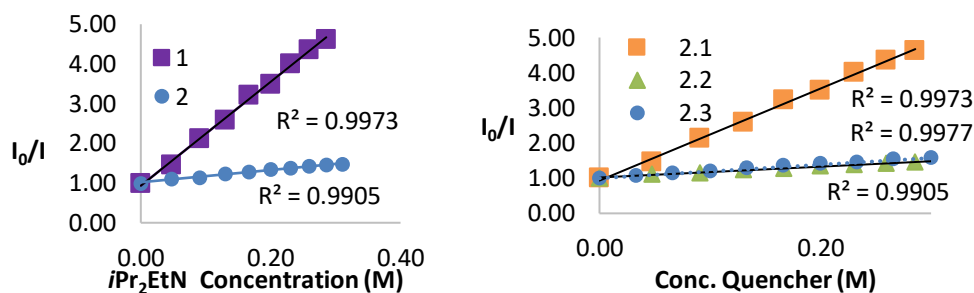


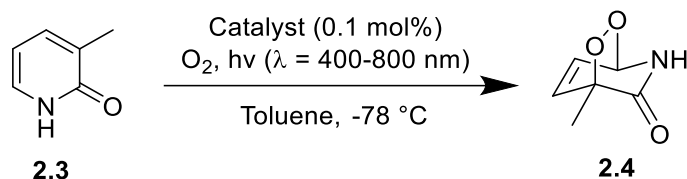
**Figure 2.17 A (Left).** Stern Volmer quenching studies of **1.1** ( $8 \times 10^{-7}$  M) and **1.2** ( $3 \times 10^{-7}$  M). **B (Right).** Stern Volmer quenching with **1.1**, **1.2**, and **1.3** (1.0 mM) with Hünig's base in chloroform. Catalysts **1.1**, **1.2**, and **1.3** were excited at 675 nm and emission was collected from 630 – 800 nm.  $I_0$  is in reference to 676.5 nm.

for **1.3** should not be considered when evaluating its ability to transfer electron until it can be repeated with an absorbance less than one. Therefore, catalysts **1.1** and **1.2** effectively accept an electron to Hünig's base and show potential to be effective photocatalysts in photoredox processes. For the remainder of this chapter, the reactivity of **1.1** and **1.2** will be further analyzed whereas **1.3** was not investigated due to purification issues, as mentioned above.

## 2.4 Silicon phthalocyanines in an energy transfer reaction

Next, the ability for photocatalysts **1.1** and **1.2** to promote an energy transfer reaction was investigated and compared to a literature standard (Table 2.2).<sup>112</sup> The

**Table 2.2** The [4+2]-cycloaddition of pyridone **2.3** to endo-peroxide **2.4**.



Entry <sup>a</sup>	Catalyst:	Time	Light Source/Wattage	Isolated Yields (%)
1	<b>1.1</b>	18 h	LED/100	25
2	<b>1.2</b>	18 h	LED/100	67
3	<b>TPP</b>	18 h	LED/100	36
4 <sup>b</sup>	<b>TPP</b>	45 min	Sodium Vapor Lamp/800	97

<sup>a</sup>All reactions were performed at 0.11 M concentration with respect to **2.3** in toluene at -78 °C for 18 h. <sup>b</sup>Literature conditions from reference 51.

photocatalytic reaction chosen was a [4+2]-cycloaddition of singlet oxygen with pyridine-2(1*H*)-one (**2.3**) to form endo-peroxide **2.4**. During the reaction, the excited photocatalyst transfers energy to molecular oxygen to form singlet oxygen, which reacts with the diene

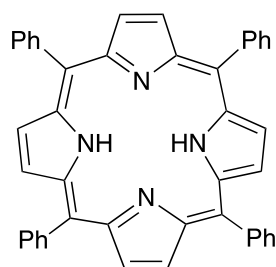


**Figure 2.18** Tetraphenylporphyrin (TPP)

of **2.3**.<sup>113</sup> We chose to promote the reaction via a 100 watt, white LED light bulb, which is an affordable, readily available light source that fits the absorbance range of both **1.1** and **1.2**. Both silicon phthalocyanine catalysts promoted the formation of **2.4** using conditions similar to the literature,<sup>113</sup> but with a lower intensity light source (Table 2.2, entries 1 and

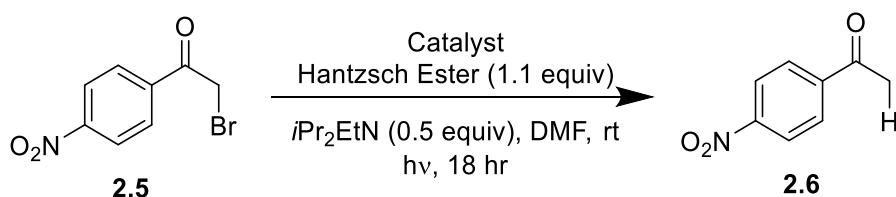
2). Trihexylsilyl catalyst **1.2** provided higher yields compared to pentyl catalyst **1.1**. We believe the low yields with **1.1** was a result of catalyst decomposition during the reaction, due to the inability to recover the catalyst during work up. This result is consistent with the irreversible redox properties discovered in the cyclic voltammetry studies shown in Figure 2.4. Therefore, we believe the bulkiness of the trihexylsilyl group on **1.2** is important in the overall stability of these structures. Bach and coworkers had originally employed the photocatalyst tetraphenylporphyrin (TPP) and an 800 watt sodium vapor lamp, resulting in significantly higher yields than our catalysts in less time (Entry 4). Employing TPP as the catalyst with the LED light source, resulted in a significant drop in yield to 36% (Entry 3), which is also dramatically lower than the yield with catalyst **1.2**. This suggests that **1.2** does a better job of activating oxygen versus TPP with this simple light source.

## **2.5 Silicon phthalocyanines in an electron transfer reaction**

The photocatalysts **1.1** and **1.2** were then examined in a photoredox catalysis reaction, specifically a reductive dehalogenation reaction (Table 2.3).<sup>114</sup> This reaction was chosen to compare the performance of our organic photocatalysts against the popular Eosin Y catalyst, again using a commercially-available LED bulb with the literature's reaction conditions. The excited photocatalyst accepts an electron by reducing **2.5** and breaking the bromine-carbon bond to produce an electron-deficient radical on the  $\alpha$ -carbon, which picks up a hydrogen radical to form **2.6**.<sup>115</sup> We believe pentyl catalyst (**1.1**) resulted in no yield due to instability of **1.1**. Once the reaction was completed, we were unable to recover the catalyst. We believe this lack of stability suggests the solvent is possibly interacting with **1.1**, or the light source was too high energy and **1.1** decomposed during the reaction. Trihexylsilyl catalyst **1.2** successfully promoted the reaction with just under 40% yield

(entry 2). This is lower than the literature yield of 83% with Eosin Y and a different light source (entry 11). We also noticed while performing the reaction with trihexylsilyl catalyst **1.2**, that the solution was dark black in color, suggesting that the reaction was too concentrated for the light to penetrate, limiting the amount of catalyst being excited. Therefore, we diluted the reaction to 1.25 mM (with respect to the catalyst) and the yield increased to 59% (entry 3), closing the gap in yield with published Eosin Y results (entry 11). The literature utilized a blue LED light source, which is optimal for Eosin Y, and we again wanted a more representative comparison using Eosin Y with our 100 watt, white LED bulb (entry 10). The light source decreased Eosin Y's yield (entry 10) and resulted in

**Table 2.3** Dehalogenation Reaction



Entry <sup>a</sup>	Catalyst	Catalyst (mM)	LED Light Source	Solvent	Yield (%)
1	<b>1.1</b>	6.25	White	DMF	0
2	<b>1.2</b>	6.25	White	DMF	38
3	<b>1.2</b>	1.25	White	DMF	59
4	<b>1.1</b>	1.25	Red	DMF	25
5	<b>1.2</b>	1.25	Red	DMF	27
6	<b>1.1</b>	1.25	Red	Chloroform	31
7	<b>1.2</b>	1.25	Red	Chloroform	22
8	<b>1.1</b>	1.25	White	Chloroform	31
9	<b>1.2</b>	1.26	White	Chloroform	21
10	Eosin Y	6.25	White	DMF	55
11 <sup>b</sup>	Eosin Y	6.25	Blue	DMF	83

<sup>a</sup>All reactions were performed at 0.05 M concentration with respect to **2.5** in specified solvent at room temperature for 18 h using specified LED light source. <sup>b</sup>Literature conditions from reference 117.

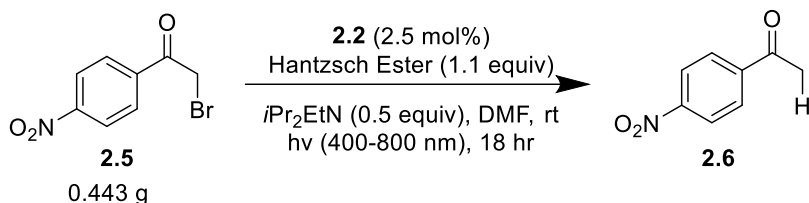


a similar yield compared to our catalyst **1.2** (entry 3). Since catalysts **1.1** and **1.2** absorb red light between ~600-700 nm, with a maximum at 675 nm, we employed a commercially-available red LED source to investigate the effect on the reaction (entries 4 and 5). Because the red LED has a wavelength range of 615-630 nm, we did expect to see lower than optimal yields, since the light source does not include the maximum absorbance wavelength for **1.1** and **1.2**. To our surprise, under these conditions, catalyst **1.1** generated 25% product. We contributed this new reactivity to less degradation of catalyst **1.1** with the less intense red LEDs compared to our white LED (a comparison of 24 W to 100 W). Catalyst **1.2** had a decrease in yield (entry 5) with the red light compared to the white LED (entry 3), and we attribute this to the lower wattage light source and the light wavelength falling outside of the maximum wavelength absorbance of **1.2**.

Since our CV studies showed irreversible and reversible reductions for **1.1** and **1.2**, respectively, in chloroform and we were concerned that DMF could be reacting with our catalysts, the dehalogenation reaction was run in chloroform with both catalysts (Table 2.3, entries 6-9). Both the red and the white LED light sources were employed, showing a slight increase in product with catalyst **1.1** over DMF with no difference between the two light sources in chloroform (31% yield, entries 6 and 8). Catalyst **1.2** resulted in a decrease in yield versus reactions run in DMF, again resulting in the same yield regardless of the light source (entries 7 and 9). The redox potentials of **1.1** and **1.2** suggest they should have similar reactivity, but solvent and the wattage of the light source can have a negative effect on these catalysts, especially **1.1**, since there is evidence that it is less stable. Changing the solvent from DMF, increased the yield of **1.1** but had a negative effect on catalyst **1.2**.

DMF is used exclusively in the literature for this reaction, suggesting it could have a stabilizing effect on the reaction intermediates.

**Table 2.4** Large Scale of Dehalogenation Reaction and Catalyst Stability Study.



Entry <sup>a</sup>	% Yield	% Recovered Catalyst
1	53	100
2	55	100
3	64	76

<sup>a</sup>All reactions were performed at 0.05 M concentration with respect to **2.5** in specified solvent at room temperature for 18 hr using specified LED light source, recycling the same sample of **1.2**.

Finally, we performed a large-scale reaction with catalyst **1.2** as well as a catalyst recyclability study. The goal was to recycle the catalyst over three reactions to determine stability, starting with close to half a gram of starting material. Table 2.4 shows the yield of the reaction does not decrease with the scale up nor does it change if the catalyst is recycled, suggesting **1.2** is stable to undergo the electron transfer for several cycles for the first two reactions. Entry 3 showed that while the yield is not affected, we did start to see decomposition of **1.2** since less was recovered from the reaction.

## 2.6 Conclusions and outlook

In conclusion, silicon phthalocyanines are viable options for photocatalysis. We have shown silicon phthalocyanines are able to undergo electron and energy transfer processes competitive with existing photocatalysts. The redox potentials of our silicon phthalocyanines are competitive with known organocatalysts, such as Eosin Y.

One study that could be insightful is a solvent study for the photoredox processes using cyclic voltammetry for redox potentials and Stern Volmer quenching studies for efficiency of electron transfer. With our study, we saw solvent had an effect on the performance of catalysts **1.1** and **1.2**. While **1.2** had better performance in DMF, it was less efficient in chloroform whereas **1.1** was able to participate and have a conversion. This could give better insight to which solvents/ligands are more stabilizing for electron transfer. These catalysts were very particular in terms of solubility and preferred relatively nonpolar solvents. While the literature seems to show predominately polar solvents (acetonitrile, DMF, etc.) for photochemistry, exploring moderately polar solvents (hexanes, dichloromethane, chloroform, tetrahydrofuran, etc.) that increase in polarity could show a trend where solvent polarity is important for these processes. One potential study we could analyze is the dehalogenation reaction with **1.2** which was run in dichloromethane. Looking at the CVs, we see better stabilization in chloroform compared to dichloromethane. I think we would have seen better yields in this solvent system compared to what we did with chloroform. While **1.1** did not have reversible reduction peaks in either solvent, it maintained its electrochemical profile between solvent systems. Therefore, I do not think we will see a significant change in yield for **1.1** in chloroform; however, **1.2** did change its electrochemistry. By performing a solvent study, we might see more solvents that improve the electrochemistry and efficiency in the photoredox reactions. Looking at the Stern Volmers, we could see if solvent also has an influence on the rate or efficiency of electron transfer, in combination with the CV study, and whether solvents can improve the rate of electron transfer. For example, our Stern Volmer studies were conducted in chloroform, and we saw **1.1** was faster than **1.2**. Would this be true in different solvents?

Performing a solvent study for CVs and Stern Volmers could provide better solvent conditions to maximize the performance of the catalysts that will be more competitive with popular photocatalysts.

For future catalyst designs, the bulkier axial ligands clearly help with stabilizing the catalysts for purification and electron transfer. I include purification because **1.1** could not tolerate chromatography or multiple purification methods on the same sample. Catalyst **1.2** was able to undergo chromatography and even recyclability as shown in the scale up dehalogenation reaction. It was very disappointing **1.3** was difficult to purify and was only used for half the characterization experiments for this project. Looking at the CVs and Stern Volmer experiments, it had great potential for photocatalysis and might have been competitive with **1.2**. When running TLCs, there was never separation in any of the various solvent system combinations that were tried. It would be interesting to try varying the ligands with more polar groups would have allowed for better separation during column chromatography or would have been more amenable to another purification method (recrystallization, filtration, etc). For example, would substituting a methoxy group on the phenyl rings of the triphenylsilyl chloride starting material have impacted the polarity enough to allow separation between product and unreacted starting material? Would having a strong withdrawing group on the phenyl ring, such as trifluoromethyl, increased the reactivity of the reaction by producing a better electrophile for the deprotonated silicon phthalocyanine dihydroxide to attack? Instead of just having two completely nonpolar structures, there might be a minor difference between the two when adding substituents on the aryl rings to afford better separation.

Another advantage to derivatizing the axial ligands is to explore the electrochemistry of ligands varying in electronics. We see a difference in redox potentials between **1.1** and **1.2/1.3** where the only difference is the size of the substituent and an additional silicon. For **1.2** and **1.3**, there is not much variation between their potentials. However, I think adding electron donating or withdrawing groups would impact the electrochemistry. While substitution on the peripheral ligands of the phthalocyanine rings would have a greater impact on the redox potentials since that is what is participating in the redox processes, I think the ease of synthesis for adding axial ligands is worth investigating first. This theory is supported by research done on silicon phthalocyanines with fluorinated axial ligands (pentafluorophenoxy, pentafluoro, and fluorophenoxy),<sup>116,117</sup> where incorporating fluorines on the axial positions had significant changes in the electrochemistry, generating better electron-accepting catalysts.

To help determine which ligands would best impact electrochemistry, computational models can help predict the redox properties of future potential photocatalysts.<sup>118,119,120</sup> Using the ground state redox potentials, the excited state potentials are calculated because the excited state is where the chemistry is occurring. Using computations, the redox properties of structures varying in axial and peripheral ligands can be predicted to analyze how these variations directly influence the electronic properties. Again, the electrochemistry might not change when varying the axial ligands, but ultimately we believe these changes will help the structure stability and purification of the compounds. I would expect to see greater changes when the peripheral ligands are substituted with a variety of substituents. Analyzing these structures computationally would be more interesting than looking at the axial ligands. While looking at the difference

substitution has on these structures would be very useful, we can also use the predicted redox properties to explore which derivatives would be compatible with future substrates. While there can be variabilities between computations and wet chemistry, ideally the computational models could better predict the redox properties of potential photocatalysts without undergoing the complex synthesis to obtain the photocatalysts. This method could also help explore derivatives of future photocatalysts and improve the efficiency in developing better photocatalysts.

## **2.7 Experimental**

### **General Information**

All reactions were carried out under a N<sub>2</sub> atmosphere using oven dried glassware. Amyl alcohol and pyridine were distilled prior to use. Toluene was dried by passing through a column of activated alumina before use and stored over molecular sieves. All other solvents and chemicals were obtained from commercial sources and used without further purification. Flash column chromatography was performed on silica gel (32–63 microns). <sup>1</sup>H NMR spectra were recorded on a Bruker Avance III (400 or 300 MHz). Chemical shifts are reported in ppm with TMS or chloroform as an internal standard (TMS 0.00 ppm for <sup>1</sup>H and <sup>13</sup>C or CHCl<sub>3</sub> 7.26 ppm and 77.16 for <sup>1</sup>H and <sup>13</sup>C, respectively). <sup>13</sup>C NMR spectra were recorded on a Bruker Avance III (101 or 75 MHz) with complete proton decoupling. The data reported for <sup>1</sup>H NMR are as follows: chemical shift, multiplicity (s = singlet, d = doublet, t = triplet, q = quartet, dd = doublet of doublet, td = triplet of doublets, dt = doublet of triplet, sept = septet, m = multiplet). Steady-state emission spectra were acquired on an Edinburgh FS5 fluorescence spectrometer equipped with a 150 W

Continuous Wave Xenon Lamp source for excitation. Absorbance scans were taken on a Shimadzu UV-2600 UV-Vis Spectrophotometer using 1 cm quartz cuvette at 25 °C. Cyclic voltammetry (CV) performed on a CH Instruments 601D potentiostat with a 3 mm diameter glassy carbon working electrode, a Pt wire (99.99%) counter electrode, and a saturated calomel electrode (SCE). The glassy carbon electrode was manually prepared by polishing the surface with a 0.05  $\mu\text{m}$  Alumina suspension. Solutions for electrochemical characterization contained 100 mM tetrabutylammonium hexfluorophosphate (TBAPF<sub>6</sub>) which was further purified by recrystallization in ethanol, dried under vacuum at 80 °C over 24 hours. Dichloromethane was purged with N<sub>2</sub> prior to any measurements taken and between measurements.

*Bis-pentyloxy silicon phthalocyanine (1.1)*

The synthesis of **1.1** was adapted from the literature.<sup>104</sup> In a flame-dried four-dram vial equipped with a stir bar, sodium hydride (2 equiv, 0.33 mmol) was added under nitrogen and washed with pentane (3 X 5 mL). Amyl alcohol (2 equiv, 0.33 mmol) was added to the vial with sodium hydride, and the solution stirred in 3 mL of dry toluene for 15 minutes. The solution was then added to a 50 mL round bottom flask with **2.1** (1 equiv, 0.165 mmol) and a stir bar under nitrogen. The mixture was diluted with 12 mL of dry toluene and refluxed overnight under nitrogen. The mixture was then concentrated via rotary evaporation and filtered with cold chloroform. The filtrate was collected and concentrated via rotary evaporation to afford **1.1** as a dark blue solid without further purification. Yield: 48%. <sup>1</sup>H NMR (300 MHz, CDCl<sub>3</sub>)  $\delta$  (ppm): 9.658 (m,  $J$  = 2 Hz, 8 H), 8.352 (m,  $J$  = 3 Hz, 8 H), -0.117 (t,  $J$  = 15.1 Hz, 6 H), -0.377 (m,  $J$  = 7.6 Hz, 4 H), -1.401 (m,  $J$  = 14.8 Hz, 4 H), -1.677 (m,  $J$  = 13.8 Hz, 4 H).

*Bis(tri-*n*-hexylsiloxy)-silicon phthalocyanine (1.2)*

The synthesis of **1.2** was adapted from the literature. To a flame-dried 5 mL round bottom flask equipped with a stir bar, under nitrogen was added **2.2** (1 equiv, 0.072 mmol), trihexylsilylchloride (2 equiv, 0.145 mmol), and 2.5 mL of distilled pyridine. A reflux condenser was added, and the mixture refluxed for 48 hours under nitrogen. The reaction was then concentrated via rotary evaporation and the resulting blue solid was purified by column chromatography (silica gel, 1% CHCl<sub>3</sub>/hexane) to give **1.2** as a blue solid. Yield: 56%. <sup>1</sup>H NMR (300 MHz, CDCl<sub>3</sub>) δ (ppm): 9.656 (m, *J* = 3 Hz, 8 H), 8.335 (m, *J* = 9 Hz, 8 H), 0.850 (m, *J* = 14.9 Hz, 12 H), 0.731 (t, *J* = 6.6 Hz, 18 H), 0.383 (m, *J* = 15.2 Hz, 12 H), 0.043 (m, *J* = 15.2 Hz, 12 H), -1.26 (m, *J* = 16.4 Hz, 12H), -2.421 (m, *J* = 18 Hz, 12 H).

## General Procedures for Photocatalytic Reactions

*Synthesis of Endoperoxide 2.4*

The synthesis of endoperoxide **2.4** was adapted from the literature.<sup>113</sup> In a flame-dried four-dram vial equipped with a stir bar, pyridone **2.3** (1 equiv, 1.4 mmol) was added with 0.1 mol% of photocatalyst and 10 mL of dry toluene under nitrogen and then sealed with a septa vial cap. The solution was then bubbled with oxygen and placed in a -78 °C bath for 18 hours and irradiated by a 100 W LED lamp. The solution was then warmed to room temperature, and the solid was filtered and washed with diethyl ether. The combined organic layers were dried over NaSO<sub>4</sub>, filtered, and concentrated via rotary evaporation. The solid was collected without further purification to afford endoperoxide **2.4**. <sup>1</sup>H NMR (300 MHz, CDCl<sub>3</sub>) δ (ppm): 6.864 (dd, *J* = 2.4 Hz, 13.2 Hz, 7.9 Hz, 1 H), 6.497 (dd, *J* =



1.8 Hz, 1.8 Hz, 7.9 Hz, 1 H), 5.764 (td,  $J = 1.8$  Hz,  $J = 1.9$  Hz,  $J = 1.8$  Hz,  $J = 8.0$  Hz, 1 H), 1.645 (s, 3 H).

### *Reductive Dehalogenation of $\alpha$ -Halogenated Carbonyl 2.6*

The synthesis of **2.6** was adapted from the literature.<sup>114</sup> In a flame-dried four-dram vial equipped with a stir bar, **2.5** (1 equiv, 0.5 mmol) was added under nitrogen. DMF (10 mL), Hünig's base (2 equiv, 1 mmol), Hantzsch ester (1.1 equiv, 0.55 mmol), and photocatalyst (1.25 mM, 0.0125 mmol) were added under nitrogen to the vial and sealed with a septa vial cap. The solution was degassed by "freeze- pump-thaw" cycles (x3) via syringe needle. The vial was then irradiated by a 100 W LED lamp for 18 hours at room temperature. The reaction was then diluted with diethyl ether, washed (3x) with water and the water layer was washed (2x) with diethyl ether. The combined organic layers were dried over NaSO<sub>4</sub>, filtered, and concentrated via rotary evaporation. Purification of **2.6** was achieved by column chromatography (silica gel, 25% Et<sub>2</sub>O/hexanes). <sup>1</sup>H NMR (300 MHz, CDCl<sub>3</sub>)  $\delta$  (ppm): 8.337 (d,  $J = 8.8$  Hz, 2 H), 8.133 (d,  $J = 8.8$  Hz, 2 H), 2.702 (s, 3 H)

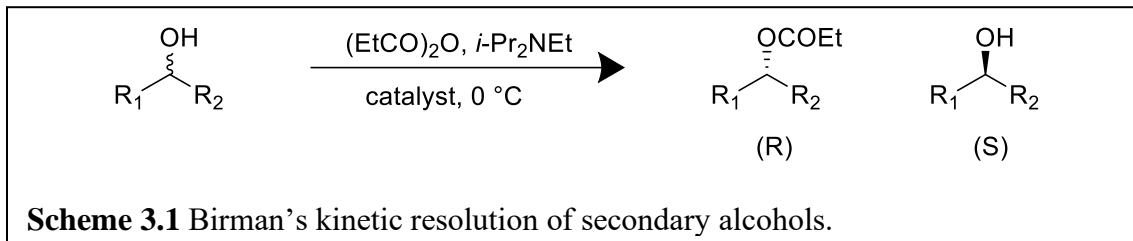
# CHAPTER 3

## INVESTIGATING THE ELECTRONIC EFFECT ON ISOTHIOUREA-BASED CATALYSTS IN COMPETITION STUDIES WITH TRANS-2-PHENYLCYCLOHEXANOLS

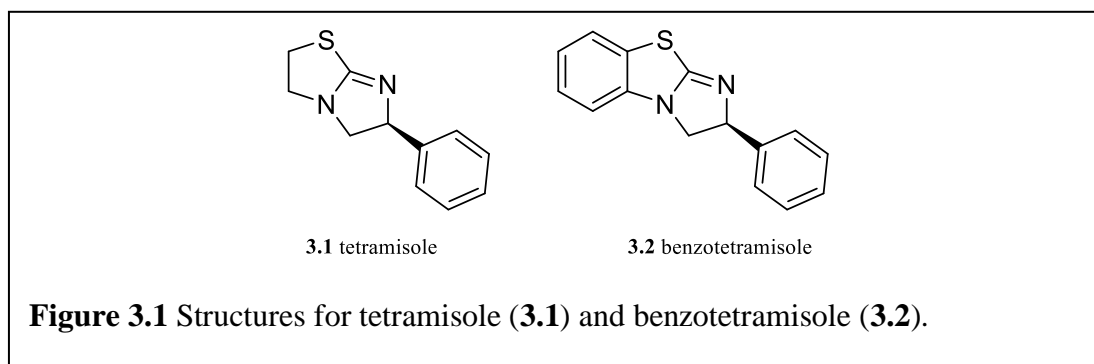
### 3.1 Introduction

Small molecule organocatalysis offers various advantages over traditional metal or enzyme-based catalysis, including easy availability, low toxicity, and they are inexpensive.<sup>121</sup> Organocatalysis is defined as “the use of small organic molecules to catalyze organic transformations” and have played large roles in the highly selective synthetic development of Tamiflu, Ibuprofen,<sup>122</sup> and many other chiral natural products.<sup>121,123,124,125</sup> Many of these organocatalysts, such as enamine- and iminium-based catalysts, are nucleophilic, where upon nucleophilic attack with a reagent, a charged, cationic catalyst intermediate is generated during the reaction.<sup>129</sup> These charged, cationic species are believed to be involved in intermolecular interactions with substrates containing pi systems, known as a cation-pi interactions, and these interactions are often implicated in how these catalysts achieve highly enantioselective reactions.<sup>126,127,128</sup> Within the last 30 years, a large focus on how organocatalysts achieve enantioselectivity has centered around the importance of cation- $\pi$  interactions.<sup>129</sup> These interactions between chiral charged catalyst intermediates and pi systems of substrates can be manipulated to aid in enantioselective reactions by either blocking one face of a reactive substrate or

positioning a reactive functional group near the reaction site, resulting in high selectivities.<sup>125</sup> In 2004, the Birman research group began analyzing a series of chiral nucleophilic amidines and bicyclic isothioureas as catalysts for the kinetic resolution of



chiral alcohols in hopes to achieve selective acyl transfer catalysts (Scheme 3.1).<sup>130</sup> A kinetic resolution is a separation process of two enantiomers in a racemic mixture where one enantiomer is selectively transformed into a different compound.<sup>131</sup> At the time, enzymatic processes were the primary tool used in kinetic resolutions but can be difficult to synthesize.<sup>122,130</sup> For the next several years, the Birman group developed three generations of nucleophilic amidine catalysts, which are imine derivatives of amides that allow resonance between two nitrogens, achieving moderate to excellent enantioselectivity in the resolution of various secondary alcohols.<sup>130,132,133,134,135</sup> Figure 3.1 shows two isothiourea catalysts, tetramisole (**3.1**) and benzotetramisole (**3.2**) that provided the highest

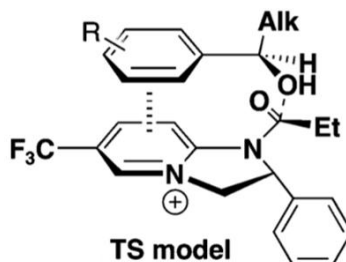


selectivity and conversions seen at that time, especially with benzotetramisole.<sup>133,134</sup>

Birman hypothesized that the success of these catalysts depended on the transition state.

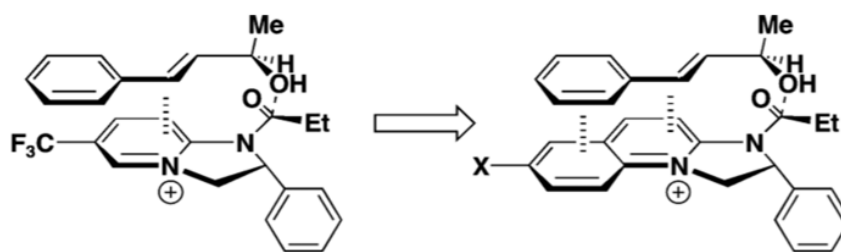
This transition state contains the cationic catalyst intermediate formed after

nucleophilically attacking the acylating reagent and its attraction to the  $\pi$  system of the alcohol, which is modeled after the transition state theorized with an amidine catalyst (Figure 3.2). With the chiral phenyl group blocking one side of the catalyst, the attraction



**Figure 3.2** Transition state of the cation- $\pi$  and  $\pi$ - $\pi$  interaction suggested by the Birman group in the resolution of chiral alcohols for amidine-based catalysts. Adapted with permission from Birman, V. B.; Jiang, H. Kinetic Resolution of Alcohols Using a 1,2-Dihydroimidazo[1,2-a]quinoline Enantioselective Acylation Catalyst, *Org. Lett.*, **2005**, 7, 3445-3447. Copyright 2021 American Chemical Society.

to the substrate can only occur on one side and the bulky alkyl group of the alcohol only allows one position, or alcohol enantiomer, for acylation to occur. This suggested cation- $\pi$  interaction allowed the Birman group to selectively resolve many substrates that contained  $\pi$  systems. The Birman group noted that to achieve the desired selectivity, the placement

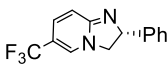
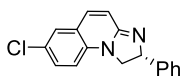
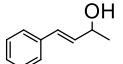
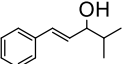
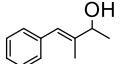
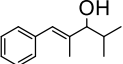
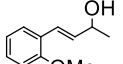
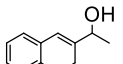
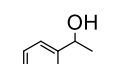
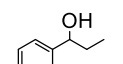
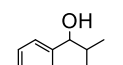
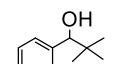
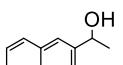
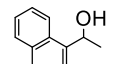
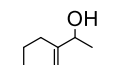


**Figure 3.3** Birman catalyst development for better  $\pi$  overlap. Adapted with permission from Birman, V. B.; Jiang, H. Kinetic Resolution of Alcohols Using a 1,2-Dihydroimidazo[1,2-a]quinoline Enantioselective Acylation Catalyst, *Org. Lett.*, **2005**, 7, 3445-3447. Copyright 2021 American Chemical Society.

of the alcohol  $\pi$  system was important for interaction with the catalyst cation. In the library of alcohols that the Birman group tested (Table 3.1) with these amidine and isothioureia

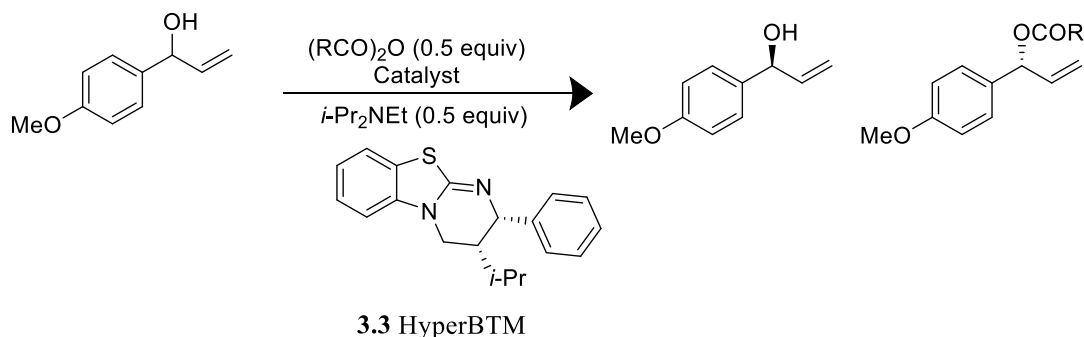
catalysts, if the placement of the alcohol  $\pi$  system was too far from the alcohol (Figure 3.3), then it cannot interact with the catalyst to form the cation- $\pi$  interaction.<sup>134</sup> This

**Table 3.1** Alcohol study by Birman for catalysts with different pi systems.

$  \begin{array}{c}  \text{OH} \\    \\  \text{R}_1-\text{C}-\text{R}_2 \\  (\pm)  \end{array}  \xrightarrow[\text{catalyst, } 0^\circ\text{C}]{(\text{EtCO})_2\text{O, } i\text{-Pr}_2\text{NEt}}  \begin{array}{c}  \text{OCOEt} \\    \\  \text{R}_1-\text{C}-\text{R}_2 \\  (\text{R})  \end{array}  +  \begin{array}{c}  \text{OH} \\    \\  \text{R}_1-\text{C}-\text{R}_2 \\  (\text{S})  \end{array}  $				
entry	substrate	$\text{F}_3\text{C}$  selectivity	 selectivity	
1		11	27	
2		21	24	
3		9	17	
4		13	22	
5		6	31	
6		26	57	
7		26	33	
8		36	41	
9		50	59	
10		85	117	
11		42	74	
12		56	55	
13		11	17	

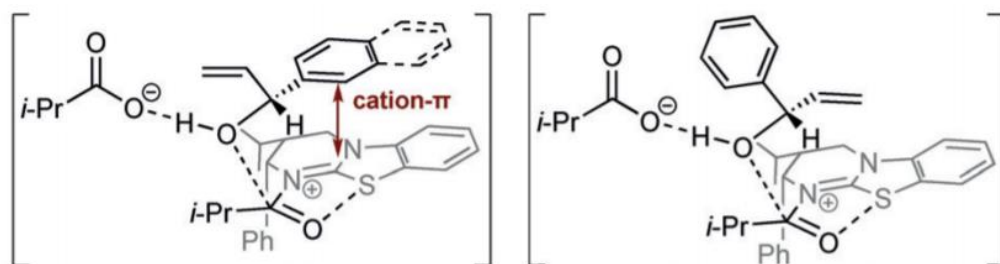
strengthened the theory that the electrostatic interaction between the catalyst cation and substrate  $\pi$  system is extremely important for selectivity.

To add to this theory of cation- $\pi$  interactions directing selectivity, Smith and coworkers have investigated kinetic resolutions where multiple  $\pi$  systems are present, determining if the suspected cation- $\pi$  interaction has a preference when more than one  $\pi$  system is available.<sup>136,137</sup> At the time, limited research had been done on chiral catalysts distinguishing between two planar or two  $sp^2$  groups. Using a derivative of benzotetramisole (**3.2**), Smith and coworkers utilized HyperBTM (**3.3**) to selectively



**Scheme 3.2** Smith's kinetic resolution of secondary alcohols with HyperBTM.

acylate enantiomers of secondary containing aryl-alkenyl ( $sp^2$  vs.  $sp^2$ ) substituents (Scheme 3.2). Using HyperBTM, Smith and coworkers studied a large library of alcohols, modifying the aryl and alkenyl systems of the alcohol and saw incredible selectivities as

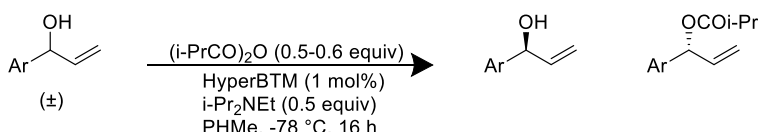
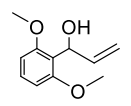
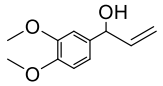
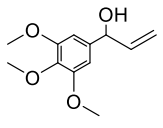
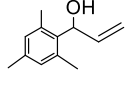
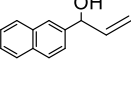
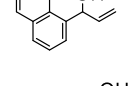
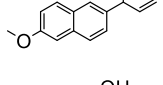
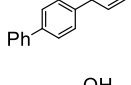
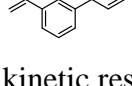


**Scheme 3.3** Proposed transition states by Smith and coworkers for multiple possible cation- $\pi$  interactions.<sup>136,137</sup>

high as about 2000 even though the alcohol was surrounded on two sides by  $\pi$  systems.<sup>136</sup>

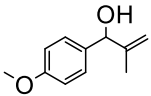
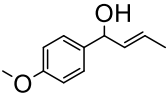
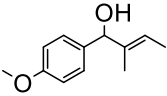
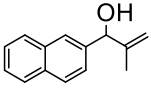
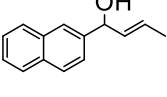
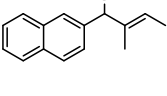
Smith and coworkers presented two potential transition states that explained where the selectivity originated as seen in Scheme 3.3.<sup>136</sup> One possibility is the acyl ammonium intermediate formed by the catalyst forms a cation- $\pi$  interaction with the  $\pi$  system of the phenyl group, or the acyl ammonium intermediate is forming a cation- $\pi$  interaction with the  $\pi$  system of the alkene. To elucidate which transition state was occurring, the Smith

**Table 3.2** Conversions and selectivities of substituted aryl alcohols in acylation kinetic resolution by Smith.

<div style="text-align: center;">  </div>			
entry	substrate	conversion	selectivity
1		37	110
2		60	44
3		51	33
4		22	11
5		49	1980
6		46	108
7		47	5
8		42	13
9		48	26

group performed several kinetic resolutions, derivatizing the electronics and sterics of the aryl and alkenyl systems individually. They saw increasing the electron density of the aryl

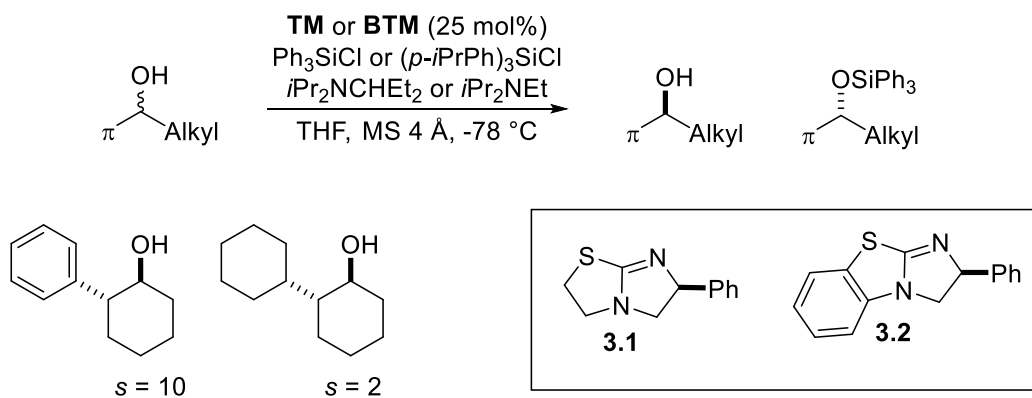
**Table 3.3** Conversion and selectivities of substituted alkenyl group in acylation kinetic resolution by Smith.

$  \begin{array}{c}  \text{OH} \\    \\  \text{Ar}-\text{CH}-\text{CH}=\text{CH}-\text{R}_2 \\    \\  \text{R}_1 \\  (\pm)  \end{array}  \xrightarrow[\text{HyperBTM (1 mol\%)}]{\text{(i-PrCO)}_2\text{O (0.5-0.6 equiv)}}  \begin{array}{c}  \text{OH} \\    \\  \text{Ar}-\text{CH}-\text{CH}=\text{CH}-\text{R}_2 \\    \\  \text{R}_1  \end{array}  +  \begin{array}{c}  \text{OCOi-Pr} \\    \\  \text{Ar}-\text{CH}-\text{CH}=\text{CH}-\text{R}_2 \\    \\  \text{R}_1  \end{array}  $ <p style="text-align: center;">             i-Pr<sub>2</sub>NEt (0.5 equiv)              P<sub>H</sub>Me, -78 °C, 16 h         </p>			
entry	substrate	conversion	selectivity
1		45	10
2		57	N/D
3		38	3
4		47	24
5		47	11
6		53	8

group by electron-donating groups (Table 3.2) gave significantly higher selectivities, whereas increasing the electron density of the alkenyl group (Table 3.3) with additional alkyl groups, lowered the selectivity. From this, they theorized the aryl group is the dominating  $\pi$  system in the transition state that participates in the cation- $\pi$  interaction. Therefore, the Smith group was able to produce a system where the cation- $\pi$  interaction is selective even when provided multiple  $\pi$  “binding sites.”



The Wiskur group is also interested in how the selectivity is obtained with isothiourea catalysts. They have employed tetramisole (**3.1**) and benzotetramisole (**3.2**) in their kinetic resolution silylation reactions to selectively resolve a large library of secondary alcohols, including cyclic alcohols,  $\beta$ -hydroxyl lactones and lactams, 2-ester cyclohexanols, and 2-arylcyclohexanols, achieving selectivities as high as 100%.<sup>138,140,139</sup> The nucleophilic catalysts (**3.1** or **3.2**) attack the silyl chloride, displacing the chloride to form the charged catalyst intermediate. The alcohol then attacks the silicon, generating the silylated alcohol and restoring the nucleophilic catalyst. In these reactions, our group noticed a  $\pi$  system was imperative to achieving high selectivity, as evident in Scheme 3.4 where the difference between a phenyl group or cyclohexane significantly impacted the selectivity, and strongly indicated a cation- $\pi$  interaction is critical to the selective outcomes of the reactions. Figure 3.4 shows this hypothesized transition state.<sup>140</sup> In our studies, we



**Scheme 3.4** Previous silylation-based kinetic resolutions performed by the Wiskur group.

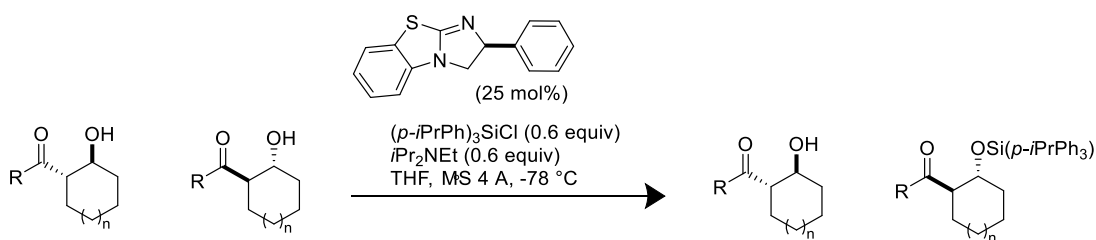
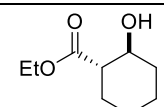
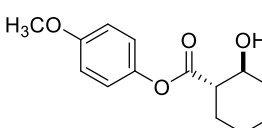
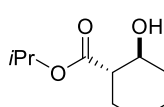
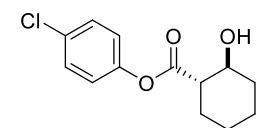
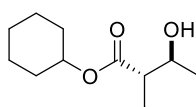
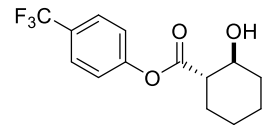
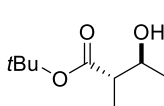
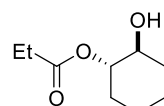
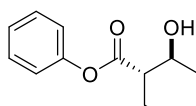
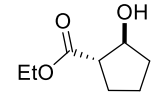


**Figure 3.4** Predicted cation-  $\pi$  interaction in transition state in the Wiskur group's silylation reactions.

analyzed how sterics and electronics of the aryl alcohols influence selectivity, with both playing pivotal roles. In one study, we analyzed a series of ester substrates with varying sterics and electronics, incorporating electron-donating or -withdrawing groups and saw significant changes in selectivity (Table 3.4).<sup>140</sup> We saw increased sterics on the ester can lower the selectivity, which is possibly preventing the pi system on the alcohol from

interacting with the catalyst intermediate. Because of the impact sterics and electronics have on the stereochemical outcome of these reactions, it is important to continue further studies to understand this interaction and how it can be manipulated to further develop selective reactions. With electron-withdrawing groups, the selectivity increased, while electron-donating decreased selectivity. This is counterintuitive because if a cation- $\pi$  interaction was occurring, increasing the electron density on the ester  $\pi$  system should

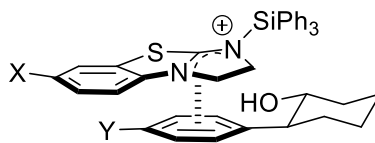
**Table 3.4** Conversions and selectivities seen with ester derivatives in kinetic resolution of chiral secondary alcohols.

<div style="text-align: center;">  <p>(25 mol%)</p> <p>(<i>p</i>-<i>i</i>PrPh)<sub>3</sub>SiCl (0.6 equiv)  <i>i</i>Pr<sub>2</sub>NEt (0.6 equiv)            THF, MS 4 Å, -78 °C</p> </div>							
Entry	Recovered alcohol	conv (%)	s	Entry	Recovered alcohol	conv (%)	s
1		36	14	6		20	4.4
2		35	10	7		43	27
3		30	8.4	8		29	34
4		6	4.7	9		38	3
5		41	3	10		45	2.7

enhance the electrostatic interaction with the catalyst cation intermediate. To further investigate, linear free energy relationships were used to determine how the ester substituents were influencing the selectivity, and it was seen that these structures were very sensitive to inductive effects. This led our group to believe a  $\pi$ - $\pi$  interaction instead of cation- $\pi$  was determining the selectivity between the carbonyl of the ester and aryl group of the catalyst or triphenylsilylchloride.<sup>140</sup> We concluded an electrostatic interaction is responsible for positioning the alcohol to allow selective reactions.

With our previous studies, we see electrostatic interactions have significant influence over substrates, however, there is still much to learn about the role these catalysts play in these interactions, and it is not given that a cation- $\pi$  interaction will dominate in each scenario. With the electrostatic study of ester derivatives, we saw an electrostatic interaction is dictating the selectivity of reactions however not necessarily the cation- $\pi$  interaction we expected but a  $\pi$ - $\pi$  interaction. If the electronics of the aryl system of the catalyst were modified, would that also inspire a different interaction other than cation- $\pi$ ? We propose looking at nonchiral isothioureia-based catalysts to give further insight in the interaction occurring between the cation catalyst intermediate and  $\pi$  systems of aryl alcohols. To simplify the catalyst, we will remove the chiral aryl system and derivatize the core aryl structure to see how this  $\pi$  system is able to interact with the alcohol. Also, we will analyze how modifying the electronics by adding electron-donating or electron-withdrawing groups also influence the ability of these catalyst to act as nucleophiles in these reactions. Using linear free energy relationship diagrams, we can try to see what interaction is occurring and what effect, resonance, electrostatic, or sterics has on these reactions.

## 3.2 Experimental Design



X, Y = EDG or EWG

**Figure 3.5** Predicted cation-pi intermediate of nonchiral isothioureia catalysts and secondary alcohols.

This study will focus on nonchiral isothioureia catalyst derivatives with varying electronic substituents to see if there is an impact on their nucleophilicity and the suspected cation- $\pi$  interaction (Figure 3.5) seen in the literature.<sup>138,140</sup> We will implement these catalysts in competition studies with two alcohols, also differing in electronics, to analyze whether these catalysts have preferences for one alcohol over the other. By increasing the electron density in the pi system of the catalysts, we believe an electron-donating group, such as methoxy, would increase the nucleophilicity of the catalyst to generate faster rates but weaken the electrostatic interaction in the cation pi intermediate, lowering the sensitivity of the catalyst. For an electron-withdrawing catalyst, such as chloro, we anticipate stronger electrostatic interactions in the cation pi intermediate since the withdrawing group is pulling electron density out of the pi system, increasing the sensitivity of the catalyst.

Therefore, we synthesized novel catalysts containing an electron-donating group, **3.5a** methoxy and one catalyst with an electron-withdrawing group, **3.5c** chloro, to compare with known unsubstituted catalyst **3.5b** (Figure 3.6). As mentioned above for the methoxy catalyst **3.5a**, we anticipate faster reaction rates since an electron-donating group

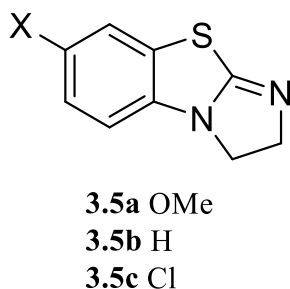
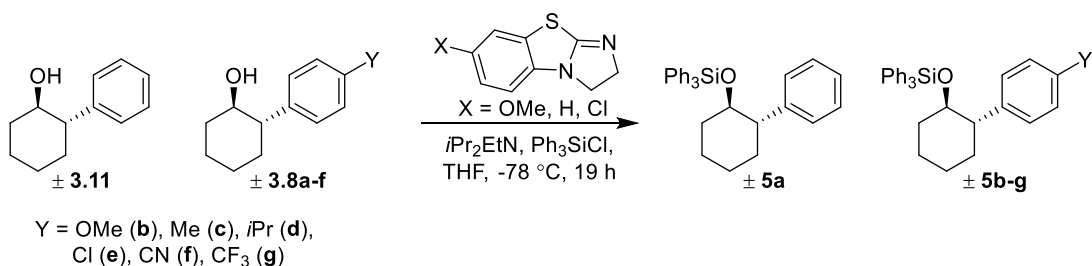


**Figure 3.6** Derivatized isothiourea-based catalysts.

would increase the nucleophilicity of the catalyst but weaken the electrostatic interaction of the cation pi intermediate whereas chloro catalyst **3.5c** would generate slower reactions as it removed electron density from the catalyst but would strengthen the electrostatic interaction of the cation-pi intermediate.

In this study, we wanted to understand the rate of each alcohol reacting with the catalyst and modified the silylation reaction developed by the Wiskur group by using two different substituted alcohols in a competition-based reaction.<sup>138,139,140</sup> In these reactions, two different 2-arylcyclohexanols, one substituted with either an electron withdrawing or electron donating group, and one with just a plain phenyl group were added in the presence



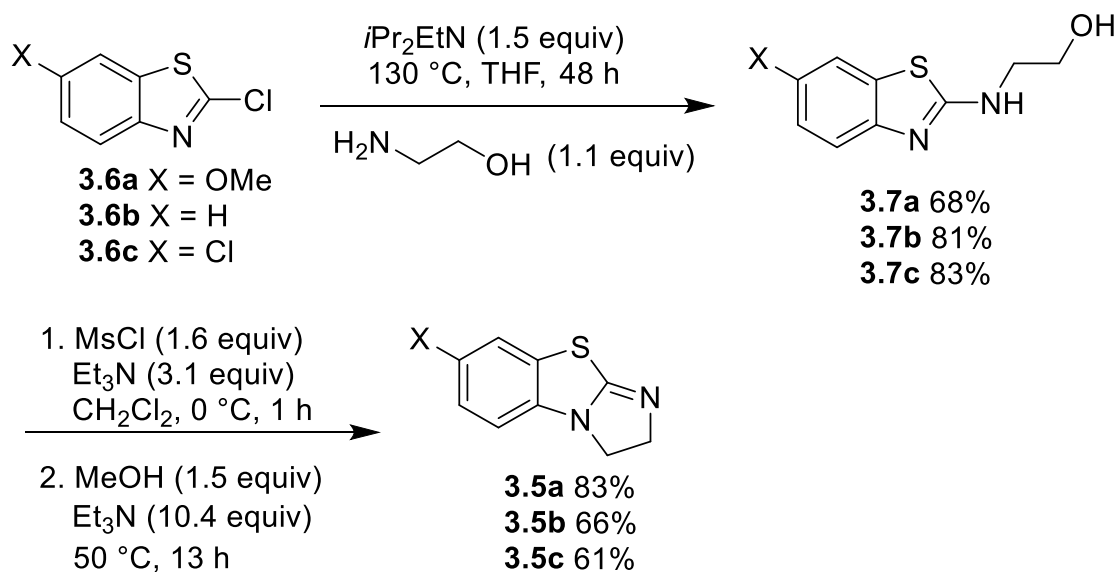
**Scheme 3.5** Reaction for competition studies.

of our isothioureia catalysts to see which alcohol would react faster (Scheme 3.5). Based off previous work by the Wiskur group, the nucleophilic catalyst attacks the silicon of the triphenylsilylchloride ( $\text{Ph}_3\text{SiCl}$ ), displacing the chloride from the silicon to form the silylated catalyst cation intermediate. The alcohol then approaches this charged intermediate, forming the cation pi interaction, and attacks the silicon, forming the silylated product and regenerating the catalyst. To see the difference in rate for the alcohols, only a half equivalent of the silylating reagent is added in reference to the total alcohol added, meaning full conversion of the alcohols is not possible. By limiting the conversion, we have a more accurate representation of how much “faster” or “slower” one alcohol is compared to another. Once the rate ratios of the products are determined from the conversion of each alcohol, the log of these ratios will be used to generate linear free energy relationship diagrams. The slope from these diagrams will provide more insight to how the electronics of these catalysts influence their substrate interactions or how sensitive each catalyst is to electronics on the substrates.

### 3.3 Synthesis of isothioureia catalysts and alcohol derivatives

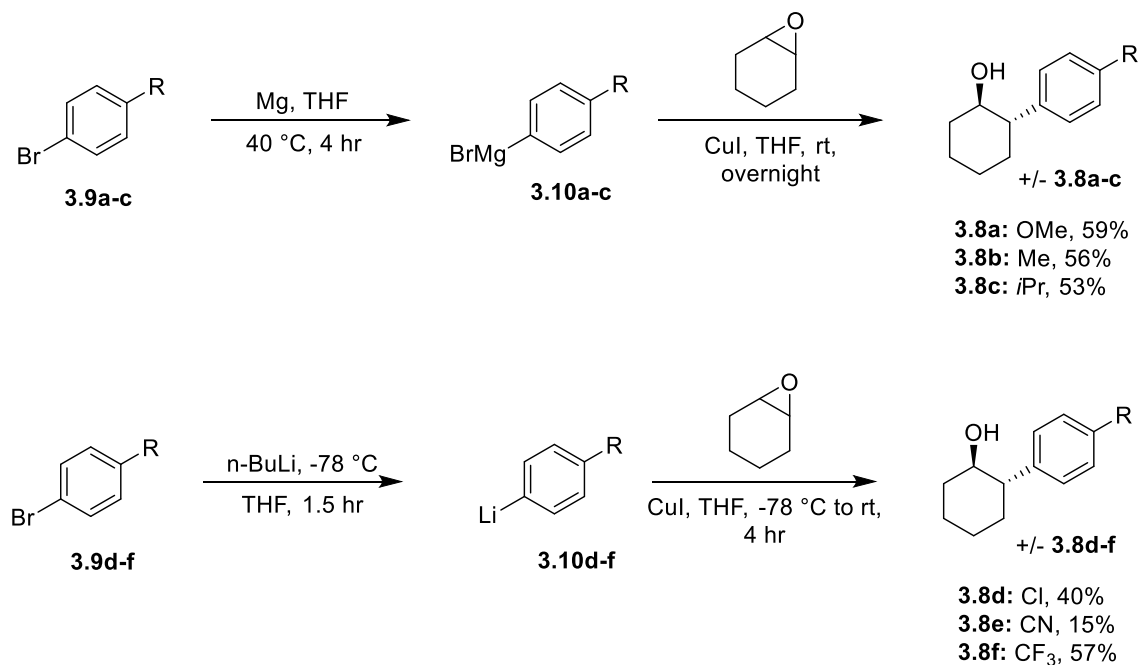
The synthesis and characterization of the isothioureia catalysts **3.5a-c** (a = OMe, b = H, and c = Cl) were adapted from literature procedures.<sup>134</sup> Scheme 3.6 depicts a general strategy for synthesizing the various catalyst derivatives. The synthesis of **3.5a-c** followed the procedure outlined by Birman with ethanolamine displacing the chloride from the appropriate 2-chlorobenzothiazole (**3.6a-c**) to generate the non-cyclized isothioureia derivatives **3.7a-c** in moderate yields.<sup>134</sup> The resulting alcohol is then protected with methanesulfonyl chloride, converting the alcohol into a better leaving group. The lone pair on the alkyl amine will form a carbon-nitrogen double bond, allowing the pi electrons from

the imine double bond in the ring to perform a nucleophilic substitution to displace the methanesulfonate, forming the third ring to afford **3.5a-c** moderate yields<sup>134</sup>



**Scheme 3.6** Synthesis of catalysts **3.5a-c**.

After the catalysts were obtained, the 2-aryl cyclohexanol derivatives (OMe (**3.8a**), Me (**3.8b**), *i*Pr (**3.8c**), Cl (**3.8d**), CN (**3.8e**), CF<sub>3</sub> (**3.8f**)) were then synthesized following



**Scheme 3.7** Synthesis of alcohol derivatives.



literature procedures (Scheme 3.7).<sup>141,142</sup> For electronic donating groups (OMe (**3.8a**), Me (**3.8b**), *i*Pr (**3.8c**)), the Grignard reagent was prepared from the appropriate para substituted-bromobenzene (**3.9a-c**). The Grignard reagent was then reacted with epoxycyclohexane to nucleophilically open the epoxide and generate the desired trans substituted alcohol in moderate yields. For electron-withdrawing groups (Cl (**3.8d**), CN (**3.8e**), CF<sub>3</sub> (**3.8f**)), a lithium halogen exchange was performed with the appropriate para substituted-bromobenzene to prepare the organo-lithium reagent that nucleophilically opens the epoxycyclohexane to generate the corresponding 2-aryl cyclohexanols with electron-withdrawing groups in moderate yields. While the Grignard method can be used for the electron-withdrawing alcohols, higher yields were observed when using the organolithium.

### 3.4 Competition studies of isothioureia catalysts

Once the catalysts and alcohols were obtained, silylation reactions were performed in the presence of two different 2-arylcyclohexanols, one substituted with either an electron withdrawing or electron donating group, and one with just a plain phenyl group to see which alcohol would react faster (Scheme 3.5). Because the electronics of the alcohols varied for each study, we expected to see a difference in the electrostatic interactions between the alcohol  $\pi$  system and the silylated catalyst intermediate, which would translate to differences in rates for each alcohol. With electron-donating alcohols and electron-withdrawing chloro catalyst **3.5c**, we expect more attractive interactions, increasing the rate of electron rich alcohols compared to electron-withdrawing alcohols, which would be less attracted to the cation intermediate. While catalysts **3.5a** and **3.5b** are not withdrawing, we still expect to see similar trends where electron-donating alcohols are faster, but these

catalysts should show smaller changes in rates. To obtain the rates from the reactions, we needed a method to determine the amount of each silylated product generated and the overall conversion. To accurately measure the conversion in the reactions, we wanted to rely on an analytical method. There are a number of different techniques that can measure conversion, including HPLC, GC, and NMR. We tried a number of these methods, which will be further discussed below.

### 3.4.1 Using HPLC to determine reaction conversion

To determine the product ratios for the reactions, and ultimately the rate ratios, we first intended to use HPLC with a silica gel column (normal phase) to determine the concentration of each silylated ether product and each remaining alcohol. Based off

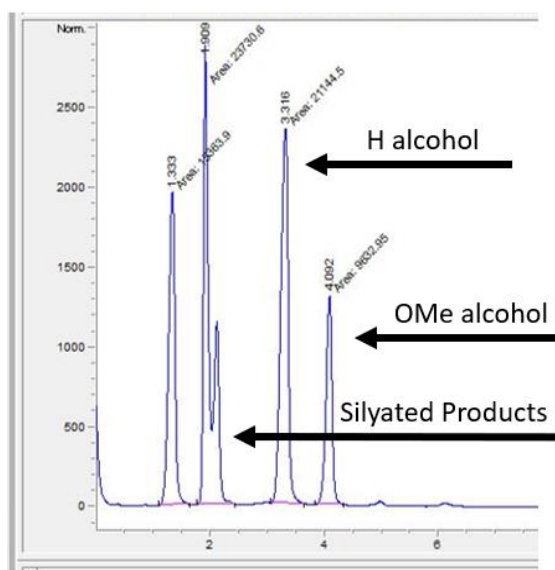


**Figure 3.7** HPLC trace of competition study.

previous work conducted by the Wiskur group,<sup>138,139,140</sup> we know the alcohols directly convert to the silylated ether with no side reactions. Therefore, we assume the amount of alcohol consumed in the reaction directly correlates to product generated and we can use

the four peaks, two silylated products and two unreacted alcohols, to determine the overall conversion of the reaction as well as the individual conversion for each alcohol. However, our initial HPLC runs showed the silylated ethers of both alcohols overlapped whereas the unprotected alcohols separated (Figure 3.7). Since the alcohols separated nicely, we decided to ascertain the concentration of the unreacted alcohols in attempts to back-calculate the concentration of the silyl ether products. For each alcohol, we generated calibration curves using the peak area of various concentrations. Using the equation produced by the calibration curve, we could input the peak area of the alcohols from our competition studies to determine the final concentration of the alcohols at the end of the reaction. From there, we could back calculate the concentration of each silylated product and determine reaction conversions. Using this method, we calculated conversions higher than 50% in our reactions, which is not valid since we limit the silyl chloride to 0.5 equivalence to the alcohols. Therefore, we wanted to implement an internal standard to see if this would improve the accuracy of the data. We wanted compounds with higher polarity

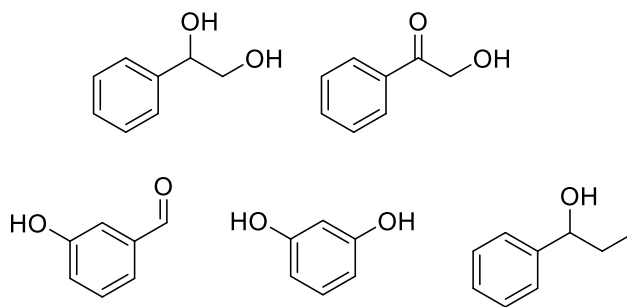


**Figure 3.8** Select compounds investigated for HPLC internal standard.

to have peaks at longer retention times to prevent the internal standard from overlapping with the alcohol and product peaks. Figure 3.8 shows different compounds we attempted to use as an internal standard; however, the internal standard either streaked on the HPLC,

overlapped with our alcohol peaks, or they were not soluble in our HPLC solvent system. When we tried to change the polarity of the solvent system, we lost the separation of our two alcohol peaks. Therefore, we decided to try Gas Chromatography (GC) to overcome these issues.

### 3.4.2 Using GC to determine reaction conversion

Using GC, we then analyzed the peaks for our unprotected alcohols and silylated ether products. Similar to HPLC, we saw clean peaks for the unreacted alcohols, however there were no peaks representative of the products (Figure 3.9). The silyl ethers either

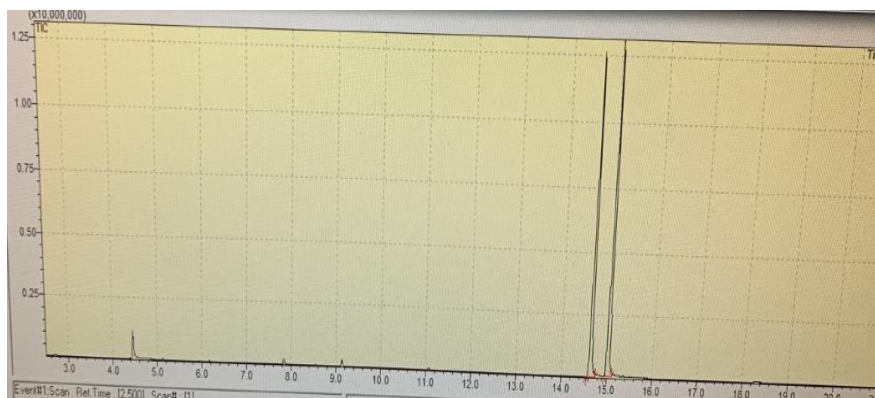


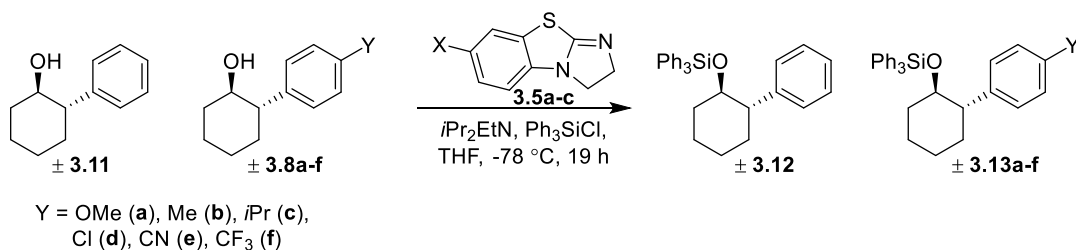
**Figure 3.9** GC trace of competition study.

fragmented or did not show up on the GC. We again generated calibration curves with the GC using only the unreacted alcohols at known concentrations in an attempt to back-calculate the product concentration. Equation 3.1 was used to determine the concentration of the recovered starting material.

$$[Alcohol] = Slope\ Calibration\ Curve * Peak\ Area$$

Using the alcohol concentration, we could determine how many mmols of alcohol was converted to the silyl ether product. Since the exact amount of alcohol added in the system was known, we could subtract the amount of alcohol remaining to determine the mmol of silyl ether product formed. Table 3.1 details the results for several competition study trials using the **3.11** and methoxy alcohol derivative **3.8a** with only data for the methoxy alcohol and product shown. For each reaction, 0.2 mmol of each alcohol is added in the reaction, meaning 0.2 mmol is the most of each alcohol we could recover. The limiting reagent in

**Table 3.5** Competition study results using the methoxy alcohol with **3.8a** to determine the amount of methoxy alcohol remaining and methoxy product generated in the reaction.



Entry	Alcohol	Mmol Recovered OMe Alcohol	Mmol OMe Product
1	OMe	0.116	0.2
2	OMe	-0.03	0.07
3	OMe	0.13	0.3
4	OMe	-0.03	0.08
5	OMe	-0.05	0.05
6	OMe	-0.02	0.10
7	OMe	0.02	0.15

the reaction was always the triphenylsilyl chloride, where we only added 0.2 mmol of silylating agent (0.5 equiv to total alcohol), meaning we can only produce 0.2 mmol of total product. Analyzing the data, we do not see very consistent results. Specifically, Entries 2-6 show too much methoxy alcohol recovered or too much methoxy silylated product produced. We theorized several possible sources of error with this method. We wondered if errors were present in the workup procedure after the reaction was quenched or in the preparation of the GC samples. Since the experiment is concentration-dependent, we wondered if the concentration of the GC samples were consistent since another lab prepared and ran the samples on the instrument. Originally, we were going to see if an internal standard would address these inconsistencies but then we turned our attention to  $^{19}\text{F}$  NMR instead.

### 3.4.3 Using $^{19}\text{F}$ NMR to determine reaction conversion

NMR is an attractive method because minimal workup is necessary and it also avoids the use of sensitive columns like with HPLC and GC. The reaction simply needs to

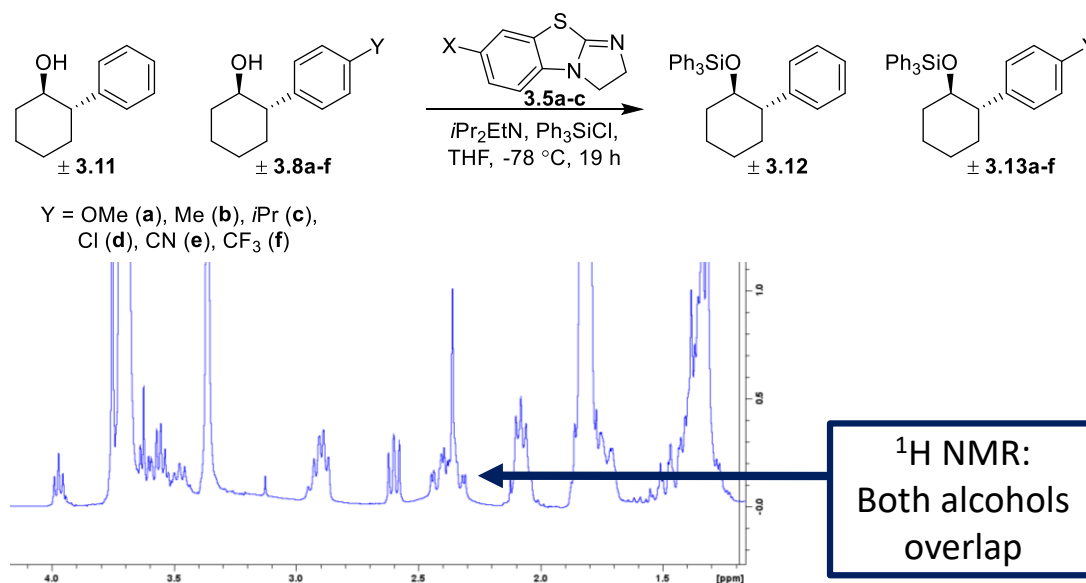
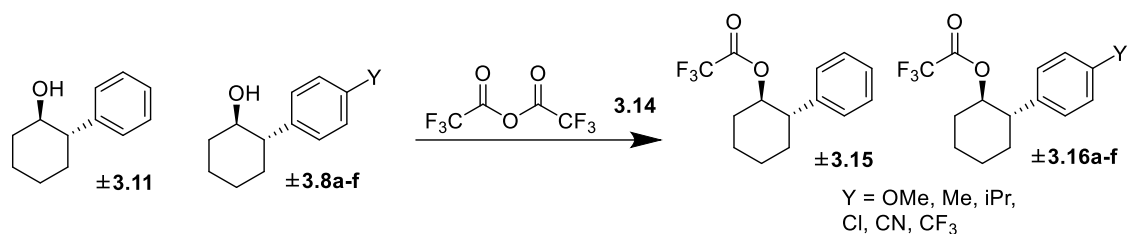


**Figure 3.10** Competition study crude  $^1\text{H}$  NMR of reaction mixture in  $\text{CDCl}_3$ .

be quenched and concentrated down, avoiding techniques such as extractions where material could be lost through multiple transfers.  $^1\text{H}$  NMR could not be used because the



**Scheme 3.8** Scheme of acylating alcohol derivatives to generate fluoro esters for  $^{19}\text{F}$  NMR.

unreacted alcohols and silylated ether peaks all overlap (Figure 3.10).  $^{19}\text{F}$  NMR is a sensitive, quantitative technique, that can provide distinct fluorine peaks even with small changes in structure.<sup>143,144</sup> We hypothesized that we could use fluorine NMR to quantitatively determine the conversion of each alcohol to product if we could introduce fluorine quantitatively into either the unreacted alcohols or the products. Trifluoroacetic anhydride is reagent that esterifies alcohols and reacts quickly and quantitatively at room temperature. We hypothesized that we could use trifluoroacetic anhydride **3.14**, to acylate the remaining alcohols at the end of our competition reaction to introduce fluorine into the molecule for  $^{19}\text{F}$  NMR (Scheme 3.8). Therefore, we took alcohols **3.11** and **3.18a-f**, acylated them with **3.14** to produce fluorinated esters **3.15** and **3.16a-f** and took  $^{19}\text{F}$  NMRs of **3.15** with each alcohol derivative to determine whether two distinctive peaks were seen for each acylated ester. Before running experiments, we also needed to verify full conversion of the alcohols to esters to ensure we would calculate accurate conversions. Therefore, we used  $^1\text{H}$  NMR to observe the singlet for alcohol **3.11** at 3.4 ppm before acylating and then after acylating. Figure 3.11 shows the peak at 3.4 ppm for the alcohol is not present after acylation, confirming full conversion of the alcohol to ester and showed a new peak at 5.1 ppm representing the acylated ester.

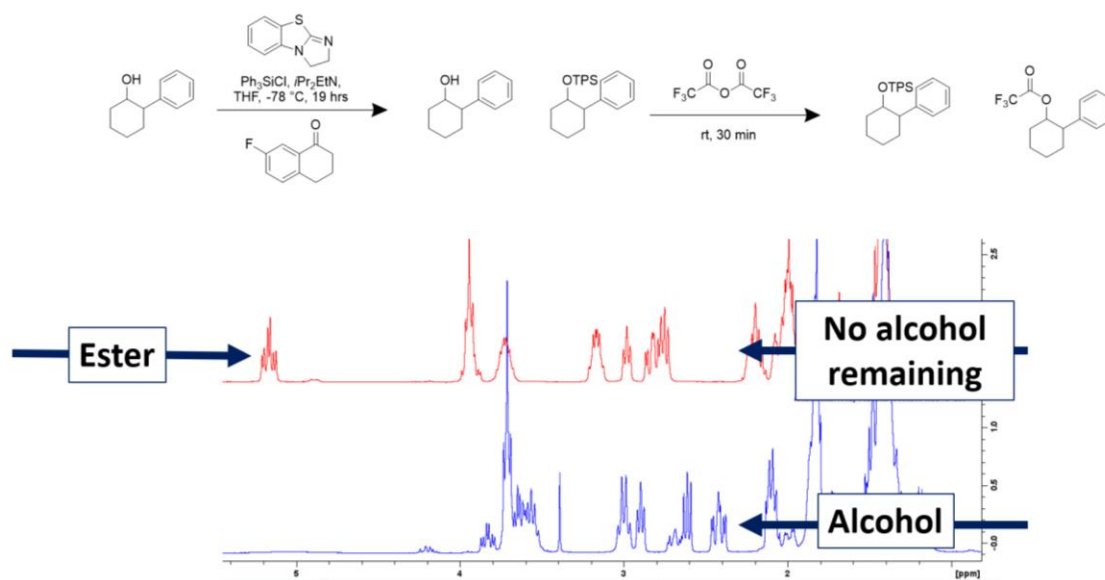
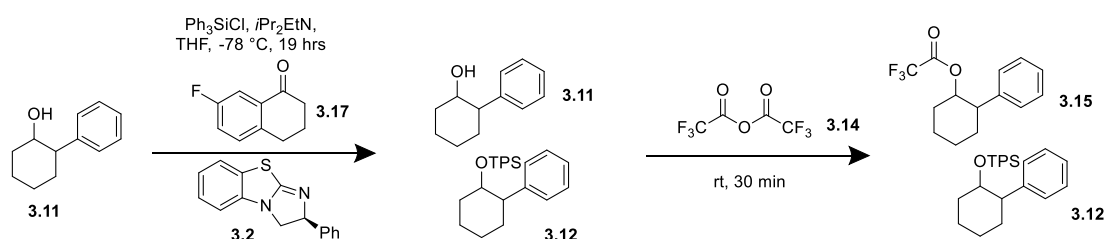


**Figure 3.11**  $^1\text{H}$  NMR comparison of crude reaction mixture before (bottom) and after (top) acylating unreacted alcohols in  $\text{CDCl}_3$ .

Once we verified the acylation of the alcohols to esters was quantitative under our reaction conditions, we did several control runs to observe the accuracy and reliability of the method. As mentioned above, the Wiskur group has thoroughly investigated the performance of chiral catalyst benzotetramisole (**3.2**).<sup>138139140</sup> Using previous studies and an internal standard, we could predict the conversion expected using this catalyst with our



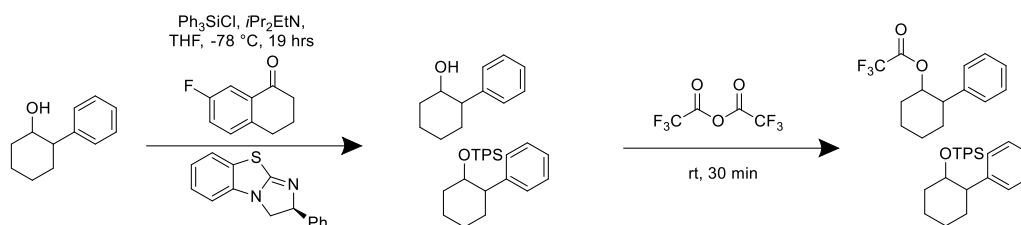
**Scheme 3.9** Controlled kinetic resolution with benzotetramisole catalyst **3.2** to generate acylated fluorinated esters.

reaction conditions (Scheme 3.9). We choose 7-fluoro-1-tetralone (**3.17**) as an internal standard because it has a singular fluorine peak that does not overlap with the acylated products or side products of the acylation. Since we limit the amount of  $\text{Ph}_3\text{SiCl}$  added and



the reaction time (19 h), we anticipated conversions between 30-45%. Table 3.6 depicts the results of two control runs **3.17** as a reference, achieving conversions within our expected ranges. Since only one alcohol is present, we could use both  $^1\text{H}$  NMR and  $^{19}\text{F}$  NMR to determine conversions and see that both are in close agreement. Therefore, we determined this method was reliable and consist for actual reaction runs. We proceeded

**Table 3.6** Control kinetic resolution runs with benzotetramisole catalyst.



Experiment	Catalyst	$^1\text{H}$ NMR conv	$^{19}\text{F}$ NMR conv
1	BTM	18%	18%
2	BTM	30%	25%

with our competition studies, again adding **3.17** for an internal standard (Table 3.7).

Looking at reaction rates, the methoxy **3.5a** and unsubstituted **3.5b** catalysts reflected consistently higher yields for each alcohol while chloro **3.5c** had consistently lower yields. Potentially, the electronics of the catalyst substituent could be influencing the nucleophilicity of the nucleophilic nitrogen with the electron withdrawing substituent (Cl) pulling electron density away from the nitrogen, reducing the yields. Therefore, the electron-donating methoxy catalyst has an increase in electron density, strengthening its nucleophilicity and generating higher yields.

Table 3.7 shows there was a general trend of donating groups on the alcohol having faster conversions and withdrawing groups on the alcohol having slower conversions. As the alcohol substituents become more electron-withdrawing, we see slower rates compared to alcohol **3.11**, resulting in rate ratios less than one for each catalyst except for methoxy

**Table 3.7** Results of competition study for catalyst and alcohol derivatives.

Y = OMe, Me, *i*Pr, Cl, CN, CF<sub>3</sub>

X = OMe, 3.5a					X = H, 3.5b					X = Cl, 3.5c				
Entry	Y	conv <sub>Y</sub> (%)	conv <sub>H</sub> (%)	K <sub>Y</sub> /K <sub>H</sub> <sup>b</sup>	Entry	Y	conv <sub>Y</sub> (%)	conv <sub>H</sub> (%)	K <sub>Y</sub> /K <sub>H</sub> <sup>b</sup>	Entry	Y	conv <sub>Y</sub> (%)	conv <sub>H</sub> (%)	K <sub>Y</sub> /K <sub>H</sub> <sup>b</sup>
1	OMe	10	10	1	7	OMe	19	14	1.4	13	OMe	8	8	1.5
2	Me	15	10	1.25	8	Me	15	16	1.1	14	Me	13	10	1.25
3	<i>i</i> Pr	14	14	1.1	9	<i>i</i> Pr	17	15	1.2	15	<i>i</i> Pr	14	12	1.23
4	Cl	18	12	1.58	10	Cl	23	23	1.0	16	Cl	7	4	0.94
5	CN <sup>c</sup>	25	32	0.68	11	CN <sup>c</sup>	11	16	0.66	17	CN <sup>c</sup>	8	13	0.60
6	CF <sub>3</sub>	17	14	1.3	12	CF <sub>3</sub>	18	23	0.78	18	CF <sub>3</sub>	14	17	0.85

<sup>a</sup>Conversions representative of two runs.

<sup>b</sup>Average of two runs.

<sup>c</sup>Cyano data average of four runs.

catalyst **3.5a**. We did expect this trend seen with **3.5b** and **3.5c** because we expected faster rates for the electron-donating alcohols because they contribute more electron density in the pi system, strengthening the expected cation pi interaction. However, we did not expect methoxy catalyst **3.5a** to show the opposite trend, where the more electron-withdrawing the alcohol, the greater the rate ratio. This suggested a cation pi interaction might not be the dominating or only interaction present in the reaction system. Although the catalyst has an electron-donating group, we should still see a decrease in rate ratio as the alcohols become less electron-donating because the pi system is more electron deficient in the cation pi interaction. If the cation pi interaction was the major contributing interaction, then we should still see similar trends as **3.5b** and **3.5c**, just a slower decrease in the rates. To

account for this difference in trend, we started looking at how the catalyst substituent could be interacting with the pi system of the alcohol, not just the cation, theorizing a pi-pi interaction could be more important in dictating the rate of the reaction. Using linear free

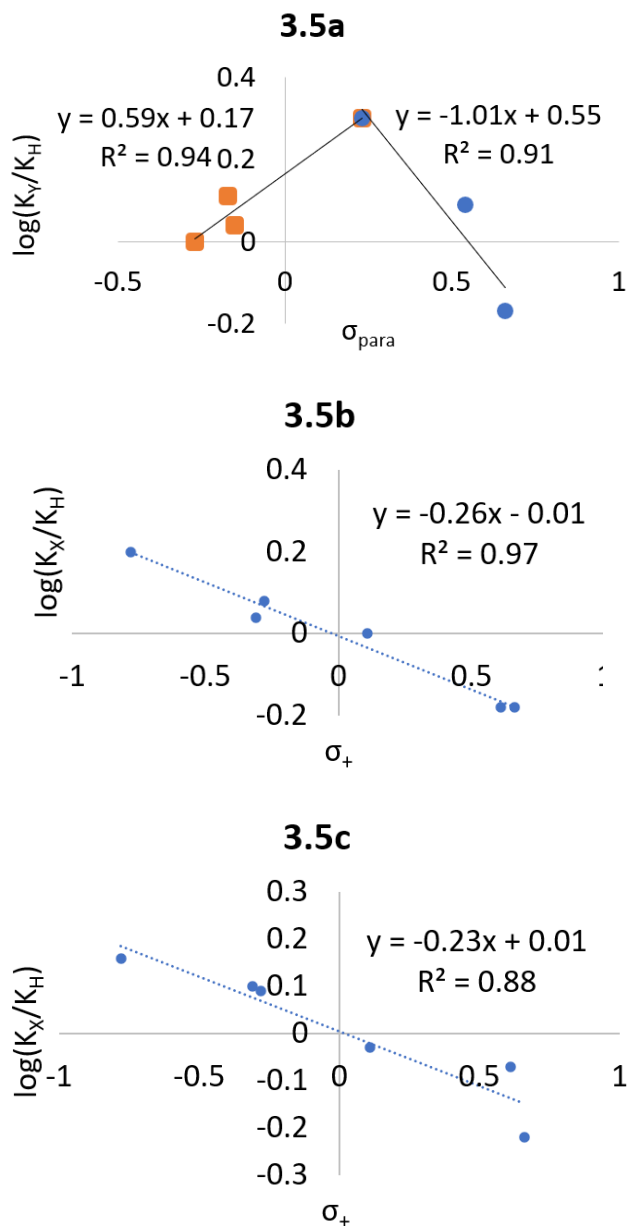


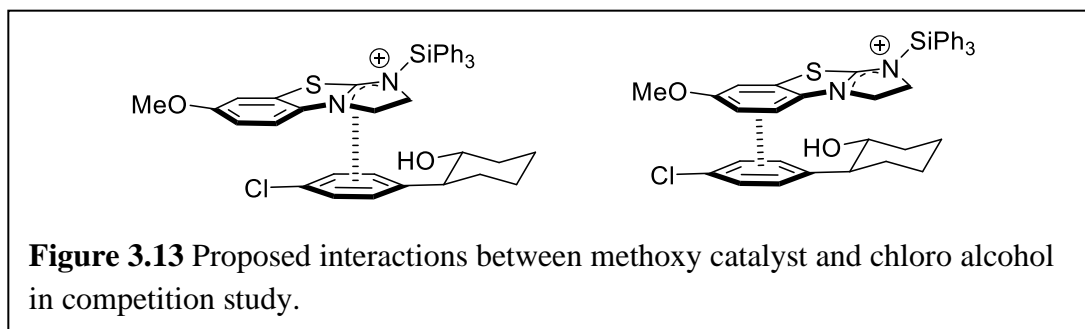
**Figure 3.12** Linear free energy relationship diagrams for **3.5a-c** using sigma plus constants.

energy relationship (LFER) diagrams, we started to explore alternate interactions to help explain this deviation from our hypothesis.

### 3.4.4 LFER studies

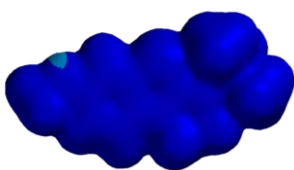
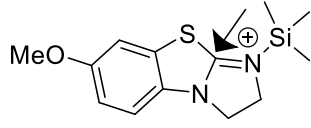
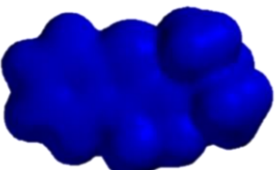
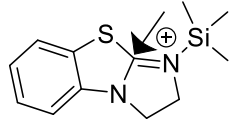
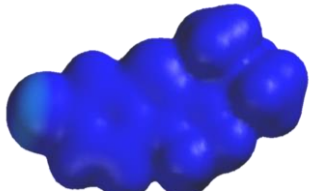
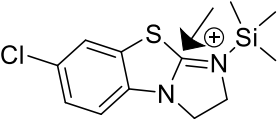
Using the rate ratios in Table 3.3, linear free energy relationship diagrams were generated for each of the three catalysts with sigma para constants for methoxy **3.5a** and sigma plus constants for unsubstituted (**3.5b**) and chloro (**3.5c**) catalysts and shown in Figure 3.12. As mentioned previously, linear free energy relationship diagrams help suggest what interaction (electrostatic, resonance, sterics, etc.) is most prevalent in a reaction.<sup>145</sup> In Figure 3.12, plus constants were used for **3.5b** and **3.5c** linear free energy diagrams, which are relevant for stabilizing cations through delocalization by resonance of the substituent.<sup>146</sup> Both catalysts showed a linear correlation with different electron-donating and -withdrawing groups, suggesting the delocalization by resonance in the phenyl group of the catalyst contributes to stabilizing the cation formed. For **3.5b** and **3.5c**, both catalysts showed similar slopes, suggesting the chloro substituent on the catalyst is not withdrawing enough to cause a major difference on the electrostatic interaction when compared to unsubstituted **3.5b**, which is validated by their similar sigma plus constants ( $H = 0$ ,  $Cl = 0.11$ ).<sup>147</sup> The negative slope reflects a buildup of positive charge in the reaction, which supports the theory that a positive charge is present in the reaction.<sup>148</sup> Looking at **3.5a**, the methoxy catalyst was plotted using sigma para constants, which are related to how the electron-withdrawing or -donating nature influence the resonance in the phenyl group. Interestingly, a bend was seen in the linear free energy relationship, which suggested a change in the reaction was occurring. For electron-donating alcohols and the chloro alcohol, we saw a positive slope, which indicates negative charge is present and can be explained by the strong electron-donating methoxy group on the catalyst aryl system. We believe the more electron-donating the alcohols became, a stronger repulsive

interaction was generated between the aryl groups of the alcohols and catalysts. Then, when the alcohols became increasingly withdrawing, a negative slope was generated, indicating a positive charge was present as seen with catalysts **3.5b** and **3.5c**. Therefore, the more electron-withdrawing the alcohols became, a repulsion between the cation and electron-deficient alcohols occurred. Consequently, we suggest two competing interactions are occurring: a cation pi interaction and a pi-pi interaction. The alcohol phenyl groups can interact with either the phenyl group the methoxy group is bonded to for the pi-pi interaction or the cation generated in the reaction to generate the cation pi interaction. The performance of the catalyst is then dependent on the compatibility of the electronics of the alcohol where we see the chloro alcohol provided the greatest ratio. We believe the weakly electron-withdrawing group can remove enough electron density from the alcohol pi system to minimize the repulsion of the catalyst aryl group but not withdrawing enough to generate a repulsion with the cation charge (Figure 3.13).



Additionally, we analyzed the electrostatic potential maps in Spartan16 software for the three catalysts as cations with trimethylsilyl in place of triphenylsilyl to analyze the charge distribution in the structure when the cation is formed (Table 3.8). Table 3.8 shows the electrostatic potential map for each catalyst cation and lists the values seen for the indicated alkene carbon adjacent to the positive nitrogen and the aryl ring of the catalysts. As expected, we see the alkene carbon adjacent to the cationic nitrogen increase in value

**Table 3.8** Electrostatic potential maps for each catalyst cation intermediate and the values for the indicated alkene carbon adjacent to the nitrogen and the aryl system.

 		 		 	
Carbon	Aryl Ring	Carbon	Aryl Ring	Carbon	Aryl Ring
375	254	383	267	395	289

\*Units are in kJ

as the substituent on the catalyst became more electron-withdrawing with the methoxy catalyst **3.5a** having the lowest value for electron density. This suggested the substituents do affect the electronics near the cation but most likely not enough to suppress the charge of the cation to avoid a repulsive interaction between the cation and an electron-withdrawing alcohol. We also see an increase in electron density in the aryl group the more electron-donating the substituent is on the catalyst, which is also expected. This could also support the idea of an increased repulsion between the aryl group of the catalyst and the pi system of the alcohols or a potential pi pi interaction between the alcohol substrates and catalyst intermediate, especially the alcohols that are more electron-donating.

Overall, the trends for all three catalysts, especially the methoxy catalyst, do suggest electronics of the substituents on the catalyst have major influence in these reactions. Comparing the linear free energy relationships of methoxy catalysts with the other two catalysts, we see a significant difference in how the catalysts interact with the substrates. Instead of an attractive interaction, such as cation pi, we believe repulsive

interactions are dictating how these reactions proceed. The electronics of the catalysts are extremely sensitive, as seen with the methoxy catalyst, and a delicate balance of minimizing the repulsive interactions that can occur with the aryl system and the cation of the catalyst intermediate is necessary for favorable outcomes in these reactions.

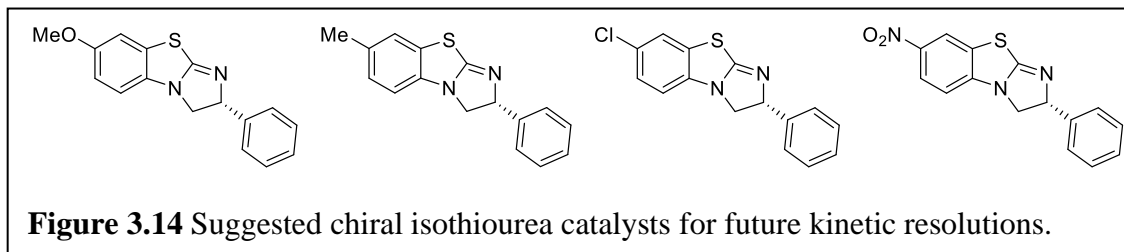
### **3.5 Conclusions and outlook**

In conclusion, electrostatic interactions are very important for these isothioureia catalysts for asymmetric catalysis. We see varying responses comparing the methoxy catalyst to the other two catalysts when the electronics of alcohol derivatives are modified, directly influencing the electrostatic interactions we believe are forming between the cationic catalyst intermediate and the pi system of the alcohols. Additionally, we see a change in slope for electron-donating methoxy catalyst versus the other catalysts, suggesting the believed cation-pi interaction is not the dominating interaction, or only interaction, dictating the selectivity in these reactions. Instead, we believe the methoxy catalyst is sensitive to the repulsive interactions that can occur between its pi system and the pi system of electron-donating alcohols as well as the repulsion between the catalyst intermediate cation and electron-withdrawing alcohols.

Future studies to continue analyzing these interactions should include electronically stronger catalysts. For example, a stronger electron-withdrawing group than chloride, such as nitro, trifluoromethyl, or cyano, is needed to more accurately see how this influences the reaction. Chlorine is very similar to hydrogen when looking at the sigma plus constants for the two, so a larger difference would be beneficial to better analyze electron-withdrawing effects on the catalyst. In theory, a larger difference in the linear free energy

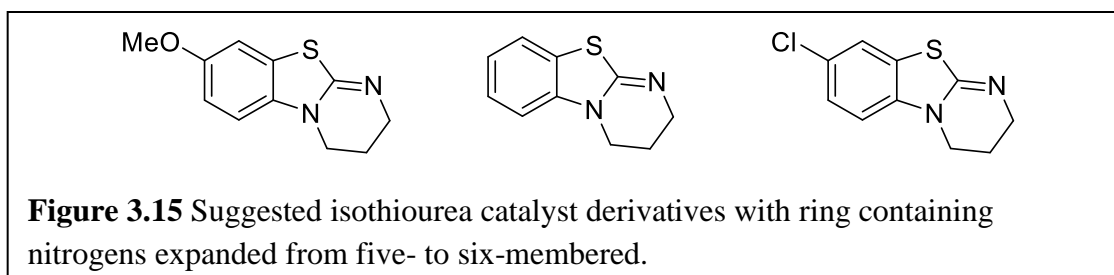
relationship slopes would be seen with the electron-withdrawing catalyst having a larger, steeper slope.

Another question is would similar trends in selectivity be seen if chiral versions of electronically-diverse catalysts were used (Figure 3.14). For many years, our lab has accepted the idea a cation pi interaction dictates the selectivity in our kinetic resolutions.



If we used the chiral version of the methoxy catalyst, would we also see a bend as we did in this study? If so, this would change future catalyst designs where more focus would be placed on compatible electronics between the alcohol and catalyst intermediate instead of a cation pi interaction. As seen with our methoxy catalyst **3.5a**, we would expect to see weakly electron-withdrawing alcohols, such as chloro, would generate better selectivities than electron-donating alcohols because the compatible electronics minimize the repulsive interactions between the two species.

It has also been shown that these benzotetramisole catalysts decompose during reactions and expanding the five membered ring containing the nucleophilic nitrogen (or imidazoline-based structure) to a six-membered ring (or tetrahydropyrimidine-based structure) has shown to better stabilize these catalysts, as seen in Hyperbenzotetramisole





as discussed previously (Figure 3.15).<sup>149</sup> Therefore, it would be worth investigating expanded forms of our derivatized benzotetramisole derivatives to see if improved conversions could be seen. Differences in selectivities have been reported between benzotetramisole and Hyperbenzotetramisole.<sup>149</sup> It would be informative to also conduct competition studies that studied the electronic interactions of these structures in addition to derivatizing the electronics to see if any differences are observed.

Since we predict two areas on the catalyst are influencing the responses seen with methoxy catalyst **3.5a**, it would be interesting to analyze how alcohols with multiple pi systems and varying electronics would respond. For example, if we used a secondary alcohol as shown in Figure 3.16 where two aryl groups are on either side of the secondary alcohol and had differing electronics, could we manipulate the electronics of the catalyst

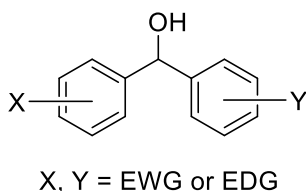


**Figure 3.16** Dual pi system of secondary alcohol for future competition studies

intermediate and alcohol to enhance their interactions as Smith did in his group's research on competing pi systems.<sup>136</sup> With the methoxy catalyst **3.5a**, we believe the catalyst intermediate has the two areas where repulsion can occur: the aryl system and the cation. Could we modify the two pi sites of the suggested alcohol in Figure 3.16 to where both aryl groups had attractive interactions with both sites on the catalyst intermediate was generated? For example, what if one ring had an electron-withdrawing group to interact with the catalyst intermediate aryl group and one had an electron-donating group to interact with the catalyst intermediate cation? Would the strength of these groups also produce

varying results? For **3.5a**, we saw the chloro alcohol had the most favorable electronics for the competition study, and we believe the alcohol is weakly withdrawing to where it removes enough electron density from its pi system without perturbing the catalyst cation. With a stronger electron-withdrawing group on the alcohol, a decrease in performance could result because the more positive charge produced from the decrease in electron density of the aryl ring could be large enough to repulse the cation. The bend seen with methoxy catalyst **3.5a** has raised many questions for how these catalysts interact with substrates and future studies will continue to explore these interactions to continue developing more efficient catalysts.

## **3.6 Experimental**

### **General Information**

All reactions were carried out under a N<sub>2</sub> atmosphere using oven dried glassware. Tetrahydrofuran and dichloromethane were dried by passing through a column of activated alumina before use and stored over molecular sieves. All other solvents and chemicals were obtained from commercial sources and used without further purification. Flash column chromatography was performed on silica gel (32–63 microns). <sup>1</sup>H NMR spectra were recorded on a Bruker Avance III (400 or 300 MHz). Chemical shifts are reported in ppm with TMS, chloroform, or methanol as an internal standard (TMS 0.00 ppm for <sup>1</sup>H and <sup>13</sup>C, CHCl<sub>3</sub> 7.26 ppm and 77.16 for <sup>1</sup>H and <sup>13</sup>C, and MeOH 3.31 ppm and 49.3 ppm for <sup>1</sup>H and <sup>13</sup>C respectively). <sup>13</sup>C NMR spectra were recorded on a Bruker Avance III (101 or 75 MHz) with complete proton decoupling. <sup>19</sup>F NMR spectra were recorded on a Bruker Avance III (400 or 300 MHz). Chemical shifts are reported with 7-fluoro-1-tetralone as an internal standard when stated. The data reported for <sup>1</sup>H NMR are as follows: chemical shift,

multiplicity (s = singlet, d = doublet, t = triplet, q = quartet, dd = doublet of doublet, td = triplet of doublets, dt = doublet of triplet, sept = septet, m = multiplet).

*General Procedure A for substituted benzothiazole addition of aminoalcohol (3.7a-c)*

To a 100 mL pressurized tube, the substituted benzothiazole (**3.6a-c**) was added (1 mmol) with stir bar, ethanol amine (1.1 equiv), diisopropylethylamine (2 equiv), and dry THF (3 mL) under N<sub>2</sub>. The tube was sealed under N<sub>2</sub> and stirred at 130 °C for 24 h, unless specified below. The solution was cooled to room temperature and washed with brine (1x, 3 mL) and dichloromethane (2x, 3 mL). The combined organic layers were dried with NaSO<sub>4</sub> and concentrated under vacuum to obtain the resulting product that was further purified by column chromatography.

*General Procedure B for ring-closure of benzothiazole (3.5a-c)*

To a 15 mL round bottom flask, the purified product of Procedure A (**3.7a-c**) was added to a solution of methylene chloride (5 mL) and triethylamine (4.3 equiv) under N<sub>2</sub> and cooled to 0 °C. After 20 minutes at 0 °C, methane sulfonyl chloride (2.5 equiv) was added under N<sub>2</sub> and the solution stirred at 0 °C for 1 hour. Once the solution warmed to room temperature, triethylamine (10 equiv) was added under N<sub>2</sub> and the solution refluxed at 40 °C for 24 hours. The solution cooled to room temperature and was washed with saturated sodium hydroxide (1x, 3 mL) and methylene chloride (2x, 3 mL). The collected organic layer was dried with NaSO<sub>4</sub> and concentrated under vacuum. The resulting solid was purified by column chromatography.

*Methoxy step 1, 3.7a*

Procedure A was followed for **3.7a**, with the tube stirring at 130 °C for 48 h. Purification was achieved by column chromatography (silica gel, gradient of 15% *i*PrOH/hexanes) to give a white solid. Yield: 68%. <sup>1</sup>H NMR (300 MHz, CDCl<sub>3</sub>) δ (ppm): 7.8939 (d, 1 H), 7.1772 (d, 1 H), 6.8950 (dd, *J* = 11.4, 1 H), 3.7853 (s, 3 H), 3.7545 (t, 2 H), 3.5207 (t, 2 H).

*Methoxy step 2, 3.5a*

Procedure B was followed for **3.5a**. Purification was achieved by column chromatography (silica gel, 1% NH<sub>3</sub> saturated MeOH/CHCl<sub>3</sub>) to give a light yellow solid. Yield: 83%. <sup>1</sup>H NMR (300 MHz, CDCl<sub>3</sub>) δ (ppm): 7.4623 (d, 1 H), 7.2501 (dd, *J* = 10.4, 1 H), 4.2705 (t, 2 H), 3.9197 (t, 2 H), 3.7845 (s, 3 H).

*Hydrogen step 1, 3.6b*

Procedure A was followed for **3.6b**. Purification was achieved by column chromatography (silica gel, gradient of 100% CH<sub>2</sub>Cl<sub>2</sub> to 50% *i*PrOH/CH<sub>2</sub>Cl<sub>2</sub>) to give a white solid. Yield: 81%. <sup>1</sup>H NMR (300 MHz, CDCl<sub>3</sub>) δ (ppm): 7.5207 (d, 1 H), 7.3848 (d, 1 H), 7.2034 (t, 1 H), 7.0057 (t, 1 H), 3.7346 (t, 2 H), 3.5162 (t, 2 H).

*Hydrogen step 2, 3.5b*

Procedure B was followed for **3.5b**. Purification was achieved by column chromatography (silica gel, 1% NH<sub>3</sub> saturated MeOH/EtOAc) to give a light yellow solid. Yield: 66%. <sup>1</sup>H NMR (300 MHz, CDCl<sub>3</sub>) δ (ppm): 7.4140 (d, 1 H), 7.2724 (t, 1 H), 7.0335 (t, 1 H), 6.8957 (d, 1 H), 4.3081 (t, 2 H), 3.9730 (t, 2 H).

*Chloro step 1, 3.7c*

Procedure A was followed for **3.7c**. Purification was achieved by column chromatography (silica gel, gradient of 30% *i*PrOH/hexanes) to give a white solid. Yield: 83%. <sup>1</sup>H NMR (300 MHz, CDCl<sub>3</sub>) δ (ppm): 7.5723 (d, 1 H), 7.3525 (d, 1 H), 7.7172 (dd, *J* = 8.6, 1 H), 3.7786 (t, 2 H), 3.5608 (t, 2 H).

*Chloro step 2, 3.5c*

Procedure B was followed for **3.5c**. Purification was achieved by column chromatography (silica gel, 10% THF/CHCl<sub>3</sub>) to give a white solid. Yield: 61%. <sup>1</sup>H NMR (300 MHz, CDCl<sub>3</sub>) δ (ppm): 7.4649 (d, 1 H), 7.2527, (dd, *J* = 10.5, 1 H), 6.8438 (d, 1 H), 4.3124 (t, 2 H), 3.9494, (t, 2 H).

*General Procedure C for alcohols 3.8a-c*

Magnesium turnings (1.8 equiv) was weighed on weigh paper and transferred and crushed with pestle and mortar. The magnesium was then transferred to a flame-dried 100 mL round bottom flask and then flame-dried again with the magnesium in the flask. The round was capped with a rubber stopper and 10 mL of dry THF was added under nitrogen. The substituted bromoalcohol (1.5 equiv) was added to the round bottom under nitrogen. The solution stirred at 40 °C for one hour and was then cooled to room temperature. A solution of copper (I) iodide (0.15 equiv) and cyclohexane oxide (1 equiv) was prepared in 10 mL of THF under nitrogen in a 4-dram vial, and the resulting slurry was added to the round bottom flask dropwise under nitrogen. The solution stirred at room temperature overnight. The reaction was quenched with saturated ammonium chloride (15 mL) and stirred for 30 minutes when no solid was seen at the bottom of the flask. The organic layer

was removed, dried with sodium sulfate, and concentrated to a solid. The solid was then purified by column chromatography (silica gel, on a gradient from 5% EtOAc/Hexanes to 25% EtOAc/Hexanes).

*Methoxy alcohol 3.8a*

Yield: 59%. %. <sup>1</sup>H NMR (300 MHz, CDCl<sub>3</sub>) δ (ppm): 7.33-7.15 (m, 2 H), 6.94-6.87 (m, 2 H), 3.82 (s, 3 H), 3.68-3.56 (m, 1 H), 2.47-2.33 (m, 1 H), 2.18-2.05 (m, 1 H), 1.95-1.70 (m, 3 H), 1.63-1.23 (m, 5 H).

*Methyl alcohol 3.8b*

Yield: 56%. %. <sup>1</sup>H NMR (300 MHz, CDCl<sub>3</sub>) δ (ppm): 7.26-7.14 (d, 4 H), 3.74-3.60 (m, 1 H), 2.49-2.30 (m, 4 H), 2.22-2.08 (m, 1 H), 1.94-1.72 (m, 3 H), 1.58-1.25 (m, 4 H).

*Isopropyl alcohol 3.8c*

Yield: 53%. %. <sup>1</sup>H NMR (300 MHz, CDCl<sub>3</sub>) δ (ppm): 7.2107 (s, 4 H), 3.6633 (m, 1 H), 3.01-2.81 (m, 1 H), 2.51-2.35 (m, 1 H), 2.20-2.06 (m, 1 H), 1.98-1.71 (m, 3 H), 1.69-1.17 (m, 10 H).

*General Procedure D for alcohols 3.8d-f*

In a flame-dried flask, the substituted bromobenzene (1.2 equiv) was added with 10 mL of dry THF with stir bar under nitrogen. The solution stirred for 15 minutes in a dry ice/acetone bath to cool -78 °C. Once at -78 °C, n-BuLi (1 equiv) was added under nitrogen and the solution stirred for one hour. Cyclohexane oxide (1 equiv) was added under nitrogen with the flask still at -78 °C. Then BF<sub>3</sub>·OEt<sub>2</sub> was added drop-wise, and the solution stirred for 4 hours at -78 °C. The reaction was quenched with NH<sub>4</sub>Cl solution (15 mL) and

stirred for 30 minutes. The organic layer was collected, dried with sodium sulfate, and concentrated to a solid. The solid was then purified by column chromatography (silica gel, on a gradient from 5% EtOAc/Hexanes to 25% EtOAc/Hexanes).

*Chloro alcohol 3.8d*

Yield: 40%. <sup>1</sup>H NMR (300 MHz, CDCl<sub>3</sub>) δ (ppm): 7.33-7.19 (m, 4 H), 3.71-3.58 (m, 1 H), 2.49-2.36 (m, 1 H), 2.15-2.02 (m, 1 H), 1.92-1.69 (m, 3 H), 1.61-1.26 (m, 4 H).

*Cyano alcohol 3.8e*

Yield: 15%. <sup>1</sup>H NMR (300 MHz, CDCl<sub>3</sub>) δ (ppm): 7.65 (d, 2 H), 7.39 (d, 2 H), 3.79-3.65 (m, 1 H), 2.60-2.49 (m, 1 H), 2.19-2.10 (m, 1 H), 1.95-1.76 (m, 3 H), 1.59-1.29 (m, 4 H).

*Trifluoromethyl alcohol 3.8f*

Yield: 57%. <sup>1</sup>H NMR (300 MHz, CDCl<sub>3</sub>) δ (ppm): 7.63-7.57 (d, 2 H), 7.45-7.35 (d, 2 H), 3.80-3.66 (m, 1 H), 2.62-2.48 (m, 1 H), 2.21-2.09 (m, 1 H), 1.98-1.75 (m, 3 H), 1.53-1.24 (m, 4 H).

*General Procedure E for competition studies*

A flame-dried 1 dram vial with oven-dried stir bar and activated 4Å molecular sieves was purged with nitrogen and sealed with a septa. A stock solution of tran-2-phenylcyclohexanol (1.6 mmol in 1 mL) was prepared under nitrogen and 0.125 mL was transferred to the 1-dram vial under nitrogen. A stock solution was prepared for the substituted alcohol (1.6 mmol in 1 mL), and 0.125 mL was transferred to the 1-dram vial under nitrogen. A stock solution of 7-fluoro-1-tetralone (1 mmol in 1 mL) was prepared

and 0.1 mL was transferred to the 1-dram vial under nitrogen. A stock solution of the catalyst was prepared and 0.1 mmol was transferred to the 1-dram vial.

Diisopropylethylamine was added to the 1-dram vial under nitrogen. THF was added under nitrogen to reach a total volume of 0.7 mL. The sides and top of the 1-dram were sealed with electric tape, and the 1-dram was placed in an isopropanol bath and cooled to -78 °C for 30 minutes. The cooled mixture was treated with a 0.67 M solution of triphenylsilylchloride in THF (0.3 mL, 0.20 mmol) and was left to react for 19 hours at -78 °C, then quenched with 0.5 mL of methanol. The solution was left to warm to room temperature and then concentrated under vacuum. Crude  $^1\text{H}$  NMRs in deuterated chloroform were taken of the resulting solid, and the NMR solution was placed back in the 1-dram vial and concentrated under vacuum again. Trifluoroacetic anhydride (1 mL) was added to the 1-dram, and the solution stirred at room temperature for 30 minutes. The solution was concentrated under vacuum for  $^1\text{H}$  and  $^{19}\text{F}$  NMRs in deuterated chloroform without purification.



## REFERENCES

- 
- <sup>1</sup> Michelin, C.; Hoffmann, N. Photosensitization and Photocatalysis - Perspectives in Organic Synthesis. *ACS Catal.* **2018**, 8 (12), 12046–12055.
- <sup>2</sup> Nicewicz, D. A.; MacMillan, D. W. C. Merging Photoredox Catalysis with Organocatalysis: The Direct Asymmetric Alkylation of Aldehydes, *Science*, **2008**, 322 (5898), 77.
- <sup>3</sup> Ischay, M. A.; Anzovino, M. E.; Du, J.; Yoon, T. P. Efficient Visible Light Photocatalysis of [2+2] Enone Cycloadditions, *J. Am. Chem. Soc.*, **2008**, 130 (39), 12886.
- <sup>4</sup> Furst, L.; Matsuura, B. S.; Narayanam, J. M. R.; Tucker, J. W.; Stephenson, C. R. J. Visible light-mediated intermolecular C-H functionalization of electron-rich heterocycles with malonates, *Org. Lett.*, **2010**, 12(13), 3104-3107.
- <sup>5</sup> Shaw, M. H.; Twilton, J. MacMillan, D. W. C. Photoredox Catalysis in Organic Chemistry, *J. Org. Chem.*, **2016**, 81 (16), 6898-6926.
- <sup>6</sup> Staveness, D.; Bosque, I.; Stephenson, C. R. J. Free Radical Chemistry Enabled by Visible Light-Induced Electron Transfer, *Acc. Chem. Res.*, **2016**, 49 (10) 2295-2306.
- <sup>7</sup> Douglas, J. J.; Sevrin, M. J.; Stephenson, C. R. J. Visible Light Photocatalysis: Applications and New Disconnections in the Synthesis of Pharmaceutical Agents, *Org. Process. Res. Dev.*, **2016**, 20 (7), 1134-1147.

- 
- <sup>8</sup> Narayanam, J. M. R.; Stephenson, C. R. J. Visible light photoredox catalysis: applications in organic synthesis, *Chem. Soc. Rev.*, **2011**, *40*, 102-113.
- <sup>9</sup> Kelly, C. B.; Patel, N. R.; Primer, D. N.; Jouffroy, M.; Tellis, J. C.; Molander, G. A., Preparation of visible-light-activated metal complexes and their use in photoredox/nickel dual catalysis, *Nat. Protoc.*, **2017**, *12*, 472-492.
- <sup>10</sup> Prier, C. K.; Rankic, D. A.; MacMillan, D. W. C., Visible Light Photoredox Catalysis with Transition Metal Complexes: Applications in Organic Synthesis, *Chem. Rev.*, **2013**, *113* (7), 5322-5363.
- <sup>11</sup> Lee, Y.; Kwon, M. S. Emerging Organic Photoredox Catalysts for Organic Transformations, *Eur. J. Org. Chem.*, **2020**, 2020 (38), 6028-6043.
- <sup>12</sup> Mancheño, O. G. Visible light-mediated organophotocatalyzed C-H bond functionalization reactions, *Org. Biomol. Chem.*, **2019**, *22*, 5475-5489.
- <sup>13</sup> Sideri, I. K.; Voutyritsa, E.; Kokotos, C. G. Photoorganocatalysis, small organic molecules and light in the service of organic synthesis: the awakening of a sleeping giant, *Org. Biomol. Chem.*, **2018**, *25*, 4596-4614.
- <sup>14</sup> Fujitsuka, M.; Majima, T. Photoinduced Electron Transfer of Porphyrin Isomers: Impact of Molecular Structures on Electron-Transfer Dynamics, *Chem. Asian J.*, **2015**, *10* (11), 2320-2326.
- <sup>15</sup> Tlili, A.; Lakhdar, S. Acridinium Salts and Cyanoarenes as Powerful Photocatalysts: Opportunities in Organic Synthesis, *Angew. Chem. Int. Ed.*, **2021**, online.
- <sup>16</sup> Kotaskova, M.; Osman, O.; Helm, M. Synthesis of new asymmetric xanthene dyes via catalyst-free S<sub>N</sub>Ar with sulfur nucleophiles, *Org. Biomol. Chem.*, **2014**, *12*, 3816.

- 
- <sup>17</sup> Morse, P. D.; Nguyen, T. M.; Cruz, C. L.; Nicewicz, D. A. Enantioselective counter-anions in photoredox catalysis: The asymmetric cation radical Diels-Alder reaction, *Tetrahedron*, **2018**, 74 (26), 3266-3272.
- <sup>18</sup> Mateos, J.; Cuadros, S.; Vega-Peñaloza, A.; Dell'Amico, L. Unlocking the Synthetic Potential of Light-Excited Aryl Ketones: Applications in Direct Photochemistry and Photoredox Catalysis, *Synlett*, **2021**, *online*.
- <sup>19</sup> Segado, M.; Reguero, M. Mechanism of the photochemical process of singlet oxygen production by phenalenone, *Phys. Chem. Chem. Phys.*, **2011**, 13, 4138-4148.
- <sup>20</sup> Pitre, S. P.; McTiernan, C. D.; Scaiano, J. C. Understanding the Kinetics and Spectroscopy of Photoredox Catalysis and Transition-Metal-Free Alternatives, *Acc. Chem. Res.*, **2016**, 49 (6), 1320-1330.
- <sup>21</sup> Bonfils, P. D.; Péault, L.; Nun, P.; Coeffard, V. State of the Art of Bodipy-Based Photocatalysts in Organic Synthesis, *Eur. J. Org. Chem.*, **2021**, 2021 (12), 1809-1824.
- <sup>22</sup> Neumann, M.; Földner, S.; Burkhard, K.; Zeitler, K. Metal-Free, Cooperative Asymmetric Organophotoredox Catalysis with Visible Light, *Angew. Chem. Int. Ed.*, **2011**, 50 (4), 951-954.
- <sup>23</sup> Hedstrand, D. M.; Kruizinga, W. H.; Kellogg, R. M. Light induced and dye accelerated reductions of phenacyl onium salts by 1,4-dihydropyridines, *Tetrahedron Lett.*, **1978**, 19 (14), 1255-1258.
- <sup>24</sup> Hari, D. P.; König, B. Eosin Y Visible Light Oxidative C-C and C-P bond Formation, *Org. Lett.*, **2011**, 13 (15), 3852-3855.

- 
- <sup>25</sup> Kee, C. W.; Chan, K. M.; Wong, M. W.; Tan, C. Selective Bromination of  $sp^3$  C—H Bonds by Organophotoredox Catalysis, *Asian J. Org. Chem.*, **2013**, 3 (4), 536-544.
- <sup>26</sup> Hari, D. P.; Schroll, P.; König, B. Metal-Free, Visible-Light-Mediated Direct C-H Arylation of Heteroarenes with Aryl Diazonium Salts, *J. Am. Chem. Soc.*, **2012**, 134 (6), 2958-2961.
- <sup>27</sup> Bosveli, A.; Montagnon, T.; Kalaitzakis, D.; Vassilikogiannakis, G. Eosin: a versatile organic dye whose synthetic uses keep expanding, *Org. Biomol. Chem.*, **2021**, 19, 3303.
- <sup>28</sup> Majek, M.; Filace, F.; Jacobi von Wangelin, A. On the mechanism of photocatalytic reactions with eosin Y, *Beilstein J. Org. Chem.*, **2014**, 10, 981-989.
- <sup>29</sup> Bobo, M. V.; Arcidiacono, A. M.; Ayare, P. J.; Reed, J. C.; Helton, M. R.; Ngo, T.; Hanson, K.; Vannucci, A. K. A Series of Green Light Absorbing Organic Photosensitizers Capable of Oxidative Quenching Photocatalysis, *ChemPhotoChem*, **2021**, 5 (1), 51-57.
- <sup>30</sup> Zhao, J.; Xu, K.; Yang, W.; Wang, Z.; Zhong, F. The triplet state of Bodipy: formation, modulation and application, *Chem. Soc. Rev.*, **2015**, 44, 8904.
- <sup>31</sup> Bumagina, N. A.; Kritskaya, A. Y.; Antina, E. V.; Berezin, M. B.; V'yugin, A. I. Effect of Alkyl, Aryl, and *meso*-Aza Substitution on the Thermal Stability of BODIPY, *Russ. J. Inorg. Chem.*, **2018**, 63, 1326-1332.
- <sup>32</sup> Yang, L.; Simionescu, Y. R.; Lough, A.; Yan, H. Some observations relating to the stability of the BODIPY fluorophore under acidic and basic conditions, *Dyes Pigm.*, **2011**, 91, 264-267.

- 
- <sup>33</sup> Wang, M.; Vicente, M. G. H.; Mason, D.; Bobadova-Parvanova, P. Stability of a Series of BODIPYs in Acidic Conditions: An Experimental and Computational Study into the Role of the Substituents at Boron, *ACS Omega*, **2018**, 3 (5), 5502-5510.
- <sup>34</sup> Gabe, Y.; Urano, Y.; Kikuchi, K.; Kojima, H.; Nagano, T. Highly Sensitive Fluorescence Probes for Nitric Oxide Based on Boron Dipyrromethene Chromophore-Rational Design of Potentially Useful Bioimaging Fluorescence Probe, *J. Am. Chem. Soc.*, **2004**, 126, 3357-3367.
- <sup>35</sup> Kollmannsberger, M.; Rurack, K.; Resch-Genger, U.; Daub, J. Ultrafast Charge Transfer in Amino-Substituted Boron Dipyrromethene Dyes and Its Inhibition by Cation Complexation: A New Design Concept for Highly Sensitive Fluorescent Probes, *Phys. Chem. A*, **1998**, 102 (50), 10211-10220.
- <sup>36</sup> Zhang, D.; Wen, Y.; Xiao, Y.; Yu, G.; Liu, Y.; Qian, X. Bulky 4-tritylphenylethynyl substituted boradiazaindacene: pure red emission, relatively large Stokes shift and inhibition of self-quenching, *Chem. Commun.*, **2008**, 39, 4777-4779.
- <sup>37</sup> Juris, A.; Balzani, V.; Belser, P.; von Zelewsky, A. Characterization of the Excited State Properties of Some New Photosensitizers of the Ruthenium (Polypyridine) Family, *Helv. Chim. Acta*, **1981**, 64 (7), 2175-2182.
- <sup>38</sup> Zhao, J.; Xu, K.; Yang, W.; Zhong, F. The triplet excited state of Bodipy: formation, modulation and application, *Chem. Soc. Rev.*, **2015**, 44, 8904-8939.
- <sup>39</sup> Huang, L.; Zhao, J. Iodo-Bodipys as visible-light-absorbing dual-functional photoredox catalysts for preparation of highly functionalized organic compounds by

---

formation of C-C bonds via reductive and oxidative quenching catalytic mechanisms, *RSC Adv.*, **2013**, 3, 23377.

<sup>40</sup> Bassan, E.; Gualandi, A.; Cozzi, P. G.; Ceroni, P. Design of BODIPY dyes as triplet photosensitizers: electronic properties tailored for solar energy conversion, photoredox catalysis and photodynamic therapy, *Chem. Sci.*, **2021**, 12, 6607.

<sup>41</sup> Dissanayake, K. C.; Ebukuyo, P. O.; Dhahir, Y. J.; Wheeler, D.; He, H. A BODIPY-functionalized Pd<sup>II</sup> photoredox catalyst for Sonogashira C-C cross-coupling reactions, *Chem. Commun.*, **2019**, 55, 4973-4976.

<sup>42</sup> Wang, D.; Malmberg, R.; Pernik, I.; Prasad, S. K. K.; Roemer, M.; Venkatesan, K.; Schmidt, T. W.; Keaveney, S. T.; Messerle, B. A. Development of tethered dual catalysts: synergy between photo- and transition metal catalysts for enhanced catalysis, *Chem. Sci.*, **2020**, 11, 6256-6267.

<sup>43</sup> Wang, D.; Solomon, N. S. D.; Pernik, I.; Messerle, B. A.; Keaveney, S. T. Development of a Tethered Palladium-BODIPY Dual Catalysis for Enhanced Photo- and Thermally Activated Catalysis, and for Promoting Sequential Reactivity, *Aust. J. Chem.*, **2020**, 73, 979-986.

<sup>44</sup> Wang, D.; Pernik, I.; Keaveney, S. T.; Messerle, B. A. Understanding the Synergistic Effects Observed When Using Tethered Dual Catalysts for Heat and Light Activated Catalysis, *ChemCatChem*, **2020**, 12 (20), 5091-5097.

<sup>45</sup> Cranston, R. R.; Vebber, M. C.; Berbigier, J. F.; Rice, N. A.; Tonnelé, C.; Comeau, Z. J.; Boileau, N. T.; Brusso, J. L.; Shuhendler, A. J.; Castet, F.; Muccioli, J.; Kelly, T. L.; Lessard, B. H. Thin-Film Engineering of Solution-Processed n-Type Silicon

---

Phthalocyanines for Organic Thin-Film Transistors, *ACS Appl. Mater. Interfaces*, **2021**, *13* (1), 1008-1020.

<sup>46</sup> Mitra, K.; Hartman, M. C. T. Silicon phthalocyanines: synthesis and resurgent applications, *Org. Biomol. Chem.*, **2021**, *19*, 1168.

<sup>47</sup> Liu, M.; Li, C. Recent Advances in Activatable Organic Photosensitizers for Specific Photodynamic Therapy, *ChemPlusChem*, **2020**, *85* (5), 948-957.

<sup>48</sup> Cranston, R. R.; Vebber, M. C.; Tonné, T.; Castet, F.; Muccioli, L.; Brusso, J. L.; Lessard, B. H. N-Type Solution-Processed Tin versus Silicon Phthalocyanines: A Comparison of Performance in Organic Thin-Film Transistors and in Organic Photovoltaics, *ACS Appl. Electron. Mater.*, **2021**, *3* (4), 1873-1885.

<sup>49</sup> Lessard, B. H. The Rise of Silicon Phthalocyanine: From Organic Photovoltaics to Organic Thin Film Transistors, *ACS Appl. Mater. Interfaces*, **2021**, *13*, 31321-31330.

<sup>50</sup> Grant, T. Synthetically facile organic solar cells with >4% efficiency using P3HT and a silicon phthalocyanine non-fullerene acceptor, *Materials Advances*, **2021**, *2*, 2594-2599.

<sup>51</sup> Stokov, K.; Schäfer, A.; Dobrindt, U.; Galstyan, A. Facile Fabrication of Silicon (IV) Phthalocyanine-Embedded Poly(vinyl alcohol)-Based Antibacterial and Antifouling Interfaces, *ACS Appl. Bio Mater.*, **2020**, *3* (6), 3751-3760.

<sup>52</sup> Cheng, G.; Peng, X.; Hao, G.; Kennedy, V. O.; Ivanov, I. N.; Knappenberger, K.; Hill, T. J.; Rodgers, M. A. J.; Kenney, M. E. Synthesis, Photochemistry, and Electrochemistry of a Series of Phthalocyanines with Graded Steric Hindrance, *J. Phys. Chem. A.*, **2003**, *107* (18), 3503-3514.

- 
- <sup>53</sup> Vebber, M. C.; Grant, T. M.; Brusso, J. L.; Lessard, B. H. Bis(trialkylsilyl oxide) Silicon Phthalocyanines: Understanding the Role of Solubility in Device Performance as Ternary Additives in Organic Photovoltaics, *Langmuir*, **2020**, *36* (10), 2612-2621.
- <sup>54</sup> Lessard, B. H.; White, R. T.; AL-Amar, M.; Plint, T.; Castrucci, J. S.; Josey, D. S.; Lu, Z.-H.; Bender, T. P. Assessing the Potential Roles of Silicon and Germanium Phthalocyanines in Planar Heterojunction Organic Photovoltaic Devices and How Pentafluoro Phenoxylation Can Enhance  $\pi$ - $\pi$  Interactions and Device Performance, *ACS Appl. Mater. Interfaces*, **2015**, *7* (9), 5076-5088.
- <sup>55</sup> Ma, D.; Pan, S.; Zhang, T.; Huang, B.; Xie, S.; Yang, H.; Peng Y. Comparison of multiple terminal functional groups dendrimer silicon(IV) phthalocyanines: Photoinduced electron/energy transfer and electrochemical properties, *Dyes and Pigments*, **2016**, *127*, 78-86.
- <sup>56</sup> Liu, M.; Li, C. Recent Advances in Activatable Organic Photosensitizers for Specific Photodynamic Therapy, *ChemPlusChem*, **2020**, *85* (5), 948-957.
- <sup>57</sup> Anderson, E. D.; Gorka, A. P.; Schernmann, M. J. Near-infrared uncaging or photosensitizing dictated by oxygen tension, *Nature*, **2016**, *7*, 13378.
- <sup>58</sup> Huang, J.; Wu, Y.; Wang, D.; Ma, Y.; Yue, Z.; Lu, Y.; Zhang, M.; Zhang, Z.; Yang, P. Silicon Phthalocyanine Covalently Functionalized N-Doped Ultrasmall Reduced Graphene Oxide Decorated with Pt Nanoparticles for Hydrogen Evolution from Water, *ACS Appl. Mater. Interfaces*, **2015**, *7* (6), 3732-3741.
- <sup>59</sup> Xiao, B.; Zhu, M.; Li, X.; Yang, P.; Qiu, L.; Lu, C. A stable and efficient photocatalytic hydrogen evolution system based on covalently linked silicon-



---

phthalocyanine-graphene with surfactant, *Int. J. Hydrog. Energy*, **2016**, *41* (27), 11537-11546.

<sup>60</sup> Yang, J.; Wang, D.; Han, H.; Li, C. Roles of Cocatalysts in Photocatalysis and Photoelectrocatalysis, *Acc. Chem. Res.*, **2013**, *48* (6), 1900-1909.

<sup>61</sup> Zhu, M.; Li, Z.; Xiau, B.; Lu, Y.; Du, Y.; Yang, P., et al. Surfactant assistance in improvement of photocatalytic hydrogen production with the porphyrin noncovalently functionalized graphene nanocomposite, *ACS Appl. Mater. Interfaces*, **2013**, *5* (5), 1732-1740.

<sup>62</sup> Liang, Y.; Wu, D.; Feng, X.; Mullen, K. Dispersion of graphene sheets in organic solvent supported by ionic interactions, *Adv. Mater.*, **2009**, *21* (7), 1679-1683.

<sup>63</sup> Zhang, X.; Hou, Y.; Xiao, X.; Chen, X.; Hu, M.; Geng, X.; Wang, Z.; Zhao, J. Recent Development of the Transition Metal Complexes Showing Strong Absorption of Visible Light and Long-Lived Triplet Excited State: From Molecular Structure Design to Photophysical Properties and Applications. *Coord. Chem. Rev.* **2020**, *417*, 213371.

<sup>64</sup> Zhu, Y.; Chen, J.; Kaskel, S. Porphyrin-Based Metal-Organic Frameworks for Biomedical Applications. *Angew. Chem. Int. Ed.* **2020**, *59*, 2-28.

<sup>65</sup> Tomal, W.; Ortyl, J. Water-Soluble Photoinitiators in Biomedical Applications. *Polymers*. **2020**, *12*, 1–31.

<sup>66</sup> Mecha, A. C.; Chollom, M. N. Photocatalytic Ozonation of Wastewater: A Review. *Environ. Chem. Lett.* **2020**, *18*, 1491-1507.

<sup>67</sup> Petzold, D.; Giedyk, M.; Chatterjee, A.; König, B. A Retrosynthetic Approach for Photocatalysis. *Eur. J. Org. Chem.* **2019**, *10*, 1193–1244.

- 
- <sup>68</sup> Michelin, C.; Hoffmann, N. Photosensitization and Photocatalysis - Perspectives in Organic Synthesis. *ACS Catal.* **2018**, 8 (12), 12046–12055.
- <sup>69</sup> Fagnoni, M.; Dondi, D.; Ravelli, D.; Albini, A. Photocatalysis for the Formation of the C-C Bond. *Chem. Rev.* **2007**, 107 (6), 2725-2756.
- <sup>70</sup> Prier, C.K.; Rankic, D. A.; MacMillan, D. W. C. Visible Light Photoredox Catalysis with Transition Metal Complexes: Applications in Organic Synthesis. *Chem. Rev.* **2013**, 113 (7), 5322-5363.
- <sup>71</sup> Tuckett, J. W.; Stephenson, C. R. J. Shining Light on Photoredox Catalysis: Theory and Synthetic Applications. *J. Org. Chem.* **2012**, 77 (4), 1617-1622.
- <sup>72</sup> Branchi, B.; Galli, C.; Gentili, P. Reactivity of Aryl and Vinyl Radicals: Abstraction of Hydrogen Atom or Reaction with a Nucleophile. *Eur. J. Org. Chem.* **2002**, 2002 (16), 2844-2854.
- <sup>73</sup> Pagire, S. K.; Föll, T.; Reiser, O. Shining Visible Light on Vinyl Halides: Expanding the Horizons of Photocatalysis. *ACS Appl. Mater. Interfaces* **2020**, 53 (4), 782-791.
- <sup>74</sup> Hockin, B. M.; Li, C.; Robertson, N.; Zysman-Colman, E. Photoredox Catalysts Based on Earth-Abundant Metal Complexes. *Catal. Sci. Technol.* **2019**, 9, 889–915.
- <sup>75</sup> Romero, N. A.; Nicewicz, D. A. Organic Photoredox Catalysis. *Chem. Rev.* **2016**, 116, 10075–10166.
- <sup>76</sup> Vega-Peñaloza, A.; Mateos, J.; Companyò, X.; Escudero-Casao, M.; Amico, L. D. A Rational Approach to Organo-Photocatalysis: Novel Designs and Structure-Property Relationships. *Angew. Chem. Int. Ed.* **2021**, 133 (3), 1082-1097.

- 
- <sup>77</sup> Sideri, I. K.; Voutyrista, E.; Kokotos, C. Photoorganocatalysis, small organic molecules and light in the service of organic synthesis: the awakening of a sleeping giant. *Org. Biomol. Chem.* **2018**, *16*, 4596.
- <sup>78</sup> Yan, D. M.; Chen, J. R.; Xiao, W. J. New Roles for Photoexcited Eosin Y in Photochemical Reactions. *Angew. Chem. Int. Ed.* **2019**, *58*, 378–380.
- <sup>79</sup> Srivastava, V.; Singh, P. Eosin Y catalysed photoredox synthesis: a review. *RSC Adv.* **2017**, *7*, 31377.
- <sup>80</sup> Hari, D. P.; König, B. Synthetic applications of eosin Y in photoredox catalysis. *Chem. Commun.* **2014**, *50*, 6688.
- <sup>81</sup> Bonfils, P. D.; Pèault, L.; Nun, P.; Coeffard, V. State of the Art of Bodipy-Based Photocatalysts in Organic Synthesis. *Eur. J. Org. Chem.* **2021**, *2021*, 1809-1824.
- <sup>82</sup> Bobo, M. V.; Arcidiacono, A. M.; Ayare, P. J.; Reed, J. C.; Helton, M. R.; Ngo, T. N.; Hanson, K.; Vannucci, A. K. A Series of Green Light Absorbing Organic Photosensitizers Capable of Oxidative Quenching Photocatalysis. *ChemPhotoChem.* **2020**, *5*, 1-8.
- <sup>83</sup> Zhao, J.; Xu, K.; Yang, W.; Wang, Z.; Zhong, F. The Triplet Excited State of Bodipy: Formation, Modulation and Application. *Chem. Soc. Rev.* **2015**, *44*, 8904–8939.
- <sup>84</sup> Johsi-Pangu, A.; Lèvesque, F.; Roth, G. H.; Oliver, S. F.; Campeau, L.; Nicewicz, D.; DiRocco, D. A. Acridinium-Based Photocatalysis: A Sustainable Option in Photoredox Catalysis. *J. Org. Chem.* **2016**, *81*, 7244-7249.
- <sup>85</sup> Zilate, B.; Fischer, C.; Sparr, C. Design and application of aminoacridinium organophotoredox catalysts. *Chem, Commun.* **2020**, *56*, 1767.

- 
- <sup>86</sup> Sharma, S.; Sharma, A. Recent Advances in Photocatalytic Manipulations of Rose Bengal in Organic Synthesis. *Org. Biomol. Chem.* **2019**, *17*, 4384–4405.
- <sup>87</sup> Le, T.; Galmiche, L.; Masson, G.; Allain, C.; Audebert, P. A straightforward synthesis of a new family of molecules: 2,5,8-trialkoxyheptazines. Application to photoredox catalyzed transformations. *Chem. Commun.* **2020**, *56*, 10742.
- <sup>88</sup> Le, T.; Courant, T.; Merad, J.; Clémence, A.; Audebert, P.; Masson, G. s-Tetrazine Dyes: A Facile Generation of Photoredox Organocatalysts for Routine Oxidations. *J. Org. Chem.* **2019**, *84*, 16139-16146.
- <sup>89</sup> Rabe, E.; Corp, K.; Huang, X.; Ehrmaier, J.; Flores, R. G.; Estes, S. L.; Sobolweski, A. L.; Domcke, W.; Schlenker, C. W. Barrierless Heptazine-Driven Excited State Proton-Coupled Electron Transfer: Implications for Controlling Photochemistry of Carbon Nitrides and Aza-Arenes. *J. Phys. Chem. C.* **2019**, *123*, 29580-29588.
- <sup>90</sup> Saritha, R.; Annes, S. B.; Ramesh, S. Metal-free, regioselective, visible light activation of 4CzIPN for the arylation of 2*H*-indazole derivatives. *RSC Adv.* **2021**, *11*, 14079.
- <sup>91</sup> Mitra, K.; Hartman, M.C.T. Silicon Phthalocyanines: synthesis and resurgent applications. *Org. Biomol. Chem.* **2021**, *19*, 1168-1190.
- <sup>92</sup> Liu, M.; Li, C. Recent Advances in Activable Organic Photosensitizers for Specific Photodynamic Therapy, *ChemPlusChem.* **2020**, *85*, 948–957.
- <sup>93</sup> Grant, T.M.; Josey, D.S.; Sampson, K.L.; Mudigonda, T.; Bender, T.P.; Lessard, B.H. Boron subphthalocyanines and silicon phthalocyanines for use as active materials in organic photovoltaics, *Chem. Rec.* **2019**, *19*, 1093–1112.

- 
- <sup>94</sup> Baron, E. D.; Malbasa, C. L.; Santo-Domingo, D.; Fu, P.; Miller, J. D.; Hanneman, K. K.; Hsia, A. H.; Oleinick, N. L.; Colussi, V. C.; Cooper, K. D. Silicon Phthalocyanine (Pc 4) Photodynamic Therapy Is a Safe Modality for Cutaneous Neoplasms: Results of a Phase 1 Clinical Trial. *Lasers Surg. Med.* **2010**, *42*, 888–895.
- <sup>95</sup> Chen, X.; Guo, Q.; Dong, S.; Chen, J.; Xie, S.; Ma, D.; Chen, L.; Yang, H.; Huang, Y.; Peng, Y. Distribution, Trafficking, and in Vitro Photodynamic Therapy Efficacy of Cholesterol Silicon(IV) Phthalocyanine and Its Nanoparticles in Breast Cancer Cells. *ACS Appl. Bio Mater.* **2019**, *2*, 5976–5984.
- <sup>96</sup> Sen, P.; Nyokong, T. A Novel Axially Palladium(II)-Schiff Base Complex Substituted Silicon(IV) Phthalocyanine: Synthesis, Characterization, Photophysicochemical Properties and Photodynamic Antimicrobial Chemotherapy Activity against *Staphylococcus Aureus*. *Polyhedron*. **2019**, *173*, 114135.
- <sup>97</sup> Lessard, B. H.; Dang, J. D.; Grant, T. M.; Gao, D.; Seferos, D. S.; Bender, T. P. Bis(Tri- n -Hexylsilyl Oxide) Silicon Phthalocyanine: A Unique Additive in Ternary Bulk Heterojunction Organic Photovoltaic Devices. *ACS Appl. Mater. Interfaces* .**2014**, *6*, 15040–15051.
- <sup>98</sup> Daziano, J.-P.; Steenken, S.; Chabannon, C.; Mannoni, P.; Chanon, M.; Julliard, M. Photophysical and Redox Properties of a Series of Phthalocyanines: Relation with Their Photodynamic Activities on *TF-I* and Daudi Leukemic Cells, *Photochem. Photobiol.*, **1996**, *64*, 712-719.
- <sup>99</sup> Li, Z.; Lieberman, M. Axial Reactivity of Soluble Silicon(IV) Phthalocyanines. *Inorg. Chem.*, **2001**, *40*, 932-939.

- 
- <sup>100</sup> Huang, J.; Wu, Y.; Wang, D.; Ma, Y.; Yue, Z.; Lu, Y.; Zhang, M.; Zhang, Z.; Yang, P. Silicon Phthalocyanine Covalently Functionalized N-Doped Ultrasmall Reduced Graphene Oxide Decorated with Pt Nanoparticles for Hydrogen Evolution from Water. *ACS Appl. Mater. Interfaces*. **2015**, *7*, 3732-3741.
- <sup>101</sup> Xiao, B.; Zhu, M.; Li, X.; Yang, P.; Qiu, L.; Lu, C. A stable and efficient photocatalytic hydrogen evolution system based on covalently linked silicon-phthalocyanine-graphene with surfactant. *Int. J. Hydrog. Energy*. **2016**, *41*, 11537.
- <sup>102</sup> Shaw, M.; Twilton, J.; MacMillan, D.W.C. Photoredox Catalysis in Organic Chemistry. *J. Org. Chem.* **2016**, *81*, 6898–6926.
- <sup>103</sup> Koziar, J. C.; Cowan, D. O. Photochemical Heavy-Atom Effects. *Acc. Chem. Res.* **1978**, *11*, 334–341.
- <sup>104</sup> Chen, X.; Ma, D.; Cai, K.; Pan, S. Effect of Axial Ligands on the Photophysical Properties of New Silicon ( IV ) Phthalocyanines, *J. Coord. Chem.*, **2015**, *68* (4), 732–740.
- <sup>105</sup> Opeyemi, O.M.; Louis, H.; Opara, C.I.; Oyebanji, O.F.; Magu, T.O. Porphyrin and phthalocyanines-based solar cells: fundamental mechanisms and recent advantages, *Adv J Chem A*, **2019**, *2*, 21-44.
- <sup>106</sup> LeGourriec, D.; Andersson, M.; Davidsson, J.; Mukhtar, E.; Sun, L.; Hammarstrom, L. *J. Phys. Chem. A*, **1999**, *103*, 557-559.
- <sup>107</sup> Wheeler, B.L.; Nagasubramanian, G.; Bard, A.J.; Schechtman, L.A.; Dininny, D.R.; Kenney, M.E. A Silicon Phthalocyanine and a Silicon Naphthalocyanine: Synthesis,

---

Electrochemistry, and Electrogenenerated Chemiluminescence. *J. Am. Chem. Soc.*, **1984**, *106*, 7404-7410.

<sup>108</sup> Biyiklioglu, Z.; Bas, H. Synthesis and electrochemistry of non-aggregated axially disubstituted silicon phthalocyanines bearing benzoxazine substituents. *Inorganica Chim. Acta*, **2015**, *427*, 293-298.

<sup>109</sup> Demirkapi, D.; Sirin, A.; Turanli-Yildiz, B.; Cakar, Z.P.; Sesalan, B.S. The synthesis of new silicon phthalocyanines and analysis of their photochemical and biological properties. *Synth. Met.*, **2014**, *187*, 152-159.

<sup>110</sup> Baş, H.; Biyiklioglu, Z. Non-Aggregated Axially Naphthoxazin Group Substituted Silicon Phthalocyanines: Synthesis and Electrochemistry. *J. Organomet. Chem.* **2015**, *791*, 238–243.

<sup>111</sup> Mau, A.W.-H.; Johansen, O.; Sasse, W. H. F. Xanthene Dyes as Sensitizers for the Photoreduction of Water. *Photochemistry and Photobiology*, **1985**, *41*, 503-509.

<sup>112</sup> Wiegand, C.; Herdtweck, E.; Bach, T. Enantioselectivity in Visible Light-Induced, Singlet Oxygen [2+4] Cycloaddition Reactions (Type II Photooxygenations) of 2-Pyridones. *Chem. Commun.* **2012**, *48*, 10195–10197.

<sup>113</sup> Bach, T.; Bergmann, H.; Harms, K. Enantioselective Intramolecular [2+2]-Photocycloaddition Reactions in Solution. *Angew. Chem. Int. Ed.* **2000**, *39*, 2302-2304.

<sup>114</sup> Neumann, M.; Földner, S.; König, B.; Zeitler, K. Metal-Free, Cooperative Asymmetric Organophotoredox Catalysis with Visible Light. *Angew. Chem. Int. Ed.* **2011**, *50*, 951–954.

- 
- <sup>115</sup> Narayanam, J. M. R.; Tucker, J. W.; Stephenson, C. R. J. Electron-Transfer Photoredox Catalysis: Development of a Tin-Free Reductive Dehalogenation Reaction. *J. Am. Chem. Soc.* **2009**, *131*, 8756–8757.
- <sup>116</sup> Lessard, B. H.; Grant, T. M.; White, R.; Thibau, E.; Lu, Z.; Bender, T. P. The position and frequency of fluorine atoms changes the electron donor/acceptor properties of fluorophenoxy silicon phthalocyanines within organic photovoltaic devices, *J. Mater. Chem. A.*, **2015**, *3*, 24512.
- <sup>117</sup> King, B.; Daszczyński, A. J.; Rice, N. A.; Peltekoff, A. J.; Yutronkie, N. J.; Lessard, B. H.; Brusso, J. L. Cyanophenoxy-Substituted Silicon Phthalocyanines for Threshold Voltage n-Type Organic Thin-Film Transistors, *ACS Appl. Electron. Mater.*, **2021**, *3*, 2212-2223.
- <sup>118</sup> Shirley, H.; Sexton, T. M.; Liyanage, N. P.; Perkins, M. A.; Autry, S. A.; McNamara, L. E.; Hammer, N. I.; Parkin, S. R.; Tschumper, G. S.; Delcamp, J. H. Probing the Effects of Electron Deficient Aryl Substituents and a  $\pi$ -System Extended NHC Ring on the Photocatalytic CO<sub>2</sub> Reduction Reaction with Re-pyNHC-Aryl Complexes, *ChemPhotoChem*, **2021**, *5*, 353-361.
- <sup>119</sup> David, E.; Mishra, K.; Thirumoorthy, K.; Palanisami, N. Aggregation induced emission (AIE)-active N-arylated ferrocenyl pyrazole-based push-pull chromophores: Structural, photophysical, theoretical and effect of substitution on second-order non-linear optical properties, *Appl. Organomet. Chem.*, **2021**, *35*, online.



- 
- <sup>120</sup> Medina, E.; Pinter, B. Electron Density Difference Analysis on the Oxidative and Reductive Quenching Cycles of Classical Iridium and Ruthenium Photoredox Catalysts, *J. Phys. Chem. A.*, **2020**, *124*, 4223-4234.
- <sup>121</sup> Parella, R.; Jakkampudi, S.; Zhao, J. C.-G. Recent Applications of Asymmetric Organocatalytic Methods in Total Synthesis, *ChemistrySelect*, **2021**, *6*, 2252-2280.
- <sup>122</sup> Hayashi, Y. Time Economy in Total Synthesis, *J. Org. Chem.*, **2021**, *86*, 1-23.
- <sup>123</sup> Marques-Lopez, Herrera, R.; Christmann, M. Asymmetric organocatalysis in total synthesis – a trial by fire, *Nat. Prod. Rep.*, **2010**, *27*, 1138-1167.
- <sup>124</sup> Kumar, P.; Dwivedi, N. Proline Catalyzed  $\alpha$ -Aminooxylation Reaction in the Synthesis of Biologically Active Compounds, *Acc. Chem. Res.*, **2013**, *46*, 289-299.
- <sup>125</sup> Sheng, F.; Wang, J.; Tan, W.; Zhang, Y.; Shi, F. Progresses in organocatalytic asymmetric daromatization reactions of indole derivatives, *Org. Chem. Front.*, **2020**, *7*, 3967.
- <sup>126</sup> Ishihara, K.; Fushimi, M. Design of a Small-Molecule Catalyst Using Intramolecular Interactions for Enantioselective Diels-Alder and Mukaiyama-Michael Reactions: L-DOPA-Derived Monopeptide-Cu(II) Complex, *Org. Lett.*, **2006**, *8*, 1921-1924.
- <sup>127</sup> Discolo, C. A.; Touney, E. E.; Pronin, S. V. Catalytic Asymmetric Radial-Polar Crossover Hydroalkoxylation, *J. Am. Chem. Soc.*, **2019**, *141*, 17527-17532.
- <sup>128</sup> Yang, X.; Bumbu, X. D.; Liu, P.; Li, X.; Jiang, H.; Uffman, E. W.; Guo, L.; Zhang, W.; Jiang, X.; Houk, K. N.; Birman, V. B. Catalytic, Enantioselective N-Acylation of Lactams and Thiolactams Using Amidine-Based Catalysts, *J. Am. Chem. Soc.*, **2012**, *134*, 17605-17612.

- 
- <sup>129</sup> Yamada, S.; Fossey, J. S. Nitrogen cation- $\pi$  interactions in asymmetric organocatalytic synthesis, *Org. Biomol. Chem.*, **2011**, *9*, 7275.
- <sup>130</sup> Birman, V.; Uffman, E.; Jiang, H.; Li, X.; Kilbane, C. 2,3-Dihydroimidazo [1, 2-a] pyridines: a new class of enantioselective acyl transfer catalysts and their use in kinetic resolution of alcohols, *J. Am. Chem. Soc.*, **2004**, *126*, 12226-12227.
- <sup>131</sup> Sumit, Chandra, D.; Sharma, U. Merging kinetic resolution with C-H activation: an efficient approach for enantioselective synthesis, *Org. Biomol. Chem.*, **2021**, *19*, 4014.
- <sup>132</sup> MacMillan, D.W.C. The advent and development of organocatalysis. *Nature*, **2008**, *455*, 304-308.
- <sup>133</sup> Birman, V. B.; Jiang, H. Kinetic Resolution of Alcohols Using a 1,2-Dihydroimidazo[1,2-a]quinoline Enantioselective Acylation Catalyst, *Org. Lett.*, **2005**, *7*, 3445-3447.
- <sup>134</sup> Birman, V. B.; Li, X. Benzotetramisole: A Remarkably Enantioselective Acyl Transfer Catalyst, *Org. Lett.*, **2006**, *8*, 1351-1354.
- <sup>135</sup> Birman, V. B.; Li, X.; Jiang, H.; Uffman, E. W. Influence of electronic and steric factors on 2, 3-dihydroimidazo [1, 2-a] pyridine-based enantioselective acylation catalysts, *Tetrahedron*, **2006**, *62*, 285.
- <sup>136</sup> Musolino, S. F.; Ojo, O. S.; Westwood, N. J.; Taylor, J. E.; Smith, A. D., Isothiourea-Catalysed Acylative Kinetic Resolution of Aryl-Alkenyl ( $sp^2$  vs.  $sp^2$ ) Substituted Secondary Alcohols, *Chem. Eur. J.*, **2016**, *22*, 18916-18922.
- <sup>137</sup> Greenhalgh, M.; Smith, S. M.; Walden, M. D.; Taylor, J. E.; Brince, Z.; Robinson, E. R. T.; Fallan, C.; Cordes, D. B.; Slawin, A. M. Z.; Richardson, H. C.; Grove, M. A.;

- 
- Cheong, P. H.; Smith, A. D. A C=O... Isothiouonium Interaction Dictates Enantiodiscrimination in Acylative Kinetic Resolutions of Tertiary Heterocyclic Alcohols, *Angew. Chem. Int. Ed.*, **2018**, *57*, 3200-3206.
- <sup>138</sup> Wang, L.; Akhani, R. K.; Wiskur, S. L. Diastereoselective and Enantioselective Silylation of 2-Arylcyclohexanols, *Org. Lett.*, **2015**, *17*, 2408-2411.
- <sup>139</sup> Akhani, R. K.; Moore, M. I.; Pribyl, J. G.; Wiskur, S. L., Linear Free-Energy Relationship and Rate Study on a Silylation-Based Kinetic Resolution: Mechanistic Insights, *J. Org. Chem.*, **2014**, *79*, 2384-2396.
- <sup>140</sup> Zhang, T.; Redden, B.; Wiskur, S. Investigation of electrostatic interactions towards controlling silylation-based kinetic resolutions, *Eur. J. Org. Chem.*, **2019**, *2019*, 4827-4831.
- <sup>141</sup> Erturk, E.; Tezeren, M. A.; Atalar, T.; Tilki, T. Regioselective ring-opening of epoxides with ortho-lithioanisoles catalyzed by BF<sub>3</sub>·OEt<sub>2</sub>, *Tetrahedron*, **2012**, *68*, 6463.
- <sup>142</sup> Shevchenko, G. A.; Oppelaar, B.; List, B. An Unexpected  $\alpha$ -Oxidation of Cyclic Ketones with a 1,4-Benzoquinone by Enol Catalysis, *Angew. Chem. Int. Ed.*, **2018**, *57*, 10756-10759.
- <sup>143</sup> Marsh, E. N. G.; Suzuki, Y. Using <sup>19</sup>F NMR to Probe Biological Interactions of Proteins and Peptides, *ACS Chem. Biol.*, **2014**, *9*, 1242-1250.
- <sup>144</sup> Howe, P. Recent Developments in the use of fluorine NMR in synthesis and characterisation, *Progress in Nuclear Magnetic Resonance Spectroscopy*, **2020**, *118-119*, 1-9.

- 
- <sup>145</sup> Biedermann, F.; Schneider, H.-J. Experimental Binding Energies in Supramolecular Complexes, *Chem. Rev.*, **2016**, *116*, 5216-5300.
- <sup>146</sup> Hansch, C.; Gao, H. Comparative QSAR: Radical Reactions of Benzene Derivatives in Chemistry and Biology, *Chem. Rev.*, **1997**, *97*, 2995-3059.
- <sup>147</sup> Hansch, C.; Leo, A.; Taft, R. W. A Survey of Hammett Substituent Constants and Resonance and Field Parameters, *Chem. Rev.*, **1991**, *91*, 165-195.
- <sup>148</sup> McGraph, J. M.; Pluth, M. D. Linear Free Energy Relationships Reveal Structural Changes in Hydrogen-Bonded Host-Guest Interactions, *J. Org. Chem.*, **2014**, *79*, 11797-11801.
- <sup>149</sup> Birman, V. B.; Li, X. Homobenzotetramisole: An Effective Catalyst for Kinetic Resolution of Aryl-Cycloalkanols, *Org. Lett.*, **2008**, *10*, 1115-1118.